Challenge Journal of STRUCTURAL MECHANICS

Vol.2 No.2 (2016)

ISSN 2149-8024

TULPAR ACADEMIC PUBLISHING

Challenge Journal of Structural Mechanics

E-mail: *cjsmec@challengejournal.com*

Web page: *cjsmec.challengejournal.com*

TULPAR Academic Publishing
www.tulparpublishing.com

Challenge Journal of Structural Mechanics

CONTENTS

TULPAR ACADEMIC PUBLISHING

Challenge Journal of Structural Mechanics

Shear capacity of post-installed anchors according to ACI318 and TS500

Özlem Çalışkan [a,*], Salih Yılmaz [b], Hasan Kaplan [c]

[a] *Department of Civil Engineering, Bilecik Şeyh Edebali University, 11210 Bilecik, Turkey*
[b] *Department of Civil Engineering, İzmir Katip Çelebi University, 35620 Izmir, Turkey*
[c] *Department of Civil Engineering, Pamukkale University, 20070 Denizli, Turkey*

ABSTRACT

Applications of strengthening works have accelerated gradually due to earthquakes in recent years. Different strengthening methods are being used in order to bring the structures with insufficient strength to those levels specified by current codes. In most of the applications, the bonding between the new structural elements and the concrete of the old structure is established with the chemical anchors. Although they are used widespread in the practice, there are not any sufficient details in Turkish Standards for the design and application of these anchors. In this work, a comparison of ACI318 and the Turkish Standards for anchor shear strength is given. As the result, it has been concluded that there are vital differences between ACI and the Turkish Standards and that an immediate revision is needed for the Turkish Standards.

ARTICLE INFO

Article history:
Received 3 March 2016
Accepted 28 April 2016

Keywords:
Post-installed anchors
Shear capacity;
TS500
ACI318
Edge distance

1. Introduction

Anchors are used to maintain integrity of structural elements that are separately constructed. They are frequently used for connections especially between reinforced concrete – steel and reinforced concrete – reinforced concrete. Due to increase in the number of strengthening applications of structures in recent years, there is also a considerable increase the use of post-installed anchors (Yılmaz and Kaplan, 2009). In these applications both chemical and mechanical usages of anchor are possible, whereas chemical anchors are mostly preferred, as they are more economical. Depending on their direction and locations, these anchors may resist shear or tension forces, or both of them.

In the literature, there exist many studies about anchors. In most of them, the tensile capacity of anchors are studied. On the other hand, the concrete elements used in those had a compressive strength greater than 30 MPa in most cases (Cook et al., 1992; McVay et al., 1996; Primavera et al., 1997; Fujikake et al., 2003; Zamora et al., 2003). The experiments with a concrete compressive strength lower than 20 MPa are a minor part of all the literature (Özkul et al., 2001; Eligehausen et al., 2006; Gürbüz, 2007; Kaya, 2007). Although tensile strength of anchors are well-studied, research on shear strength of anchors are limited in number (Fuchs et al., 199; Muratli et al., 2004; Özturan et al., 2004). The effects of edge distance and the spacing on the shear strength are researched and it was observed that the shear strength is proportional with the edge distance. ACI Committee 349 shear strength formula presents the estimated acceptable lower limit for the test results of the work by Ueda et al. (1990). The researchers, who evaluated the data base for anchor experiments, which is compiled by ACI Comitee 349 and 355, have observed that the concrete edge distance in the direction of loading has a significant effect on the shear strength of anchors. They have also observed that the embedment depth and diameter have a minor effect on the shear strength of anchor and that there is not any linear relationship between the shear capacity of anchor and the compressive strength of concrete. (Alqedra and Ashour, 2005).

In literature, various methods were presented to determine the anchor shear capacity. However, in the recent years, common approach is to find the capacities for different failure modes separately and to take the lowest strength as the anchor shear capacity into consideration. In parallel with that approach, an important revision was made after the 2002 version of ACI318 (2008) and the

* *Corresponding author*. Tel.: +90-228-2141561 ; Fax: +90-228-2141222 ; E-mail address: ozlem.caliskan@bilecik.edu.tr (Ö. Çalışkan)
ISSN: 2149-8024 / DOI: http://dx.doi.org/10.20528/cjsmec.2016.04.009

calculation methods for anchor tensile and shear capacities were changed. On the other hand, even though there isn't any regulation in TS500 about the anchors, which are post-installed in to the concrete, a separate section about strengthening of structures was added to Turkish Earthquake Code in 2007. In this section, it was referred to formula of shear friction, which is given in TS500 (2000) for the shear capacity of anchor elements. In this formula, which was not changed since the version of TS500 in 1984, only the capacity that corresponds to steel failure is taken into consideration. Weaker failure modes caused by the failures in concrete are neglected. However, the compressive strength of concrete in strengthened structures in Turkey is extremely low and the anchor workmanship is not sufficient in quality. Two extreme cases in Fig. 1 clearly shows the possible lower limits of anchor quality.

Fig. 1. Concrete quality and anchor workmanship in some strengthened structures.

In this study, anchor strengths were calculated for different embedment depth, base concrete strength according to ACI318 and TS500 standards. Both standards are compared and some revisions are proposed for TS500.

2. Material and Method

2.1. ACI318 method

ACI318 identifies three different failure modes for the ultimate case, when anchor shear capacity is reached: Steel failure, concrete breakout and concrete pryout. These failure modes are illustrated in Fig. 2. Generally it can be expressed that in cases where the anchor bar is near to free edge, the breakout and pryout capacities are governing the anchor capacity, and in cases where this distance is far, failure of the anchor bar is determining the ultimate strength.

With consideration of the failure of steel, the anchor strength can be calculated by Eq. (1).

$$V_{sa} = n * A_{se} * f_{uta} . \quad (1)$$

Here, n represents the number of anchors in the group, A_{se} represents the sectional area of the anchor (mm^2) and f_{uta} represents the tension strength of steel (N/mm^2).

When the failure is at concrete breakout mode, the breakout capacity can be found by Eq. (2) for single anchor, and in Eq. (3) for group anchors.

$$V_b = 0{,}6\left(\frac{l_e}{d_0}\right)^{0,2}\sqrt{d_0}\sqrt{f'_c}n(c_{a1})^{1,5} , \quad (2)$$

$$V_b = 0{,}7\left(\frac{l_e}{d_0}\right)^{0,2}\sqrt{d_0}\sqrt{f'_c}n(c_{a1})^{1,5} . \quad (3)$$

Here, l_e load bearing length of anchor for shear, f'_c specified compressive strength of concrete, d_0 outside diameter of anchor.

For pryout failure, the formula given by ACI318 is shown for a single anchor in Eq. (4) and for group anchors in Eq. (5). Pryout capacity can be calculated depending on the axial breakout capacity.

$$V_{cp} = k_{cp} * N_{cp} , \quad \text{(for a single anchor)} \quad (4)$$

$$V_{cpg} = k_{cp} * N_{cpg} . \quad \text{(for a group of anchors)} \quad (5)$$

Here, N_{cb} nominal concrete breakout strength in tension of a single anchor, N_{cbg} nominal concrete breakout strength in tension of a group of anchors, k_{cp} is a coefficient depending on the embedment depth, k_{cp}=1.0 for h_{ef} <65 mm ; k_{cp}=2.0 for $h_{ef} \geqslant$65 mm.

The capacity is calculated for three different failure modes separately according to ACI318, and the failure mode with the lowest strength is determining the ultimate shear capacity. It is important to note that these forces corresponds to capacity estimations. For design forces ACI introduces capacity reduction factors also.

2.2. TS500 method

Turkish Earthquake Code references TS500 sliding shear formula for calculation of the anchor shear capacity. According to sliding shear formula in TS500, only the failure mode of reinforcement is taken into consideration. TS500 formula is given in the Eq. (6).

$$V_r = \mu * A_s * f_{yd} , \quad (6)$$

μ value is a constant depending on roughness of the surface, A_s is the reinforcement area (mm^2), and f_{yd} is the design yield strength of reinforcement (N/mm^2).

The lowest possible value of the friction coefficient is given as 0.6. Therefore, in this study, μ=0.6 is used, in order to determine anchor capacities according to TS500.

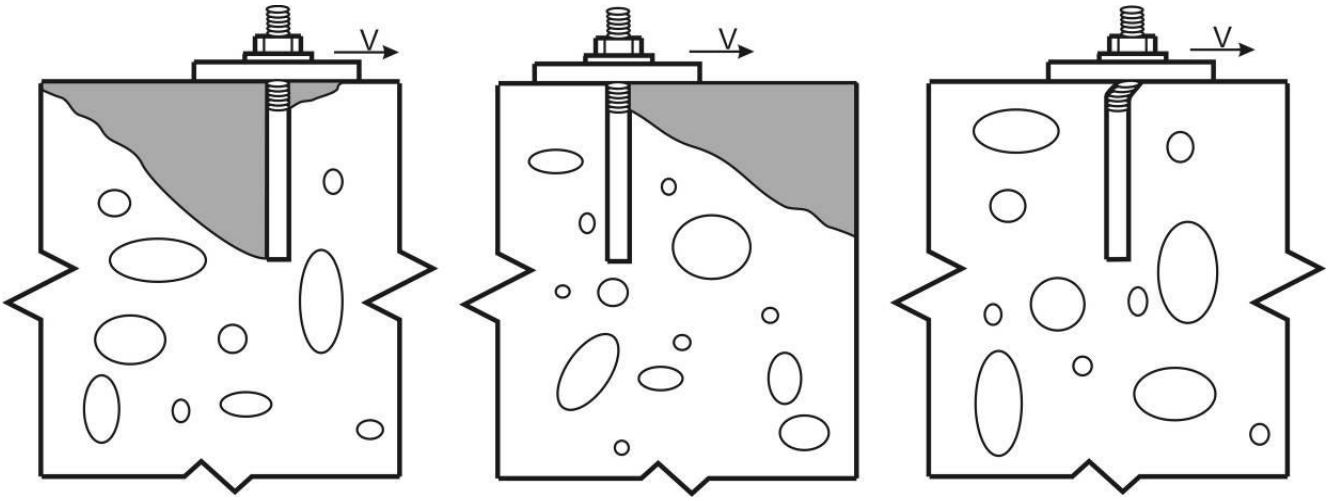

Fig. 2. Anchor failure modes.

3. Parameters

Embedment depth, base concrete strength, free edge distance and bar diameter are variable parameters. In the scope of the study, the shear capacities of anchors between 12 mm to 24 mm bar sizes are determined per ACI318 and TS500. The parameters used in the study are shown in Table 1.

Table 1. Parameters used in the work.

Depth L	Concrete Compression Strength C (MPa)	Edge distance c (mm)	Bar diameter d (mm)
10Φ	8	50	12
15Φ	12	100	14
20Φ	20	150	16
		200	18
			20
			22
			24

4. Shear Capacity of Anchors

Shear capacities of anchors with different diameter, embedment depth and edge distance, which are calculated according to TS500 and ACI318, are compared in Fig. 3 for base concrete strengths of 8, 12 and 16 MPa. Each point on the curves corresponds to a different bar size. Bar diameters from down to up are 12, 14, 16, 18, 20, 22 and 24 mm, respectively.

For anchors with edge distance equal to 100 mm and less, the TS500 values are greater than those calculated by ACI318 method in concretes with 8 MPa compressive strength. Evaluation of anchors designed per TS500 for 12 MPa concrete, all anchors with edge distance less than 50 mm are unsafe according to ACI318. While the edge distance increases to 100 mm, anchors with smaller diameters, i.e. 16 mm and smaller, can be safely designed by TS500. However, the problem is the same for greater bar sizes. For C16 concrete class, TS500 design forces for edge distance equal to 50 mm are not safe according to capacity determined per ACI318. Greater edge distances results in safer design loads. Accordingly, the decrease in concrete strength and the increase in reinforcement diameter are negatively affecting the reliability of the TS500 formula.

In Fig. 4, the ACI318 and TS500 design forces for anchors are given for varying edge distances. These graphics are given for three different embedment depths (10Φ, 15Φ ve 20Φ) and for three different reinforcement diameters (12, 16 and 20 mm). Edge distance directly affect the capacity of anchor according to ACI318 formulation, However, TS500 formulation results in the same capacity for different edge distances. If the edge distance is great enough, which corresponds to minority of actual cases in practice, then TS500 gives safe results. For example, for an anchor bar with 10Φ embedment depth, the TS500 formula is on the safe side with respect to ACI318, when the edge distance is greater than 100 mm for 12mm bars installed in to C8 block. This lower limit, which defines reliability of TS500 formula, increases to 150 mm for Φ20 mm bars.

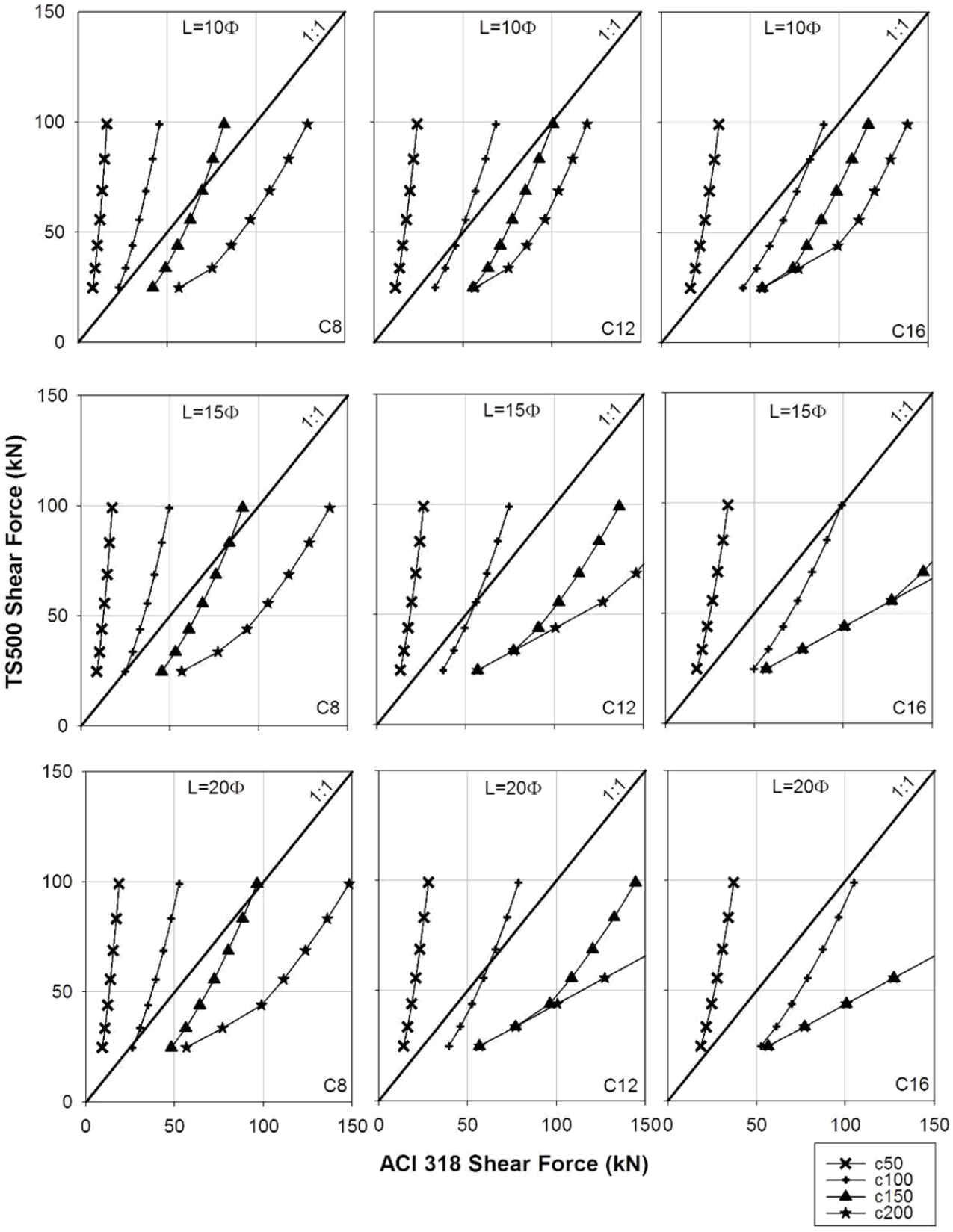

Fig. 3. ACI318 - TS500 comparison of shear forces.

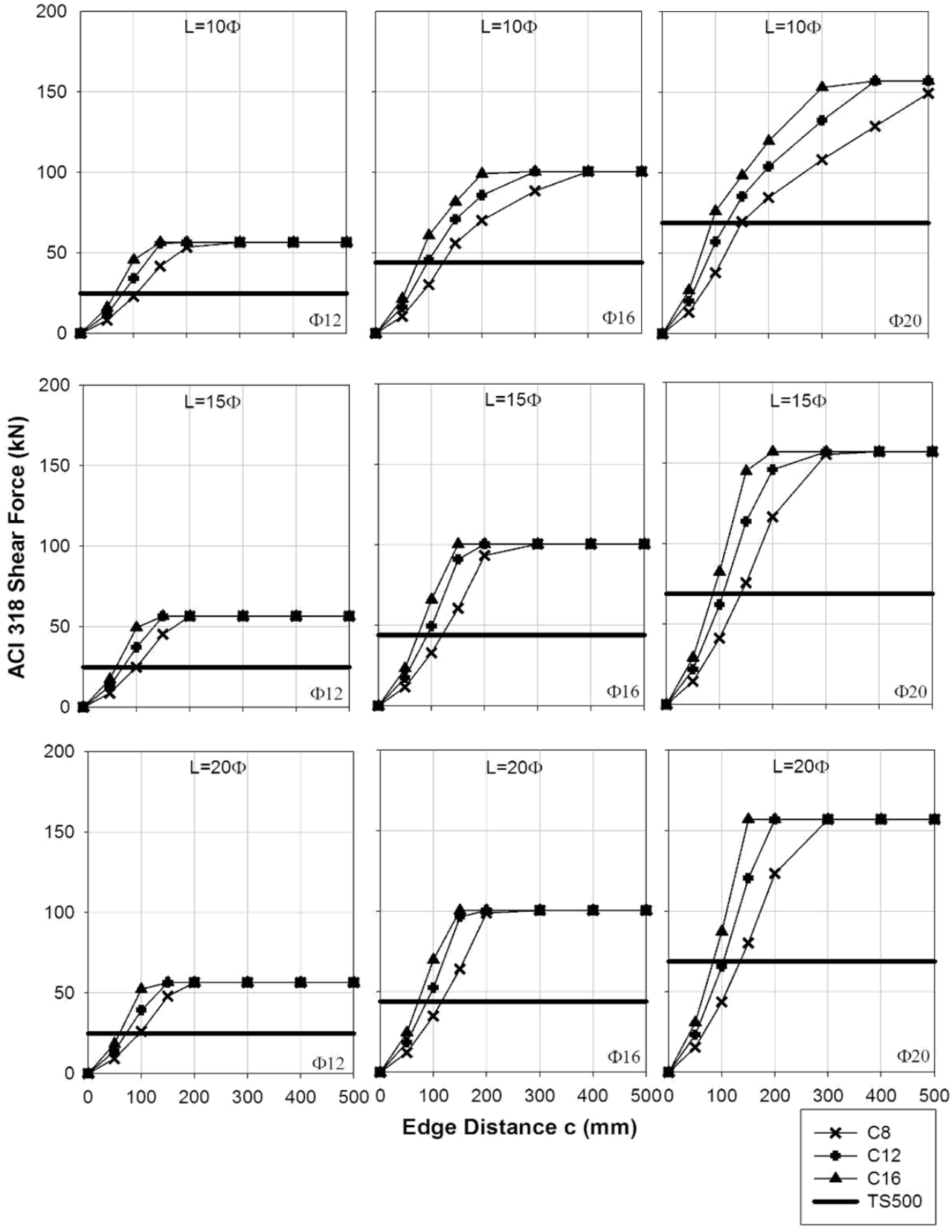

Fig. 4. ACI318 – TS500 shear forces with varying edge distances.

5. Conclusions

In this study, ACI318 and TS500 methods, which are used for determining anchor shear capacity, are compared for low strength base concrete. Current Turkish Earthquake Code (2007) references to sliding shear formula of TS500 for anchor capacity.

In ACI318 method, besides bar diameter and steel strength, concrete strength and the free edge distance of anchor are effective parameters for shear capacity. However, in TS500 formula, the anchor strength is not affected by concrete compressive strength and edge distance. As a result, the shear design of anchors with small free edge distance or embedded to low strength concrete according to TS500 may cause to misleading results. Therefore, an immediate revision is needed either in Turkish Earthquake Code or TS500.

From the results of this study, it is possible to conclude that TS500 formulae results in safe result for the most of the cases while free edge distance is higher than 15Φ. Therefore, designers can utilize either TS500 or ACI318 methods accordingly. However, it should be noted ACI capacity reduction factors were not utilized for this study. Use of those would definitely result in a worse condition for TS500 approach.

Acknowledgement

This study has been supported by National Scientific and Technological Research Foundation of Turkey (TÜBİTAK) under grant number 107M572.

References

ACI Committee 349 (1978). Code requirements for nuclear safety - related concrete structures and commentary.

ACI Committee 355 (1991). State-of-the-Art Report on Anchor to Concrete, ACI 355.1R-91, American Concrete Institute, Detroit, MI.

ACI318 (2008). Building Code Requirements for Reinforced Concrete, American Concrete Institute, Detroit, USA.

Alqedra MA, Ashour AF (2005). Prediction of shear capacity of single Anchors located near a concrete edge using neural Networks. *Computers & Structures*, 83, 2495-2502.

Cook RA, Collins D Mi, Klingner RE, Polyzois D (1992). Load-deflection behavior of cast-in-place and retrofit concrete anchors. *ACI Structral Journal*, November-December. 639-649.

DBYYHY (2007). Deprem Bölgelerinde Yapılacak Yapılar Hakkında Yönetmelik, Bayındırlık ve İskan Bakanlığı, Ankara.

Eligehausen R, Cook RA, Appl J (2006). Behavior and design adhesive bonded anchors. *ACI Structural Journal*, November-December, 822-831.

Fuchs W, Eligehausen R, Breen JE (1995). Concrete capacity design (CCD) approach for fastening to concrete. *ACI Structural Journal*, 92(1), 73-94.

Fujikake K, Nakayama J, Sato H, Mindess S, Ishibashi T (2003). Chemically bonded anchors subjected to rapid pullout loading. *ACI Materials Journal*, May-June, 246-252.

Gürbüz T (2007). Yapıların Güçlendirilmesinde Kullanılan Kimyasal Ankrajların Eksenel Çekme Etkisi Altındaki Davranışlarının Incelenmesi. *M.Sc. thesis*, İstanbul Technical University, İstanbul (in Turkish).

Kaya Y (2007). Yapıların Güçlendirilmesi Uygulamalarında Kullanılabilecek Kısmi Bağlı Ankraj Detayı ve Yüzey Temizliği Koşulları Altında Ankrajların Eksenel Çekme Davranışlarının İncelenmesi. *M.Sc. thesis*, İstanbul Technical University, İstanbul (in Turkish).

McVay M, Cook RA, Krishnamurthy K (1996). Pullout simulation of postinstalled chemically bonded anchors. *Journal of Structural Engineering*, September, 1016-1024.

Muratli, H, Klingner RE, Graves HL (2004). Breakout capacity of anchors in concrete-part 2: shear. *ACI Structural Journal*, November-December, 821-829.

Özkul H, Mutlu M Sağlam AR (2001). Beton ankrajları, Sika Teknik Bülten Sayı 4.

Özturan T, Gesoğlu M, Özel M, Güneyisi E (2004). Kimyasal, harçlı ve mekanik ankrajların çekme ve kesme yükleri altındaki davranışları. *İMO Teknik Dergi*, 208, 3105-3124..

Primavera EJ, Pinelli JP, Kalajian EH. (1997). Tensile behavior of cast-in-place and undercut anchors in high-strength concrete. *ACI Structural Journal*, September-October, 583-594.

TS500 (2000). Betonarme Yapıların Tasarım ve Yapım Kuralları. Türk Standartları Enstitüsü, Ankara.

Ueda T, Kitipornchai S, Ling K (1990). Experimental investigation of anchor bolts under shear. *ASCE Journal of Structural Engineering*, 116(4), 910-924.

Yılmaz S, Kaplan H (2009). Epoksi Ankraj Uygulamalarında dikkat edilmesi gerekli konular, İMO Denizli Bülten, Temmuz-Eylül.

Zamora NA, Cook RA, Konz RC and Consolazio GR (2003). Behavior and design of single, headed and unheaded, grouted anchors under tensile load, *ACI Structural Journal*, March-April, 222-230.

Challenge Journal of Structural Mechanics

Reliability design of the hinge kit system subjected to repetitive loading in a commercial refrigerator

Seong-woo Woo [a,*], Dennis L. O'Neal [b]

[a] *Reliability Association of Korea, 146-102 Sunyoo-ro, Yeongdeungpo-gu, Seoul 150-103, Korea*
[b] *School of Engineering and Computer Science, Baylor University, Waco, TX 76798-7356, USA*

ABSTRACT

A newly designed hinge kit system (HKS) of a commercial refrigerator was subjected to a robust reliability methodology during the design phase of the system. This methodology included setting the overall parametric accelerated life test (ALT) plan of product and identifying failure mechanisms and modes in field. The ALT included a sample size equation to improve several of the HKS design parameters. Reliability of the new HKS was targeted to be 10 years over B1. Failure sites in the HKS were identified through returned products from the field. The first ALT confirmed a failure that occurred at the housing of HKS. The missing design parameters of HKS housing for the refrigerator were that it had no support ribs in the original design. The supporting structure of HKS in the refrigerator was modified based on the action plan. Cracks were identified in a second ALT that was generated in the torsional shaft. Due to it having squared off corners, the HKS torsional shaft did not have not enough strength to withstand repetitive stresses. The shaft was modified as a consequence of the ALTs. The reliability of redesigned HKS is now guaranteed as B1 10 years. The design methods - load analysis and three ALTs were very effective in identifying the missing design parameters during the design phase. The robust design method presented in this paper might be applicable to the other mechanical systems.

ARTICLE INFO

Article history:
Received 29 March 2016
Accepted 13 May 2016

Keywords:
Robustness
Parameter design
Load analysis
Accelerated life testing

1. Introduction

When a consumer opens and closes a refrigerator door, they should be able to accomplish this with minimal effort. The hinges of a door are a component of the door that is subjected to repetitive use over the life of the refrigerator. A new hinge kit system (HKS) was designed for the refrigerator (see Fig. 1(a)) to improve the ease of opening and closing the door for the consumer. The HKS is shown in Fig. 1(b) consists of a kit cover, shaft, spring, and oil damper, etc.

The functional loss of the original HKS had been reported often by owners of the refrigerator. Thus, exact data analysis was required to find out the root cause of the defective HKS and what parameter in the HKS needed to be redesigned.

Fig. 2 shows a damaged HKS which has two cracks that appeared after a period of use. It was not known under what usage conditions the failure occurred. When comprehensive data from the field were reviewed, it was concluded that the root cause of the HKS failure was a structural design flaw–no round of torsional shaft. Moreover, due to the repetitive loading of the opening and closing of the door, this design defect eventually led to creating the cracks of HKS.

Robust design techniques, including statistical design of experiments (SDE) and Taguchi methods (1978), were developed by statisticians many years ago. Taguchi's robust design method uses parameter design to place the design in a position where random ''noise" does not cause failure and is used to determine the proper design parameters and their levels

* *Corresponding author*. Tel.: +82-42-936-1026 ; Fax: +82-42-936-2052 ; E-mail address: twinwoo@yahoo.com (S. Woo)
ISSN: 2149-8024 / DOI: http://dx.doi.org/10.20528/cjsmec.2016.05.010

(Taguchi and Shih-Chung, 1992; Ashley, 1992; Wilkins, 2000; Phadke, 1989; Byrne and Taguchi, 1987). The basic idea of parameter design is to identify, through exploiting interactions between control factors and noise factors, appropriate settings for the control factors that make the system's performance robust in relation to changes in the noise factors. Thus, the control factors are assigned to an inner array in an orthogonal array, and the noise factors are assigned to an outer array. However, a large number of experimental trials in the Taguchi product array may be required because the noise array is repeated for every row in the control array. However, for a simple mechanical structure, a lot of design parameters should be considered in the Taguchi method's robust design process. Those products with the missing or improper minor design parameters may result in recalls and loss of brand name value.

Fig. 1. Commercial refrigerator and its HKS: (a) Commercial refrigerator; (b) HKS.

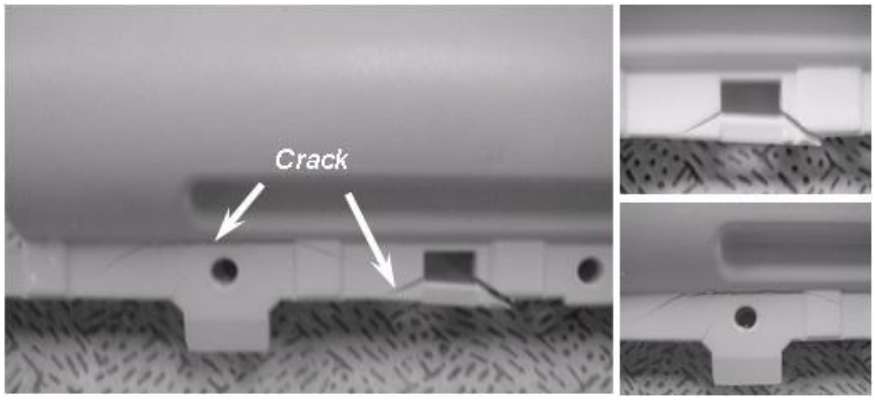

Fig. 2. A view of damaged HKS after a period of use.

The purpose of this study was to present a robust reliability evaluation methodology to the HKS as mechanical system subjective to repetitive loading in the commercial refrigerator. The method includes

- setting overall parametric ALT plan for the product,
- analyzing the failure modes of the returned product from the field, and
- improving the designs of the HKS using a tailored of ALTs with a sample size equation.

Nomenclature

AF	Acceleration factor
BX	Durability index
$C1$	Housing design of HKS
$C2$	Roundness of torsional shaft
$F(t)$	Unreliability
F	Force (kN)
$F1$	Impact force under accelerated stress conditions
$F0$	Impact force under normal conditions
h	Testing cycles (or cycles)
h^*	Non-dimensional testing cycles
KCP	Key Control Parameter
KNP	Key Noise Parameter
L_B	Target B_X life (x = 0.01X, on the condition that $x \leq 0.2$)
M	Moment around the hinge kit system (kN·m)
M_1	Moment under accelerated stress conditions
M_0	Moment under normal conditions
M_A	Moment due to the accelerated weight (kN·m)
M_{door}	Moment due to the door weight (kN·m)
n	Number of test samples
$N1$	Consumer door open/close force (kN)
r	Failed numbers
S	Stress
S_1	Mechanical stress under accelerated stress conditions
S_0	Mechanical stress under normal conditions

t_i	Test time for each sample (h)
TF	Time to failure (h)
x	$x = 0.01 \cdot X$ (on condition that $x \leq 0.2$)
Greek symbols	
η	Characteristic life
Superscripts	
β	Shape parameter in a Weibull distribution
n	Stress dependence ($n = -\left[\frac{\partial \ln(T_f)}{\partial \ln(S)}\right]_T$)
Subscripts	
0	Normal stress conditions
1	Accelerated stress conditions

2. Load Analysis and Bx Life

In the field, HKS parts of a refrigerator were failing due to cracking and fracturing (Fig. 2) under unknown consumer usage conditions. Field data indicated that the damaged products might have had structural design flaws, including sharp corner angles and not enough enforced ribs resulting in stress risers in high stress areas. These design flaws combined with the repetitive impact loads on the HKS could cause a crack to occur, and thus cause failure consumer usage conditions, HKS were subjected to different loads during the opening and closing of the refrigerator door.

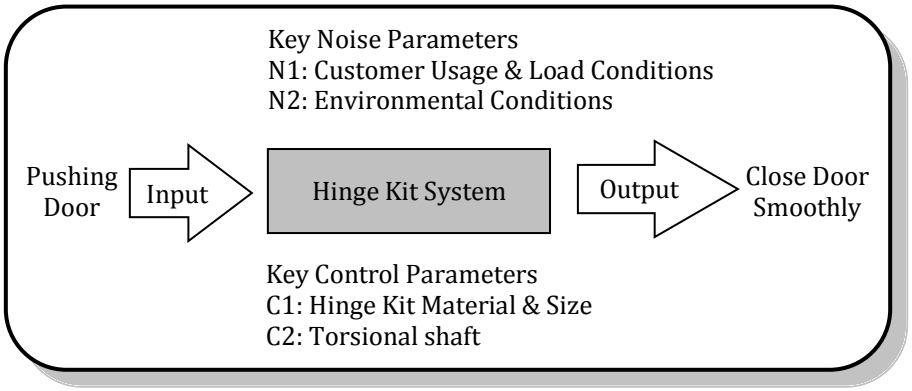

Fig. 3. Robust design schematic of HKS.

Fig. 3 shows the robust design schematic overview of the HKS. Depending on the consumer usage conditions, HKS were subjected to different loads during the opening and closing of the refrigerator door.

Because the HKS is a relatively simple structure, it can be modeled with a simple force-moment equation (see Fig. 4). As the consumer opens or closes the refrigerator door, the stress due to the weight momentum of the door is concentrated on HKS.

The number of door closing cycles will be influenced by specific consumer usage conditions. The door system of the refrigerator were required to be opened and closed between three and ten times a day in the Korean domestic market.

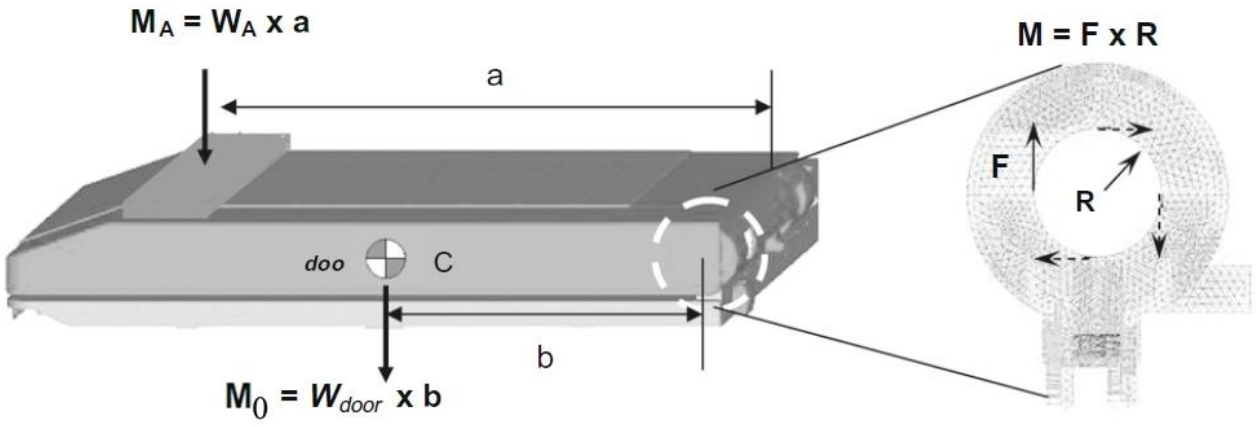

Fig. 4. Design concept of HKS.

The moment balance around the HKS can be represented as

$$M_0 = W_{door} \times b = T_0 = F_0 \times R \ . \quad (1)$$

The moment balance around the HKS with an accelerated weight can be represented as

$$M_1 = M_0 + M_A = W_{door} \times b + W_A \times a = T_1 = F_1 \times R \, . \quad (2)$$

Because F_0 is impact force in normal conditions and F_1 is impact force in accelerated weight, the stress on the HKS depends on the applied impact. Under the same temperature and efforts concept proposed by Karnopp et al. (2000), the life-stress model (LS model) proposed by McPherson (1989) and can be modified as

$$TF = A(S)^{-n} = AT^{-n} = A(F \times R)^{-n} \, , \quad (3)$$

The acceleration factor (AF) can be derived as

$$AF = \left(\frac{S_1}{S_0}\right)^n = \left(\frac{T_1}{T_0}\right)^n = \left(\frac{F_1 \times R}{F_0 \times R}\right)^n = \left(\frac{F_1}{F_0}\right)^n . \quad (4)$$

The characteristic life η_{MLE} from the Maximum Likelihood Estimation (MLE) can be derived as:

$$\eta_{MLE}^{\beta} = \sum_{i=1}^{n} \frac{t_i^{\beta}}{r} . \quad (5)$$

If the confidence level is 100(1 - α) and the number of failure is $r \geq 1$, the characteristic life, η_{α}, would be estimated from Eq. (5),

$$\eta_{\alpha}^{\beta} = \frac{2r}{\chi_{\alpha}^2(2r+2)} \eta_{MLE}^{\beta} = \frac{2r}{\chi_{\alpha}^2(2r+2)} = \sum_{i=1}^{n} t_i^{\beta} \, . \quad (6)$$

Presuming there is no failures, p-value is α and $\ln(1/\alpha)$ is mathematically equivalent to Chi-Squared value, $\frac{\chi_{\alpha}^2(2)}{2}$. The characteristic life η_{α}, would be represented as:

$$\eta_{\alpha}^{\beta} = \frac{2r}{\chi_{\alpha}^2(2)} \sum_{i=1}^{n} t_i^{\beta} = \frac{1}{ln\frac{1}{\alpha}} \sum_{i=1}^{n} t_i^{\beta} \, . \quad (7)$$

Eq. (6) is established for all cases $r \geq 0$ and can be redefined as follows:

$$\eta_{\alpha}^{\beta} = \frac{2r}{\chi_{\alpha}^2(2r+2)} \sum_{i=1}^{n} t_i^{\beta} \qquad for \geq 0 \, . \quad (8)$$

To evaluate the Weibull reliability function, the characteristic life can be converted into L_B life as follows:

$$R(t) = e^{-\left(\frac{L_{BX}}{\eta}\right)^{\beta}} = 1 - x \, . \quad (9)$$

After logarithmic transformation, Eq. (9) can be expressed as:

$$L_{BX}^{\beta} \left(ln\frac{1}{1-x}\right) \eta^{\beta} \, . \quad (10)$$

If the estimated characteristic life of p-value α, η_{α}, in Eq. (8), is substituted into Eq. (10), the B_X life equation can be obtained:

$$L_{BX}^{\beta} = \frac{2}{\chi_{\alpha}^2(2r+2)} \left(ln\frac{1}{1-x}\right) \sum_{i=1}^{n} t_i^{\beta} \, . \quad (11)$$

If the sample size is large enough, the planned testing time will proceed as:

$$\sum_{i=1}^{n} t_i^{\beta} \, . \quad (12)$$

The estimated lifetime (L_{BX}) in test should be longer than the targeted lifetime (L^*_{BX}) :

$$L_{BX}^{\beta} \cong \frac{2}{\chi_{\alpha}^2(2r+2)} \left(ln\frac{1}{1-x}\right) nh^{\beta} \geq L_{BX}^{*\beta} . \quad (13)$$

Then, sample size equation is expressed as follows:

$$n \geq \frac{\chi_{\alpha}^2(2r+2)}{2} \frac{1}{\left(ln\frac{1}{1-x}\right)} \left(\frac{L_{BX}^{*\beta}}{h}\right)^{\beta} . \quad (14)$$

However, most lifetime testing has insufficient samples. The allowed number of failures would not have as much as that of the sample size.

$$\sum_{i=1}^{n} t_i^{\beta} = \sum_{i=1}^{n} t_i^{\beta} + (n-r)h^{\beta} \geq (n-r)h^{\beta} \, . \quad (15)$$

If Eq. (15) is substituted into Eq. (13), the B_X life equation can be modified as follows:

$$L_{BX}^{\beta} \geq \frac{2}{\chi_{\alpha}^2(2r+2)} \left(ln\frac{1}{1-x}\right) (n-r)h^{\beta} \geq L_{BX}^{*\beta} . \quad (16)$$

Then, sample size equation with the number of failure can also be modified as:

$$n \geq \frac{\chi_{\alpha}^2(2r+2)}{2} \frac{1}{\left(ln\frac{1}{1-x}\right)} \left(\frac{L_{BX}^{*}}{h}\right)^{\beta} + r \, . \quad (17)$$

From the generalized sample size Eq. (17), we can proceed lifetime testing (or parametric ALT testing) under any failure conditions ($r \geq 0$). Consequently it also confirm whether the failure mechanism and the test method are proper.

For a 60% confidence level, the first term $\chi_{\alpha}^2(2r+2)/2$ in Eq. (17) can be approximated to $(r + 1)$ proposed by Ryu and Chang (2005). And if the cumulative failure rate, x, is below about 20 percent, the denominator of the second term $\ln(1/(1-x))$ approximates to x by Taylor expansion. Then the general sample size equation can be approximated as follows:

$$n \geq (r+1) \frac{1}{x} \left(\frac{L_{BX}^{*}}{h}\right)^{\beta} + r \, . \quad (18)$$

If the acceleration factors in Eq. (4) are added into the planned testing time, Eq. (18) will be modified as:

$$n \geq (r+1)\frac{1}{x}\left(\frac{L_{BX}^{*}}{h}\right)^{\beta} + r\,. \tag{19}$$

The reliability of the new HKS was targeted to be 10 years over B1. Based on the customer usage conditions, the normal range of operating conditions and cycles of the product (or parts) were investigated. Under the worst case, the objective number of cycles and the number of required test cycles can be obtained from Eq. (19).

For the worst case, the impact force around the HKS was 1.10 kN which was the maximum force applied by the typical consumer. The impact force for the ALT with accelerated weight was 2.76 kN. Using a stress dependence of 2.0, the acceleration factor was found to be approximately 6.3 in Eq. (4). The test cycles and the numbers of samples used in the ALT were calculated from Eq. (19).

For the B1 life, the required target *x* was 0.01. The test cycles and test sample numbers calculated in Eq. (8) were 34,000 cycles and six units without failure, respectively. ALT was designed to ensure a B1 of 10 years life with about a 60% level of confidence that it would fail less than once during 34,000 cycles. Fig. 5 shows the experimental setup of the ALT with labelled equipment for the robust design of HKS. Repetitive stress can be expressed as the duty effect that carries the on/off cycles and shortens part life (Ajiki et al., 1979). Fig. 6 shows the duty cycles for the impact force *F*.

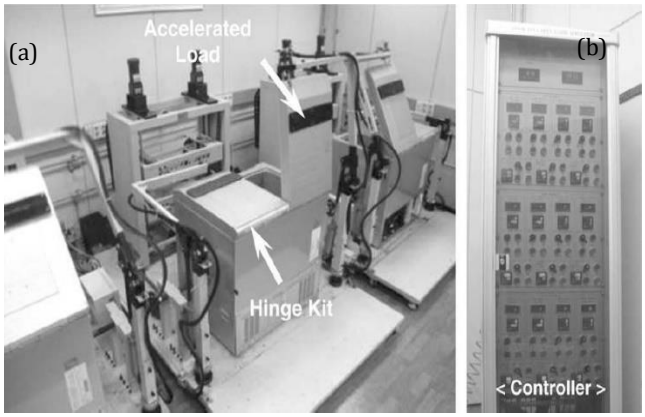

Fig. 5. Equipment used in accelerated life testing and controller: (a) ALT Equipment; (b) Controller.

ALT equipment can then be conducted on the basis of load analysis. In ALT testing, the missing parameters in the design phase can be identified.

3. Laboratory Experiments

Generally, the operating conditions for the HKS in a refrigerator were approximately 0–43 °C with a relative humidity ranging from 0% to 95%, and 0.2–0.24g's of acceleration. The closing of the door occurred an estimated average of 3 to 10 times per day. With a life cycle design point for 10 years, HKS incurs about 36,500 usage cycles (Table 1).

Table 1. Operating cycles of the HKS.

Item	Number of operations (times)			
	1 day		10 years	
	Normal	Worst	Normal	Worst
HKS	1–3	10	10,950	36,500

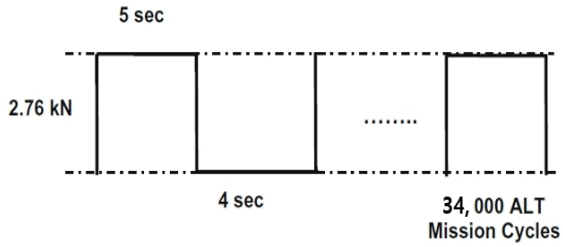

Fig. 6. Duty cycles of the repetitive impact load *F* on HKS.

The control panel was used to operate the testing equipment - the number of test time, starting or stopping the equipment, and the other. When the start button in the controller panel gave the start signal, the simple hand-shaped arms held and lifted the refrigerator door. As the door was closing, it was applied to the HKS with the maximum mechanical impact force due to the accelerated load (2.76 kN).

Fig. 7 shows a photograph comparing the failed product from the field and from 1st accelerated life testing, respectively. As shown in the picture, the shape and location of the failure in the ALT were similar to those seen in the field. Fig. 8 represented the graphical analysis of the ALT results and field data on a Weibull plot. The shape parameter in the first ALT was estimated at 2.0. From the Weibull plot, the shape parameter was confirmed to be 2.1.

The defective shape of the ALT was very similar to that of the field. From the Weibull plot, the shape parameters of the ALT and market data were found to be similar. As supported by two findings in the data, these methodologies were valid in pinpointing the weak designs responsible for failures in the field, which determined the lifetime.

Fig. 7. Failed products in field and crack after 1st ALT: (a) Failed products in field; (b) crack after 1st ALT.

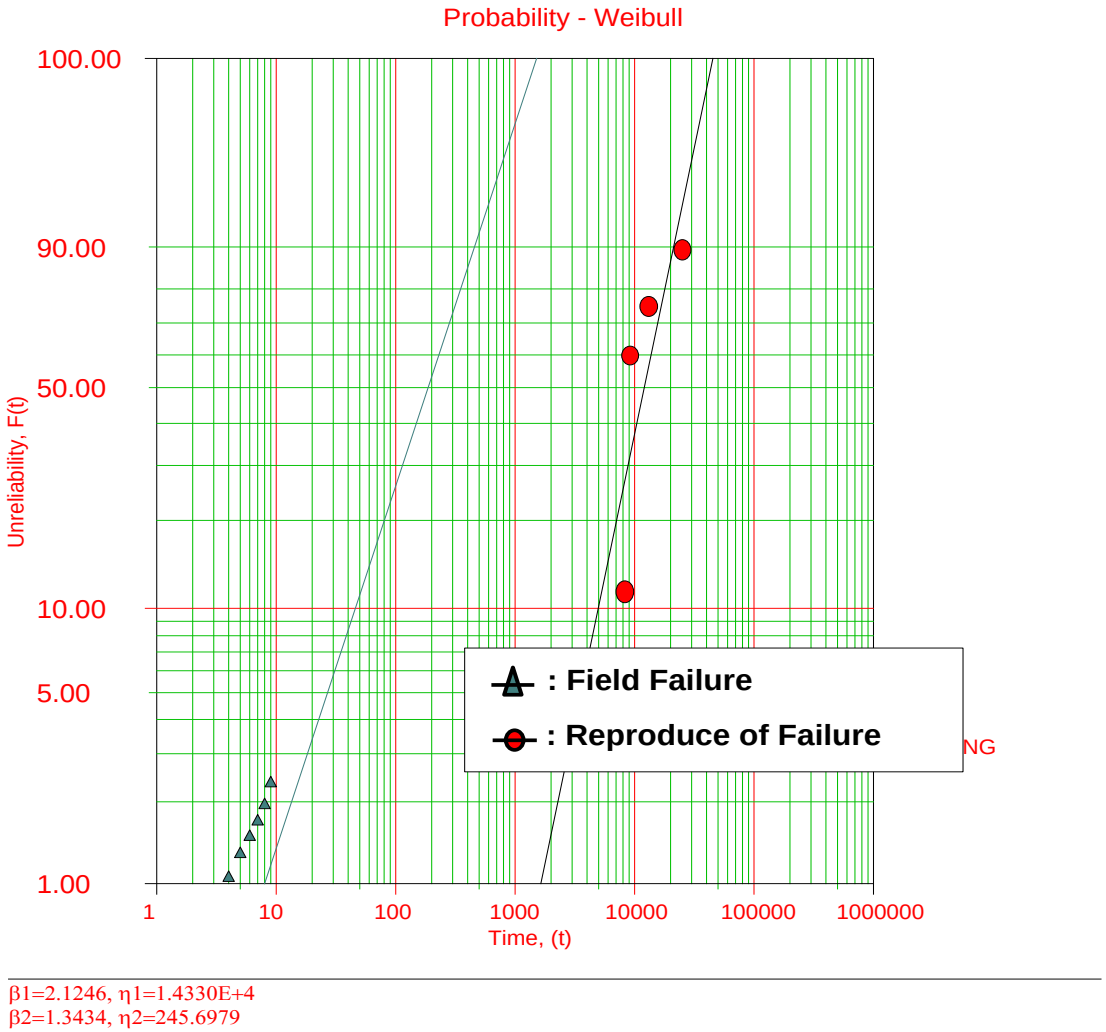

Fig. 8. Field data and 1st ALT on Weibull chart.

The fracture of the HKS in both the field products and the ALT test specimens occurred in the housing and support of the HKS (Fig. 9). The missing design variables of the HKS in the design phase came from no support structure. The repetitive applied force in combination with the structural flaws may have caused the fracturing of the HKS. The concentrated stresses of the HKS were approximately 21.2 MPa, based on finite element analysis. The stress risers in high stress areas resulted from the structural design flaws of not having any supporting ribs. The corrective action plans was to add the support ribs (Fig. 10). Applying the new design parameters to the finite element analysis, the stress concentrations of the HKS decreased from 21.2 MPa to 18.9 MPa. Therefore, the corrective action plan had to be made at the design stage before production.

The design target of the newly designed samples were more than the target life of a B1 of 10 years. The confirmed values of AF and b in Fig. 8 were 6.3 and 2.1, respectively. The recalculated test cycles and sample

size in Eq. (19) for reliability target of B1 of 10 years were 41,000 and six units, respectively. Based on the BX and sample size, three ALTs were performed to obtain the design parameters and their proper levels. In the second ALTs the crack of torsional shaft occurred due to its sharp rounding and repetitive impact stresses (Fig. 11). The torsional shaft of the HKS was modified by giving it more roundness from R0.5mm to R2.0mm at the corner of torsional shaft (see Fig. 12). Finally, the redesigned HKS could withstand the high impact force during closure of the door. With this design change, the refrigerator could also be opened and closed more comfortably.

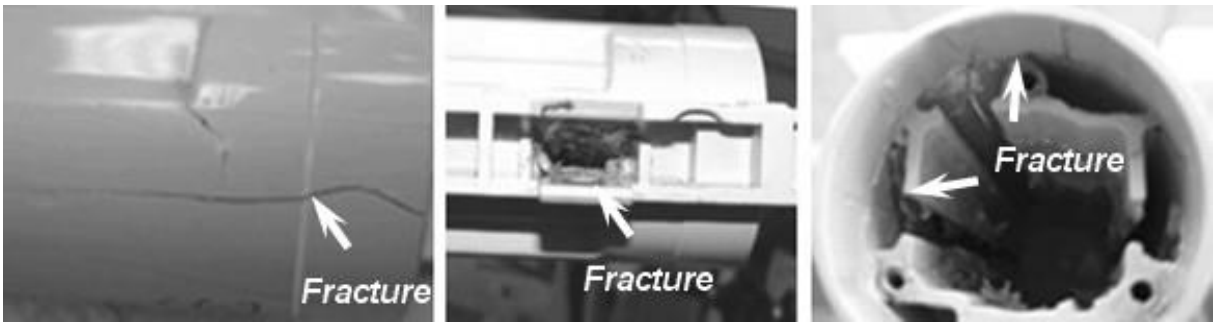

Fig. 9. Structure of failing HKS in 1st ALT Results of ALT plotted in Weibull chart.

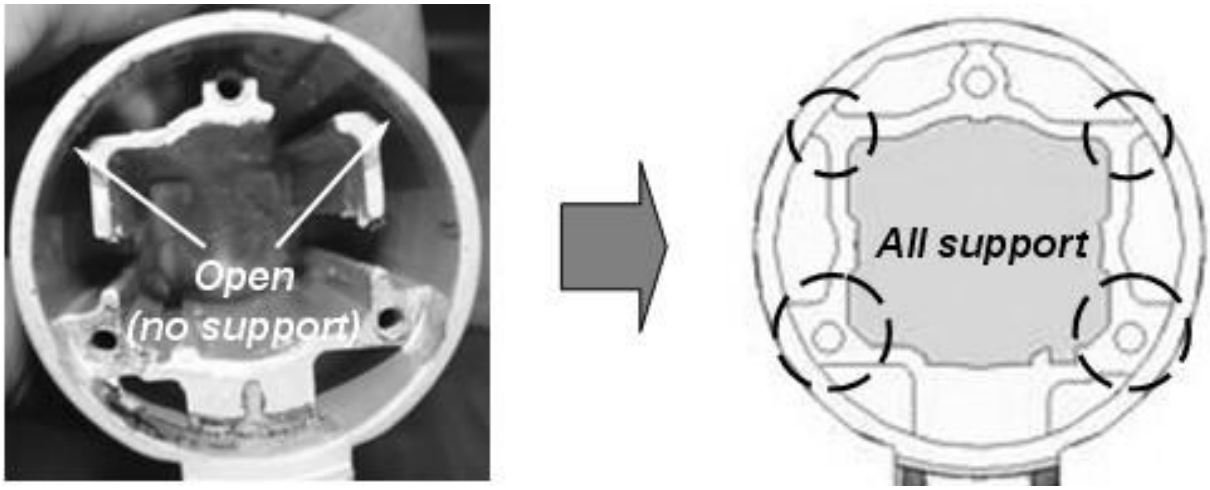

Fig. 10. Redesigned HKS structure.

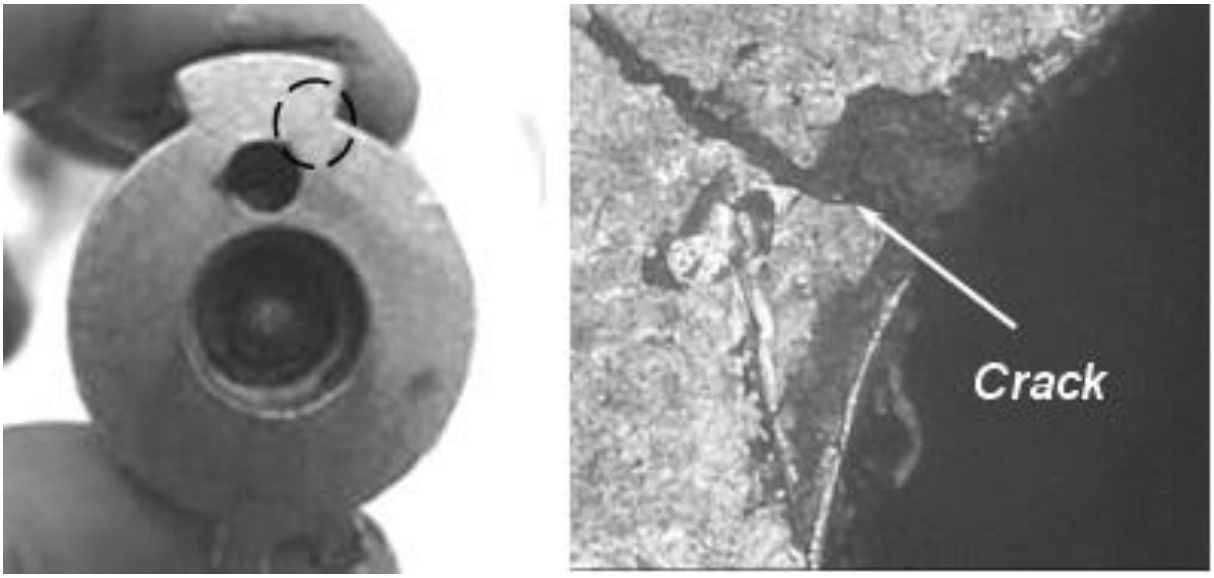

Fig. 11. Cracked torsional shaft of HKS.

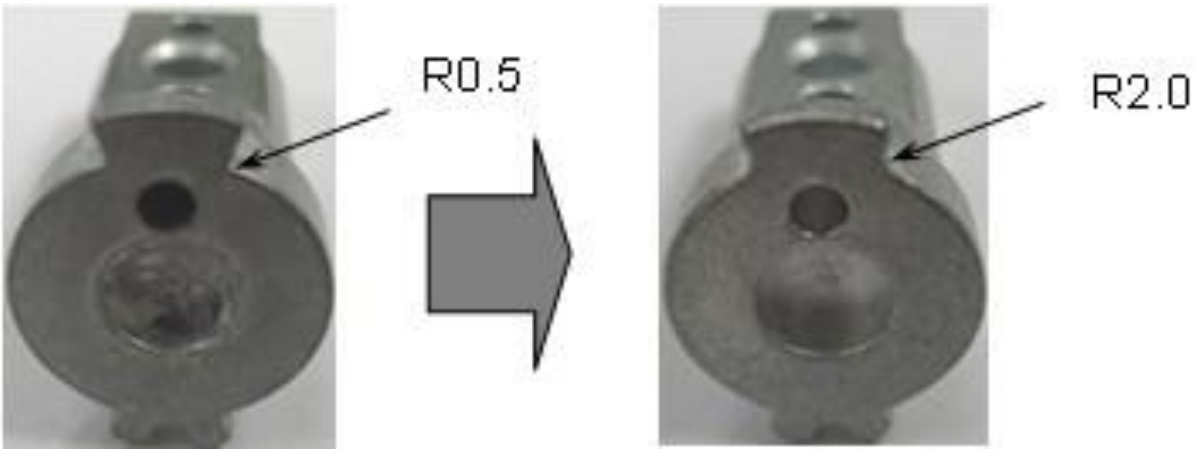

Fig. 12. Redesigned torsional shaft of HKS.

Table 4 and 5 show the design parameters confirmed from a tailored set of ALTs and the summary of the results of the ALTs, respectively. With these modified parameters, the refrigerator door could be smoothly closed for a longer period without failure. Fig. 13 shows the graphical results of the ALT plotted in a Weibull chart. Over the course of the three ALTs, the B1 life of the samples was guaranteed to be 10.0 years.

Table 4. Vital parameters based on ALTs.

CTQ	Parameters			Unit
Crack	KNP	N1	Impact force	MPa
	KCP	C1	Supporting structure	-
		C2	Corner roundness of torsional shaft	mm

Table 5. Results of ALT.

	1st ALT	**2nd ALT**	**3rd ALT**
	Initial Design	Second Design	Final Design
In 41,000 cycles, HKS has no crack	3,000 cycles: 2/6 Crack (HKS Housing)	12,000 cycles: 4/6 Crack (Torsional shaft)	41,000 cycles: 6/6 OK
HKS Structure			
Material and specification	Supporting rib C1: No → 2 supports	Roundness corner of torsional shaft C2: R0.5mm → R2.0mm	

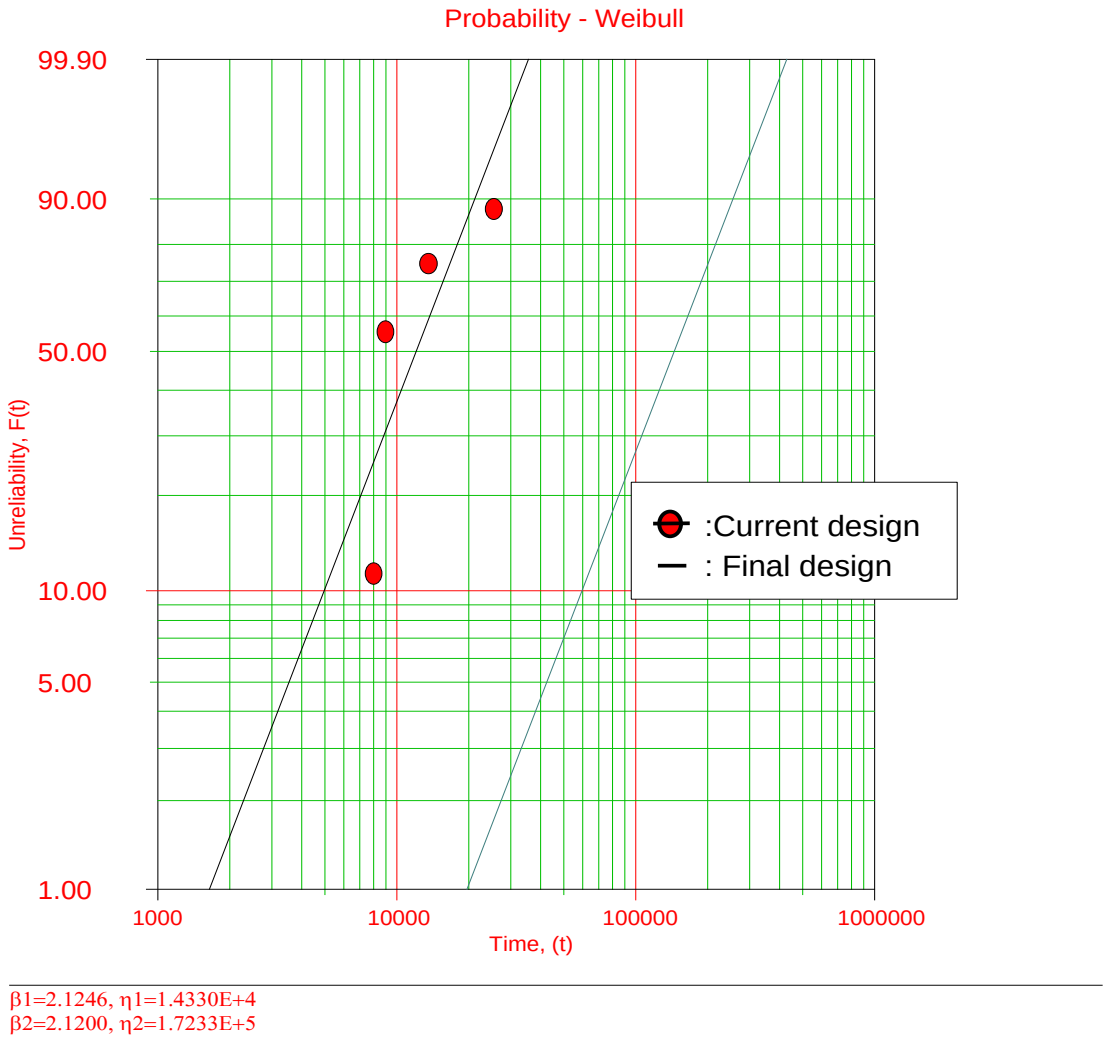

Fig. 13. Results of ALT plotted in Weibull chart.

4. Conclusions

To improve the reliability of a newly designed hinge kit system in refrigerators, robust methodologies – setting overall parametric ALT plan of product have been utilized, identifying the failure modes and mechanism investigation of fractured HKS in field, conducting a series of accelerated life testing, and redesigning the HKS based on the ALT. Based on the products that failed both in the field and in the ALTs, the primary failure of the HKS occurred due to fracturing of the HKS housing.

The missing design parameters in the design phase of the refrigerator were the housing of HKS. The corrective action plans included adding supporting ribs to the HKS. Based on second set of ALTs, cracking occurred in the torsional shaft. The additional key design parameter of the failed torsional shaft was the corner roundness. After a sequence of ALTs, the proper values for the design parameters were determined to meet the life cycle requirements - B1 of 10 years, respectively. Inspection of the failed product, load analysis, and three rounds of ALTs, indicated that the newly designed mechanical HKS was greatly improved using the new robust design methodologies. Case studies on the design flaws also were suggested by Woo and Pecht (2008), Woo et al. (2009a; 2009b; 2009c; 2009d), Woo et al. (2010a; 2010b), Woo et al. (2011), Woo (2015), Woo and O'Neal D (2015), Woo and O'Neal D (2016).

References

Ajiki T, Sugimoto M, Higuchi H (1979). A new cyclic biased THB power dissipating ICs. *In: 17th Annual Proceedings Reliability Physics*, 118–126.

Ashley S (1992). Applying Taguchi's quality engineering to technology development. *Mechanical Engineering*, 114(7), 58.

Byrne D, Taguchi S (1987). The Taguchi approach to parameter design. *Quality Progress*, 20(12), 19–26.

Karnopp D, Margolis D, Rosenberg R (2000). System Dynamics: Modeling and Simulation of Mechatronic Systems. John Wiley & Sons, New York.

McPherson J (1989). Accelerated Testing, Packaging, Electronic Materials Handbook. *ASM International*, 1, 887-894.

Phadke M (1989). Quality Engineering using Robust Design. Prentice Hall, Englewood Cliffs, New Jersey.

Ryu D, Chang S (2005). Novel concept for reliability technology. *Microelectronics Reliability*, 45(3), 611-622.

Taguchi G (1978). Off-line and on-line quality control systems. *In: Proceedings of the International Conference on Quality Control*, Tokyo, Japan.

Taguchi G, Shih-Chung T (1992). Introduction to Quality Engineering: Bringing Quality Engineering Upstream. American Society of Mechanical Engineering, New York.

Wilkins J (2000). Putting Taguchi methods to work to solve design flaws. *Quality Progress*, 33(5), 55-59.

Woo S, Pecht M (2008). Failure analysis and redesign of a helix upper dispenser. *Engineering Failure Analysis*, 15(4), 642–653.

Woo S, O'Neal D, Pecht M (2009a). Improving the reliability of a water dispenser lever in a refrigerator subjected to repetitive stresses. *Engineering Failure Analysis*, 16(5), 1597–1606.

Woo S, O'Neal D, Pecht M (2009b). Design of a hinge kit system in a Kimchi refrigerator receiving repetitive stresses. *Engineering Failure Analysis*, 16(5), 1655–1665.

Woo S, Pecht M, O'Neal D (2009c). Reliability design and case study of a refrigerator compressor subjected to repetitive loads. *International Journal of Refrigeration*, 32(3), 478-486

Woo S, Ryu D, Pecht M (2009d). Design evaluation of a french refrigerator drawer system subjected to repeated food storage loads. *Engineering Failure Analysis*, 16(7), 2224–2234.

Woo S, O'Neal D, Pecht M (2010a). Failure analysis and redesign of the evaporator tubing in a Kimchi refrigerator. *Engineering Failure Analysis*, 17(2), 369-379.

Woo S, O'Neal D, Pecht M (2010b). Reliability design of a reciprocating compressor suction reed valve in a common refrigerator subjected to repetitive pressure loads. *Engineering Failure Analysis*, 2010, 17(4), 979-991.

Woo S, O'Neal D, Pecht M (2011). Reliability design of residential sized refrigerators subjected to repetitive random vibration loads during rail transport. *Engineering Failure Analysis*, 18(5), 1322–1332.

Woo S (2015). The reliability design of mechanical system and its Parametric ALT. Handbook of Materials Failure Analysis with Case Studies from the Chemicals, Concrete and Power Industries, Elsevier, 259-276.

Woo S, O'Neal D (2015). Reliability design of mechanical systems subject to repetitive stresses. *Recent Patents on Mechanical Engineering*, 8(4), 222-234.

Woo S, O'Neal D (2016). Improving the reliability of a domestic refrigerator compressor subjected to repetitive loading. *Engineering*, 8, 99-115.

Challenge Journal of Structural Mechanics

Seismic analysis of arch dams subjected to in-phase and anti-phase ground motions

Mehmet Akköse [a,*], Ali Aydın Dumanoğlu [b], Alemdar Bayraktar [c]

[a] *Department of Civil Engineering, Karadeniz Technical University, 61080 Trabzon, Turkey*
[b] *Department of Civil Engineering, Canik Başarı University, 55080 Samsun, Turkey*
[c] *Department of Civil Engineering, Karadeniz Technical University, 61080 Trabzon, Turkey*

ABSTRACT

In this study, the response of arch dams is obtained for in-phase and anti-phase ground motions when there is no water in the reservoir. The material of the dam is considered to be linearly elastic, homogenous and isotropic. The foundation and banks of the dam, which are usually of hard rock, are assumed to be rigid. The S16E component of San Fernando Earthquake, February 9, 1971, has been used in the calculations. The response of arch dams determined for anti-phase dynamic effects is compared with that of in-phase (uniform) dynamic effects.

ARTICLE INFO

Article history:
Received 12 April 2016
Accepted 26 May 2016

Keywords:
Arch dams
Seismic analysis
Earthquake waves
Ground motions

1. Introduction

A dynamic ground motion is defined as in-phase (uniform) if the motion propagates in the same direction with the same phase and infinite velocity. However, if the motion propagates in the same direction with the opposite phase and infinite velocity, the case of the motion is defined as anti-phase (Adanur, 1998). The anti-phase ground motion may occur due to the fact that the directions of the earthquake waves are changeable. This ground motion is particularly effective in the structures, which have large structure-foundation interface or long spans. For example, bridges, long pipelines, nuclear power plants and dams. The behaviour of arch dams subjected to the anti-phase dynamic effects is the aim of this study.

In the anti-phase ground motion, quasi-static displacements occur in addition to dynamic displacements. Inertia forces cause dynamic displacements whereas relative movements of the support points according to each other at the structure-foundation interface cause the quasi-static displacements (Dumanoglu and Severn, 1984; Bayraktar and Dumanoglu, 1998). The determination of the quasi-static displacements requires the deformed shape of the structure to be calculated for a given unit displacement of each support point of structure-foundation interface. The quasi-static displacements are time-dependent and cause stresses to be added to the dynamic stresses. There are no quasi-static effects for in-phase ground motion due to the rigid body motion.

Different earthquake waves have been recorded in soil surface of each abutment of Ambiesta dam during same earthquake (Calciati, 1979). This shows that the earthquake record might be different at different points. This situation also indicates that the propagation of the earthquake waves can be different direction for both banks. Arch dams conduct reactions induced by water pressures on its surface to the foundation rock at their banks by arc effects. Therefore, a strong ground motion can cause relative movement of the abutments of arch dams. This situation can disturb the stability of the arch dams and cause their collapse.

In this study, the response of a selected arch dam is investigated by considering relative movements of their abutments according to each other when there is no water in the reservoir. The foundation and banks of the dam, which are usually of hard rock, are assumed to be

* *Corresponding author*. Tel.: +90-462-3772628 ; Fax: +90-462-3772606 ; E-mail address: akkose@ktu.edu.tr (M. Akköse)
ISSN: 2149-8024 / DOI: http://dx.doi.org/10.20528/cjsmec.2016.05.011

rigid. The possible amplitude variations of the earthquake waves are neglected. In the other words, it is assumed that the earthquake waves propagate with the same amplitude. The response of the dam determined for anti-phase dynamic effects is compared with that of in-phase (uniform).

2. Equations of Motion

The equation of motion for dynamic effects is given by the equation,

$$M\ddot{v} + C\dot{v} + Kv = F \ , \tag{1}$$

where M, C and K are mass, damping and stiffness matrices, respectively. $\ddot{v}$, $\dot{v}$ and v are total acceleration, velocity and displacement vectors, respectively. F is external load vector. The degrees of freedom of the system may be separated into two groups. First group is associated with degrees of freedom of the structure-foundation interface. Second group is related to degrees of freedom of the structure. The former will be denoted as the vector v_g and the latter as v_r. Here, suffix g denotes "ground degrees of freedom" and suffix r denotes "response degrees of freedom". According to this explanation, Eq. (1) can be expressed as follows;

$$\begin{bmatrix} M_{rr} & M_{rg} \\ M_{gr} & M_{gg} \end{bmatrix} \begin{Bmatrix} \ddot{v}_r \\ \ddot{v}_g \end{Bmatrix} + \begin{bmatrix} C_{rr} & C_{rg} \\ C_{gr} & C_{gg} \end{bmatrix} \begin{Bmatrix} \dot{v}_r \\ \dot{v}_g \end{Bmatrix} + \begin{bmatrix} K_{rr} & K_{rg} \\ K_{gr} & K_{gg} \end{bmatrix} \begin{Bmatrix} v_r \\ v_g \end{Bmatrix} = \begin{Bmatrix} 0 \\ 0 \end{Bmatrix}. \tag{2}$$

In the absence of external forces applied directly to the structure, F becomes zero-vector as shown in Eq. (2). It is also possible to separate the total displacement vectors as quasi-static, v_s, and dynamic, v_d, into two groups which are shown as;

$$\begin{Bmatrix} v_r \\ v_g \end{Bmatrix} = \begin{Bmatrix} v_{sr} \\ v_{sg} \end{Bmatrix} + \begin{Bmatrix} v_{dr} \\ v_{dg} \end{Bmatrix} . \tag{3}$$

In the Eq. (3), it is clear that v_{dg} is zero. So, v_{sg} is equal to v_g. Substituting Eq. (3) into Eq. (2), the equation of motion of the dynamic component of the response degrees of freedom can be written as;

$$M_{rr}\ddot{v}_{dr} + C_{rr}\dot{v}_{dr} + K_{rr}v_{dr} = -M_{rr}R_{rg}v_{sg} \ , \tag{4}$$

where R_{rg} contains r vectors (ground displacement shape vector) that describe the displaced shape of the structure when a unit displacement is given to the single ground degrees of freedom while all after ground degrees of freedom are held fixed. r vector owing to in-phase motion is obtained for positive unit displacement assigned to the ground degrees of freedom where in-phase motion effecting. However, r vector owing to anti-phase motion, is obtained for positive and negative unit displacements assigned to right and left bank ground degrees of freedom, respectively. From Eq. (4), dynamic components of the total displacement vectors are calculated by mode superposition technique as

$$v_{dr} = \sum_i \phi_i Y_i(t) \ , \tag{5}$$

where i is mode number, ϕ_i is ith mode vector and $Y_i(t)$ is the time-dependent modal amplitude of the response. Quasi-static components of the total displacement vectors are obtained as

$$v_{sr} = r_1 v_{1g}(\tau_1, t) + r_2 v_{2g}(\tau_2, t) + \cdots \ , \tag{6}$$

where v_{ig} is referred to displacements of the acceleration records of ground motion. This is calculated from twice integration of the acceleration records. τ_i is referred to arrival time from a certain reference point of ground motion to ith support point. Total displacements, v_r, are obtained by summing up quasi-static and dynamic displacements as follows;

$$v_r = v_{sr} + v_{dr} \ . \tag{7}$$

3. Numerical Example

In this study, arch dam Type 5, which was suggested in the symposium on Arch Dams (Arch Dams, 1968), is selected as an example for anti-phase dynamic effects. This dam is a standard double curved structure. The view in plan and the vertical crown cross-section of the idealised arch dam is shown in Fig. 1. The dimensions of the arch dam are in unit. The height of the dam is chosen as 120 m to obtain realistic results. The other dimensions of the dam are determined according to this size. An axonometric view of the finite element mesh of the whole dam is shown in Fig. 2. In the finite element mesh of the arch dam, 164, eight-node, 3D solid elements are used.

The material of arch dam is assumed to be linearly elastic, homogenous and isotropic. The elasticity modulus, mass density and Poisson's ratio of the dam are taken as $2x10^{10}$ N/m^2, 2446.48 N/m^3 and 0.15, respectively. The solution time step is 0.001. The damping ratio is chosen as %5. The program MULSAP (Dumanoglu, 1988) is employed in the response calculations. Pacoima Dam record S16E component recorded during the San Fernando Earthquake, February 9, 1971 shown in Fig. 3 is chosen for the ground motion. The component considered is applied in the upstream-downstream direction for both in-phase and anti-phase situation as shown in Fig. 4.

The response of the arch dam chosen for both situations is examined. The absolute maximum nodal displacements are obtained at arch sections. Fig. 5 shows reference lines of the arch sections. Figs. 6 and 7 give the displacements at the arch sections. The displacements calculated in the middle plane of the dam for anti-phase dynamic effect are considerably greater than those of in-phase dynamic effect.

The absolute maximum stresses obtained on the direction *x-x*, *y-y* and *z-z* at section I-I shown in Fig. 5 are given in Table 1 for upstream face and Table 2 for downstream face. These tables contain the response of the dam for both in-phase and anti-phase dynamic effects. The stresses are given at the centroid of the elements. The stresses calculated for anti-phase dynamic effect are different from those of in-phase. In particular, the stresses on the direction *x-x* have its maximum value around the axis of symmetry of the dam.

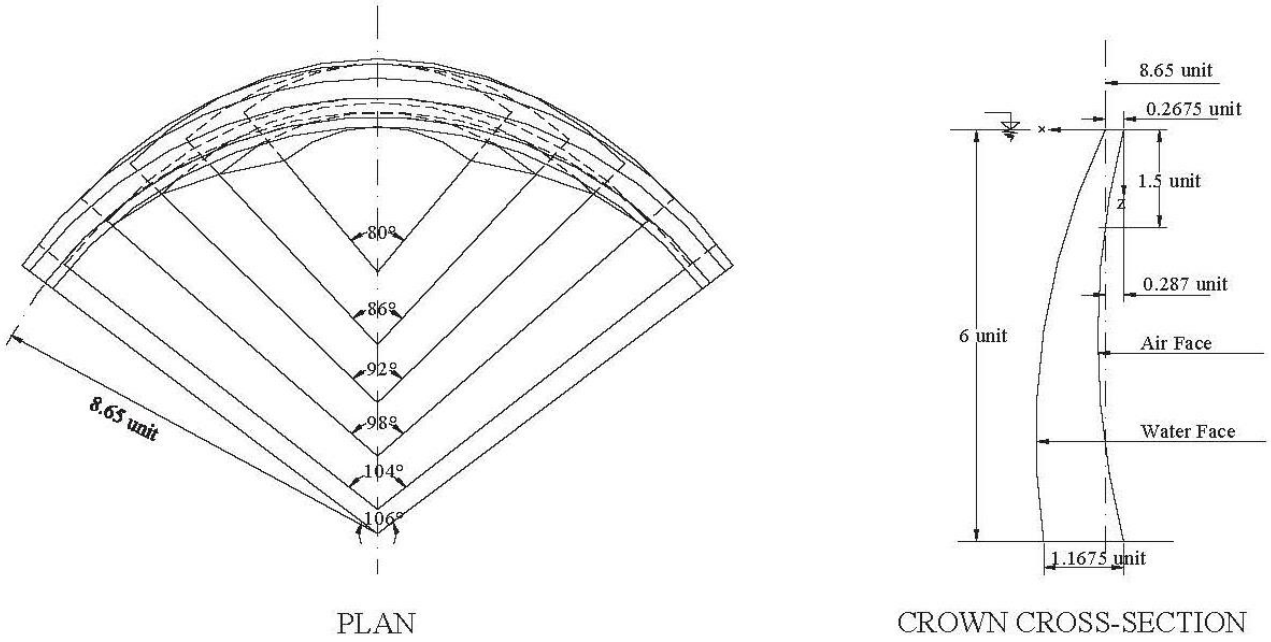

Level	0	1	2	3	4	5	6
Radius (units)	3.67	5.29	6.64	7.72	8.54	8.80	8.50
Central Angle	80°	86°	92°	98°	104°	106°	106°

Fig. 1. The view in plan and the vertical crown cross-section of arch dam Type 5.

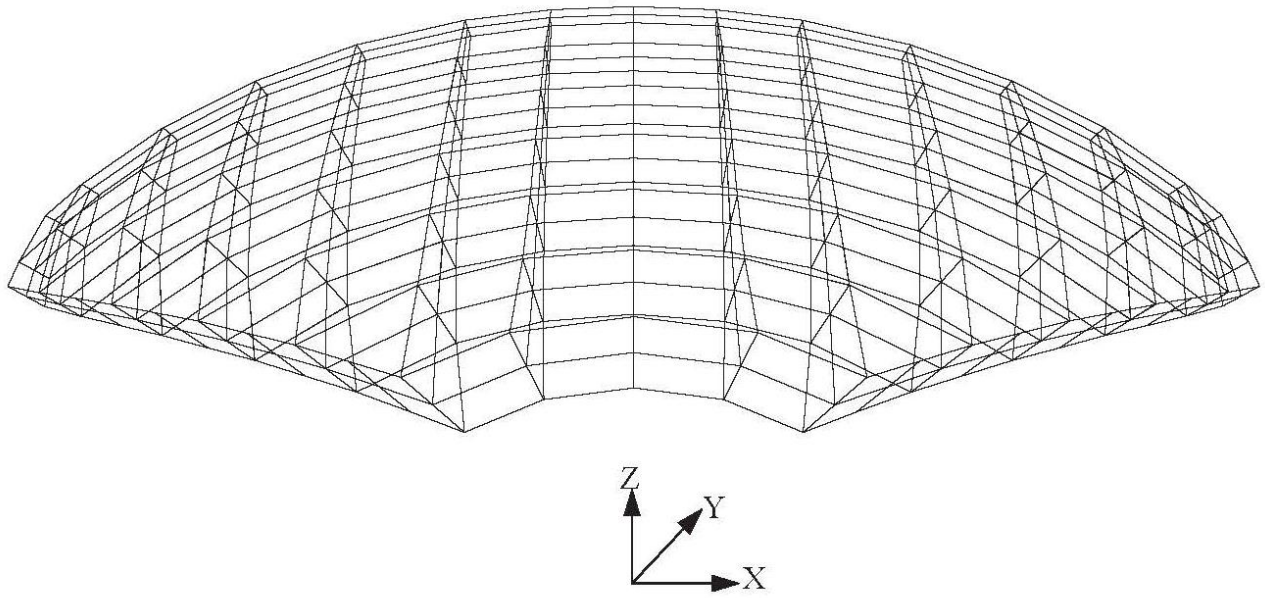

Fig. 2. The axonometric view of 3D finite element mesh of arch dam Type 5.

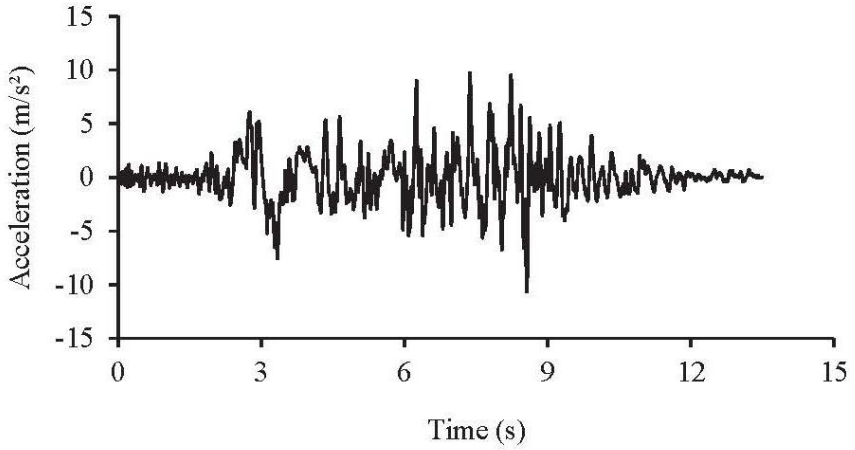

Fig. 3. S16E San Fernando Earthquake, February 9, 1971 (Pacoima dam record).

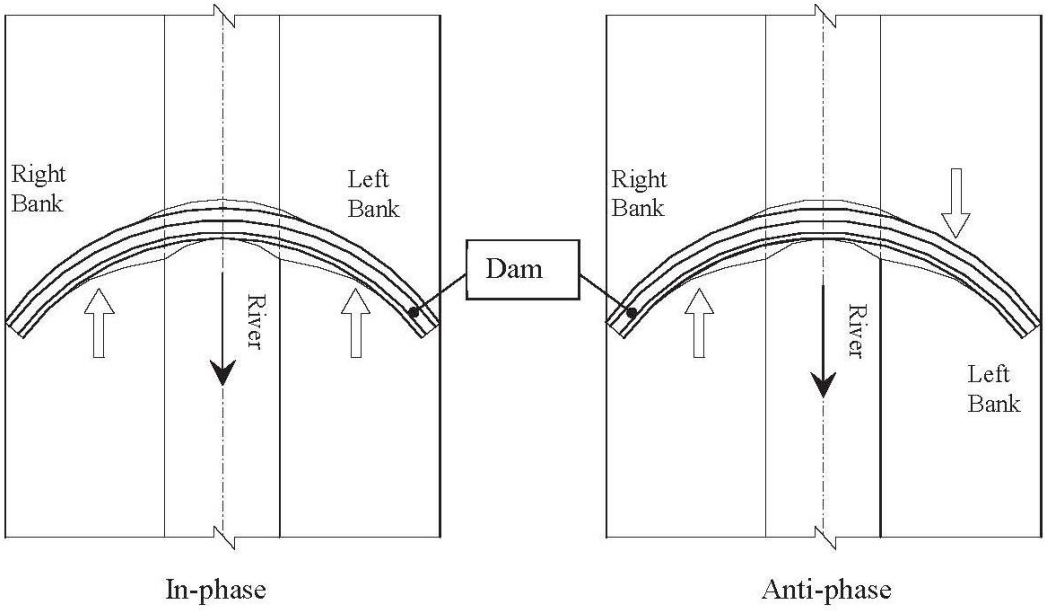

Fig. 4. Arch dam Type 5 subjected to in-phase and anti-phase ground motions in plan.

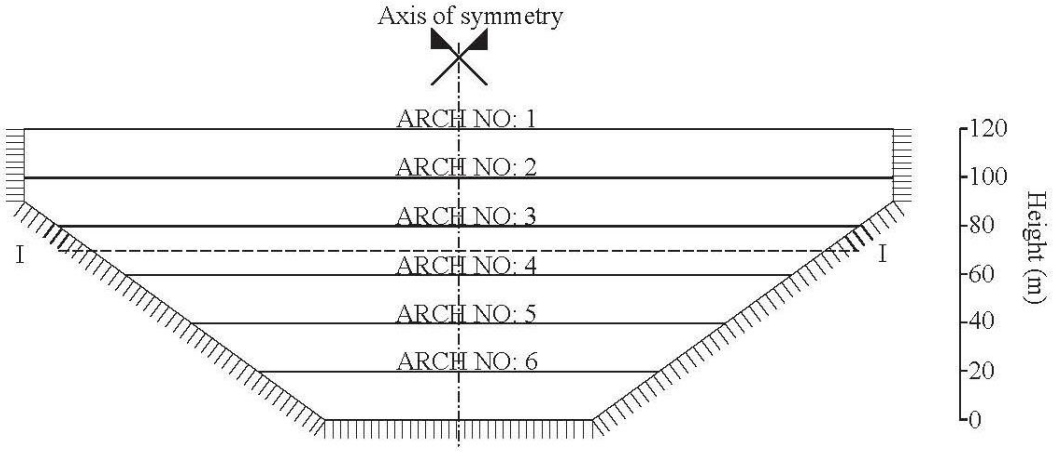

Fig. 5. The arch reference lines of arch dam Type 5.

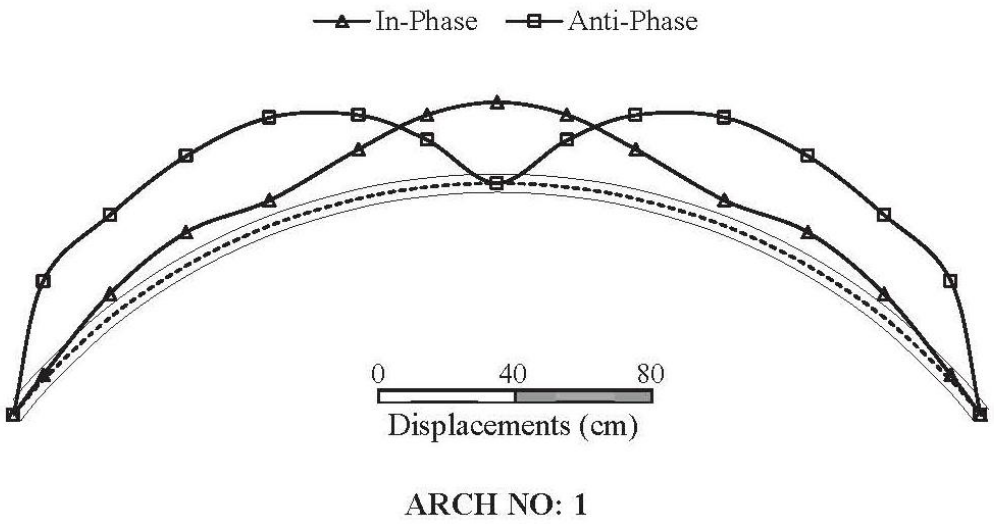

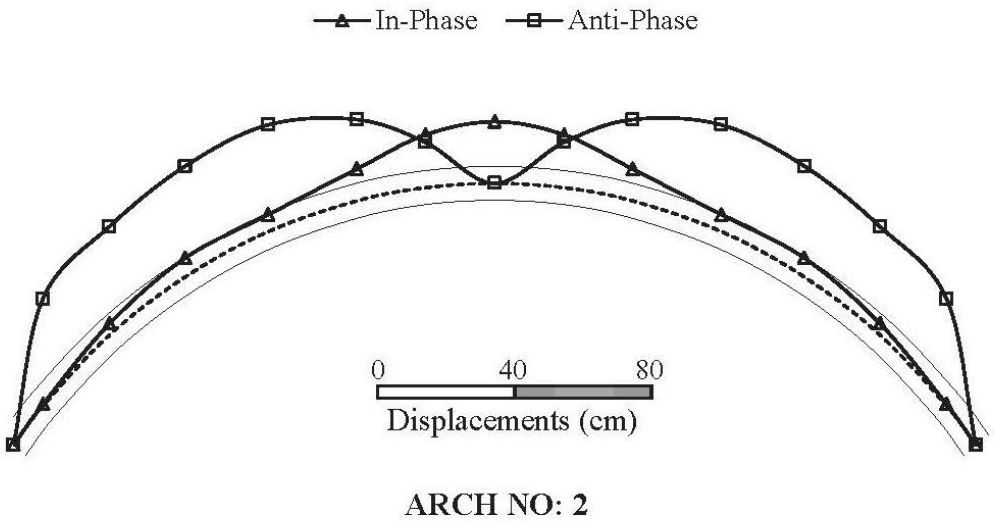

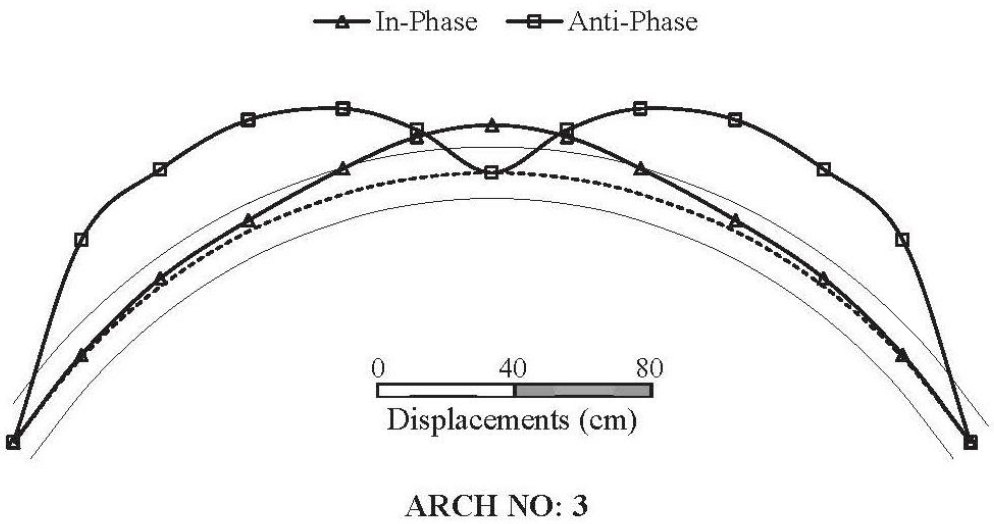

Fig. 6. The absolute maximum nodal displacements at arch section 1, 2 and 3.

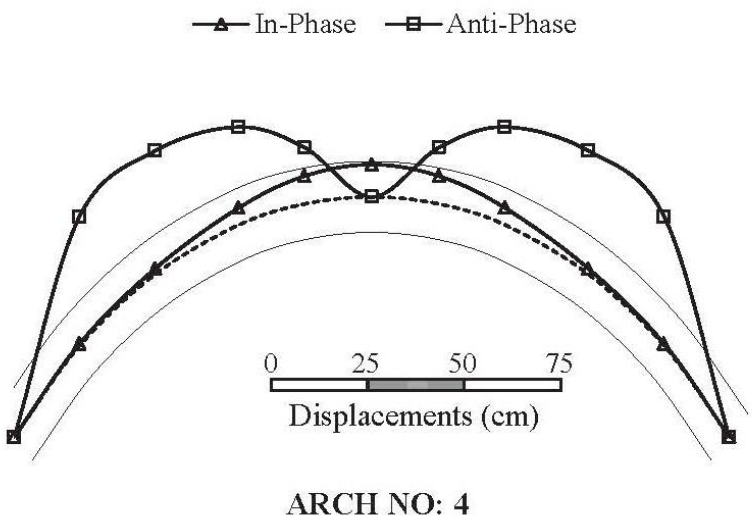

Fig. 7. The absolute maximum nodal displacements at arch section 4, 5 and 6

Table 1. The absolute maximum element stresses on upstream face at section I-I.

The Absolute Maximum Element Stresses (MPa)						
Element Number	σ_{xx}		σ_{yy}		σ_{zz}	
	In-Phase	Anti-Phase	In-Phase	Anti-Phase	In-Phase	Anti-Phase
10	3.39	1.48	0.81	0.29	3.96	2.21
16	1.69	0.36	0.71	0.39	2.62	1.79
24	1.18	1.80	0.69	0.90	2.08	2.19
34	2.30	5.77	1.07	0.26	1.57	2.03
46	5.10	6.49	0.39	0.25	3.15	1.92
58	7.72	3.02	0.39	0.29	3.93	0.80
70	7.72	3.02	0.39	0.29	3.93	0.80
82	5.10	6.49	0.39	0.25	3.15	1.92
94	2.30	5.77	1.07	0.26	1.57	2.03
106	1.18	1.80	0.69	0.90	2.08	2.19
116	1.69	0.36	0.71	0.39	2.62	1.79
124	3.39	1.48	0.81	0.29	3.96	2.21

Table 2. The absolute maximum element stresses on downstream face at section I-I.

The Absolute Maximum Element Stresses (MPa)						
Element Number	σ_{xx}		σ_{yy}		σ_{zz}	
	In-Phase	Anti-Phase	In-Phase	Anti-Phase	In-Phase	Anti-Phase
9	1.27	0.82	3.05	2.05	1.88	0.86
15	2.01	1.62	1.62	1.97	2.76	1.84
23	4.21	2.50	2.03	1.45	1.57	2.00
33	4.17	4.30	1.39	1.54	1.81	1.69
45	2.38	4.31	0.10	0.60	2.34	1.01
57	2.68	1.54	0.48	0.25	2.59	0.29
69	2.68	1.54	0.48	0.25	2.59	0.29
81	2.38	4.31	0.10	0.60	2.34	1.01
93	4.17	4.30	1.39	1.54	1.81	1.69
105	4.21	2.50	2.03	1.45	1.57	2.00
115	2.01	1.62	1.62	1.97	2.76	1.84
123	1.27	0.82	3.05	2.05	1.88	0.86

4. Conclusions

The response of arch dams is presented for anti-phase dynamic effects when there is no water in the reservoir. The dynamic effect can cause relative movements of the banks of the arch dams according to each other. This situation can disturb their stability and cause their collapse. The quasi-static displacements occurred during the anti-phase ground motion change significantly the response of the arch dams. On the numerical results presented, it is seen that the displacements increase due to the anti-phase dynamic effects and the stresses have the maximum value around the axis of symmetry of the dam. Consequently, it may be stated that the response of arch dams itself should be considered but not overlooked for anti-phase dynamic effects. However, it should be investigated the effects taken into considering fluid-structure interactions in further studies.

References

Adanur S, Dumanoglu AA (1998). Dynamic analysis of suspension bridges subjected to anti-phase ground motion, *Third_National Computational Mechanics Conference*, 16-18 November, 41-48, Istanbul (in Turkish).

Bayraktar A, Dumanoglu AA (1998). The effect of asynchronous ground motion on hydrodynamic pressures. *Computers and Structures*, 68, 271-282.

Calciati F, Castoldi R, Ciacci R, Fanelli MA (1979). Experiences gained during in situ artificial and natural dynamic excitation of large concrete dams in Italy: Analytical interpretation of results. *Thirteenth International Congress on Large Dams (ICOLD)*, New Delhi, Volume 4, R 32, 1377-1402.

Dennis TL (1968). Arch dams; A review of British research and development. *Proceedings of the Symposium Held at the Institution of Civil Engineering*, 20-21 March 1968, London, England.

Dumanoglu AA (1988). Asynchronous dynamic analysis. First *Symposium on Computer Usage in Civil Engineering*, 95-106, Istanbul (in Turkish).

Dumanoglu AA, Bayraktar A, Akkose M (2000). Comparative earthquake analysis of concrete gravity dams for uniform and asynchronous ground motion. Turkish Earthquake Foundation, TDV/TR 029-47, January (in Turkish).

Dumanoglu AA, Severn RT (1984). Dynamic response of dams and other structures to differential ground motions. *Proceedings - Institution of Civil Engineers*, Part 2, 77, 333-352, September.

Challenge Journal of Structural Mechanics

Acceleration response spectra for Tbilisi city with site effects

Paata Rekvava *, Ketevan Mdivani

Georgian National Association for Earthquake Engineering and Engineering Seismology, 0112 Tbilisi, Georgia

ABSTRACT

The utilization of time histories of earthquake ground motion has grown considerably in the field of earthquake engineering. It is very unlikely, however, that recordings of earthquake ground motion will be available for all sites and conditions of interest. Hence, there is a need for efficient methods for the simulation of strong ground motion for a given region. Due to lack of the real strong ground motion records the objective of this research is to develop a methodology for rapid generation of horizontal and vertical components of earthquake ground motion at any site for Tbilisi city. The model developed in this study provides simulation of ground motion over a wide range of magnitudes and distances at 8 earthquake sources zones of Tbilisi region (within 50 km). The research includes three main topics: (i) the stochastic simulation of earthquake ground motion at a given site of the city of Tbilisi; (ii) the estimation of acceleration time histories at a given site using the direct method of engineering seismology considering soil conditions based on the theory of the reflected waves and (iii) calculation of horizontal and vertical acceleration elastic response spectra for main sites of Tbilisi territory. The simulation procedure typically consists of multiplying deterministic modulating function with a stationary process of known power spectral density. The obtained results in the terms of normalized elastic response spectra can be widely applied in the practice of earthquake engineering in Georgia.

ARTICLE INFO

Article history:
Received 16 April 2016
Accepted 30 May 2016

Keywords:
Earthquake
Ground motion
Stochastic simulation
Acceleration response spectra

1. Introduction

In the practice of earthquake engineering an earthquake effect quantitatively is classified according to the seismic scale and by the building code. For this purpose in the seismic scale are used Peak Ground Acceleration (PGA), Peak Ground Velocity (PGV) and Peak Ground Displacement (PGD).

In the building code the seismic action usually is represented by an elastic ground acceleration response spectra and the ground acceleration time-histories.

It should be noted that, each earthquake represents individual process, which is generated under certain geographic and geological conditions, its destructive effect first of all depends on the seismic source magnitude and the epicentral distance. The normalized elastic response spectrum shape or outlines of the spectral curves of dynamic coefficient depends on the earthquake generation mechanism and ground response in the site of interest. Therefore, the elastic response spectra defined according to the recorded accelerograms in different regions, differ from each other and reflect only local site conditions.

The time-histories dynamic analysis provides the evaluation of seismic demand of structures using the recorded and artificial or simulated accelerograms that give information on earthquake intensity, its frequency content and duration, i.e. it does not exclude time factor as it occurs in the response spectrum analysis.

Proceeding from the regulations on seismic action basic conception given in the Eurocode 8 (European Standard EN 1998-1:2004), selection of the elastic response spectrum shape in the country or part of the country is possible from the certain country National annexes that are worked out by local Authorities. In accordance with the recommendations suggested by Eurocode 8

* *Corresponding author*. Tel.: +995-32-2187588 ; E-mail address: rekvavapaata@yahoo.com (P. Rekvava)
ISSN: 2149-8024 / DOI: http://dx.doi.org/10.20528/cjsmec.2016.05.012

deep geological data of the construction site should be considered and the horizontal and vertical elastic response spectra should be computed taking into account the seismic sources and the earthquake magnitudes generated from them.

In general, lack of the strong earthquake records statistic package creates certain problems for the elastic response spectra and the normalized dynamic coefficient spectral curves elaboration. Note that, an example of such problems is the capital of Georgia – Tbilisi city.

For Tbilisi city records of the strong earthquakes data are limited. During last 100 years at the territory of Tbilisi city about hundred weak earthquakes took place. Local strong earthquake occurred only on April 25, 2002, under the central part on the city with magnitude M=4.5 and recorded on the bedrock peak horizontal acceleration of 0,11g, which was amplified to the range of 0.20 to 0.30g due to dynamic response of surface soil deposits.

It is evident that, on the basis of the weak and rare earthquakes real records formation of the seismic action specified regional model is impossible. In such conditions the most straightforward procedure is to generate ground motion time histories using of regional earthquake sources zones parameters and classification according to the soils seismological and geological properties spread at Tbilisi city territory.

At the same time, according to the Georgian building code (Building Code, PN 01.01.-09, 2009) Tbilisi city is located in the seismic zone of intensity 8 degree by the MSK-64, with a maximum horizontal acceleration equals 0.17g and a return period of earthquakes 2500 years (2%/in 50 years). The normalized spectral dynamic coefficient is determined for grounds of hard (I), medium (II) and soft (III) categories and without special investigations its maximum value for all three categories grounds is accepted equal to 2.5.

It should be noted, that from the earthquake source zones of Tbilisi region (within 50 km) at the territory of the city are expected the earthquakes with magnitudes M=5.0_7.0 and corresponding seismic generated kinematics of shifting as reverse and dextral strike slip. It follows from this that it is necessary to define more precisely given in the National code the normalized spectral curves of dynamic coefficient considering the data of Tbilisi region seismological and geological properties of the grounds spread at city territory. In such conditions it is important simulation of the expected regional spatial seismic action in the form of the acceleration time-histories and elaboration the acceleration elastic response spectra and the three components spectral curves of normalized dynamic coefficient for various sites of Tbilisi city.

The objective of this study is to develop a methodology for simulation ground motions and evaluation the three components of acceleration elastic response spectra and the three components normalized spectral curves of dynamic coefficient at any site for Tbilisi city territory considering the regional seismological characteristics and geological conditions for the site of interest.

The proposed approach includes three main topics:

- the stochastic simulation of earthquake ground motion at a given site of the city of Tbilisi;
- estimation of acceleration time histories at a given site using the direct method of engineering seismology taking into account a soil properties based on the theory of the reflected waves
- calculation of the horizontal and vertical acceleration elastic response spectra and corresponding the normalized spectral curves of dynamic coefficient for main sites of Tbilisi city territory.

2. Stochastic Simulation of Earthquake Ground Motion

For simulation of possible seismic ground motions on the territory of Tbilisi city in this paper is employed the discrete nonstationary Gaussian stochastic process represented as (Rekvava and Mdivani, 2010)

$$A_{gi}(t) = E_i(t) \quad X_i(t), \qquad (i = 1, 2, 3) \ , \tag{1}$$

where $A_{gi}(t)$ determines of ground acceleration in the direction of three principal orthogonal axes with zero cross correlation between of components; $E_i(t)$ is the deterministic normalized envelope function or modulating function; $X_i(t)$ represents a typical realization of the stationary filtered white-noise process.

Normalized stationary random function with zero mean and unit-variance is characterized by $K(\tau)$ function of correlation as

$$K(\tau) = e_j^{-\alpha|\tau|}\left(cos\ \omega_j\tau + \alpha_j/\omega_j\ sin\ \omega_j|\tau|\right) \ , \tag{2}$$

where α is correlation coefficient characterizing bandwidth of the process ; ω is circular process frequency; j represents an ordinal number of process .

The modulating function $E_i(t)$ is defined in terms of so-called Berlag impulse and with $|E_i(t)|_{max}$=1 is given by

$$E_i(t) = \varepsilon\ t\ exp(1 - \varepsilon t) \ , \tag{3}$$

where ε controls the shape of the envelope function and determines the effective duration and process nonstationarity.

Generalizing the form in Eq. (1), the horizontal and vertical components of the process can be written as

$$A_{g1}(t) = \kappa\sigma_1\varepsilon t\ exp(1 - \varepsilon t)x_1(t) \ ,$$

$$A_{g2}(t) = \eta\sigma_2\varepsilon t\ exp(1 - \varepsilon t)x_2(t) \ ,$$

$$A_{g3}(t) = \upsilon\sigma_3\varepsilon t\ exp(1 - \varepsilon t)x_3(t) \ , \tag{4}$$

where σ_i is a mean square value of acceleration in the direction of principal axes and denotes random process intensity that is defined by its variance; κ, η da υ are corrective factors of the value of the horizontal and vertical components which are accordingly equal to 1.0, 0.85 and 0.7.

Thus, the formulation in Eq. (4) is completely determined with fixed values of dominant frequency ω_j using three parameters: α, ε and σ which are depended on regional seismological and geological conditions or in

the simple form on the earthquake magnitude, hypocentral distance, dominant frequency and ground characteristics at the site.

On the basis of proposed stochastic ground motion model formulated in Eq. (4) the software package ACCSIM (Rekvava and Mdivani, 2011), was developed, which allows to generate the multiple artificial accelerograms of the predicted earthquakes.

3. Parameters Estimation

For estimation of macro-seismic intensity for territory of Tbilisi city from the earthquake sources zones of Tbilisi region the two various expressions are applied (Javakhishvili et al.,1998):
for small earthquakes (M_s<6)

$$I_{Tb} = 1.5M_s - 3.4lgR + 3.1\,, \tag{5}$$

for strong earthquakes (M_s>=6)

$$I_{Tb} = 1.5M_s - 4.7lgR + 4.0\,, \tag{6}$$

where M_s is surface-wave magnitude; R=(Δ^2+h^2)$^{1/2}$ is hypocentral distance; Δ is epicentral distance; h is focal depth.

The resulting equation for larger horizontal values of peak horizontal acceleration is defined by (Smit et al., 2000)

$$log\ PGA_{h1} = 0.72 + 0.44M_s - log\ R - 0.00231K + 0.28p\,, \tag{7}$$

and

$$K = \sqrt{\Delta^2 + h^2 + 4.5^2}\,, \tag{8}$$

where p is 0 for 50-percentile values and 1 for 84-percentile.

Empirical relations between the surface-wave magnitude of the earthquake and a hypocentral distance derived for shallow-focus near-source earthquakes under an average soil site conditions are given by the following formula (Mikhailova and Aptikaev, 1996)

$$lgT = 0.15M_s + 0.25lgR + C_1 + C_2 \pm 0.2\,, \tag{9}$$

where C_1 is parameter of fault mechanism (C_1=-0.1 for reverse, C_1=0 for strike slip, C_1=0.1 for dextral strike slip); C_2–coefficient of influence not taken into consideration factors that is equal to 1.11;
Duration of the ground motion is computed by

$$lgD = 0.15M_s + 0.50lgR + C_1 + C_2 \pm 0.30\,, \tag{10}$$

where C_1 is parameter of fault mechanism (C_1=-0.25 for reverse, C_1=0.0 for strike slip, C_1=-0.12 for dextral strike slip; C_2=-0.15 for hard ground; C_2=0 for medium ground; C_2=0.15 for soft ground; a mean value of ratio C_3 is equal to 1.3.

The calculated parameters for the borderline territory of Tbilisi city are listed in Table 1. It should be noted that for computation of PGA has been used 84-percentile. On the basis of empirical data the more intensive horizontal component of PGA_{h1} is obtained 1.28 times greater than other one and the vertical component is 2/3 of the maximum horizontal component.

For 10 sites of Tbilisi city territory (350 square kilometers) were also determined (Fig. 1) minimum hypocentral distances, *PGA* for 2% and 1% probabilities of being exceeded in 50 years, values of the dominant periods and duration of oscillation. As an illustration in Table 2 are given parameters generated from the high potential seismic generating zone #3 which is situated to the north-west of Tbilisi region. Note, that values of PGA in Table 2 correspond to 2% probability of being exceeded in 50 years and are by 15% less than computed for 1% probability of being exceeded in 50 years.
The main parameter ω_j of the ground motion model has been determined based on the Eq. (9) using the expression:

$$\omega_j = 2\pi/T_j\,. \tag{11}$$

Table 1. Quantitative characteristics of the predicted ground motion on the borderline of Tbilisi city.

Zone	R (km)	I_{TB} (deg)	T (sec)	D (sec)	PGA_{h1} (m/sec²)	PGA_{h2} (m/sec²)	PGA_{h3} (m/sec²)
From focus with M=5							
2	10.6	7	0.13	1.63	2.11	1.65	1.41
5	8.38	7	0.12	1.45	2.20	1.72	1.47
From focus with M=5.5							
7	10.7	8	0.15	2.06	2.38	1.86	1.59
From focus with M=6							
4	11.2	8	0.18	2.66	2.53	1.98	1.69
6	10.0	8	0.18	2.51	2.57	2.01	1.72
8	16.0	7	0.2	3.18	2.38	1.86	1.67
From focus with M=6.5							
1	29.4	7	0.28	5.42	2.32	1.81	1.55
From focus with M=7							
3	16.3	9	0.28	5.08	2.81	2.20	1.88

The value of the correlation degree characterizing parameter α was evaluated based on the analysis of the Georgian earthquakes records data (Rekvava and Mdivani, 2011) depending on ω and for 1(x), 2(y) and 3(z) components consists of

$$\alpha_{i1} = 0.204\omega_i\,; \quad \alpha_{i2} = 0.253\omega_i\,; \quad \alpha_{i3} = 0.41\omega_i\,. \quad (12)$$

The mean square value of acceleration σ was accepted considering that

$$\sigma_i = PGA_i/3\,, \qquad i = 1,2,3\,. \quad (13)$$

The parameter ε is determined on the basis of the given duration of intensive iscillations above-mentioned records and is equal to

$$\varepsilon_i = 0.02\omega_i\,. \quad (14)$$

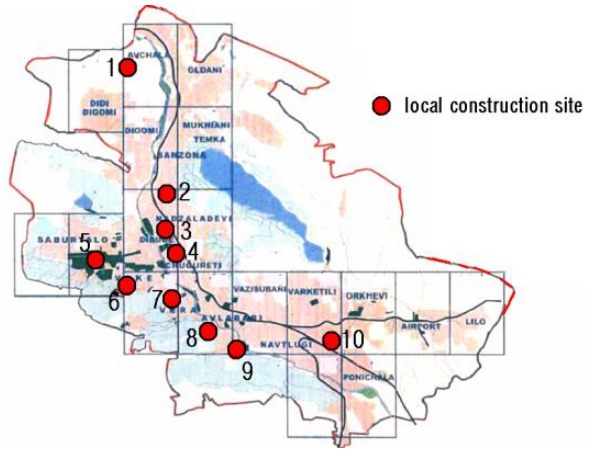

Fig. 1. Location of the sites on the territory of the city.

Thus calculated parameters are represented in Table 3, but mean square values of the horizontal and vertical accelerations for earthquake generated from the high potential seismic generating zone #3 are given in Table 4.

Table 2. Quantitative characteristics of the predicted ground motion for the concrete sites of Tbilisi city.

Zone	M	Parameters	Site									
			1	2	3	4	5	6	7	8	9	10
3	7	R_{min}, km	15.6	20.0	21.2	23.3	18.1	21.6	25.1	26.8	30.0	33.7
		PGA_{h1}, (m/sec²)	2.83	2.72	2.69	2.65	2.77	2.69	2.62	2.58	2.53	2.47
		PGA_{h2}, (m/sec²)	2.21	2.13	2.10	2.07	2.16	2.10	2.04	2.02	1.98	1.93
		PGA_{h3}, (m/sec²)	1.89	1.81	1.80	1.77	1.85	1.79	1.74	1.72	1.69	1.65
		T, sec	0.281	0.299	0.303	0.31	0.291	0.305	0.316	0.321	0.331	0.34
		D, sec	4.98	5.63	5.8	6.08	5.35	5.86	6.3	6.52	6.9	7.31

Table 3. Parameters for generation of regional synthetic accelerograms.

Zone	ω_j (sec^{-1})	α_{j1} (sec^{-1})	α_{j2} (sec^{-1})	α_{j3} (sec^{-1})	ε_j (sec^{-1})	Δt=0.04T_j (sec)
From focus with M=5						
2	48.3	9.85	12.1	19.8	0.97	0.005
5	52.3	10.67	13.1	21.4	1.05	0.0048
From focus with M=5.5						
7	41.8	8.53	10.5	17.1	0.84	0.006
From focus with M=6						
4	34.8	7.1	8.7	14.3	0.7	0.007
6	34.8	7.1	8.7	14.3	0.7	0.007
8	31.4	6.4	7.9	12.9	0.63	0.008
From focus with M=6.5						
1	22.4	4.5	5.6	9.2	0.45	0.011
From focus with M=7						
3	22.4	4.6	5.6	9.2	0.45	0.011

Table 4. Mean square values of accelerations for concrete sites from Zone 3.

Mean square value of acceleration (m/sec²)	Probability of exceeding in 50 years	Site									
		1	2	3	4	5	6	7	8	9	10
σ_1	2% /50	94	91	90	88	92	90	87	84	84	82
	1% /50	109	104	103	102	106	103	100	97	97	95
σ_2	2% /50	73	71	70	69	72	70	68	67	66	64
	1% /50	85	81	81	79	83	80	78	77	76	74
σ_3	2% /50	63	60	60	59	62	60	58	57	56	55
	1% /50	72	70	69	68	71	69	67	66	65	63

4. Determination of Multilayer Ground Motion based on the Theory of Reflected Waves

Method of the multiple reflected waves gives a possibility to determine for a certain concrete territory by geologic profile conformity to natural laws of seismic oscillation of the multilayer ground surface, under motion of bedrock as foundation according a law of given accelerogram.

For analytical drawing of accelerogram of the ground surface oscillation let consider, a wave picture at any time in the ground area, with different thickness and horizontal borderline. It is accepted an assumption that the ground is elastic and waves are propagated in the vertical direction (Fig. 2). In the form of seismic influence in this case is used recorded on the bedrock accelerogram from the database of ground motions with known earthquake (Rekvava and Mdivani, 2011).

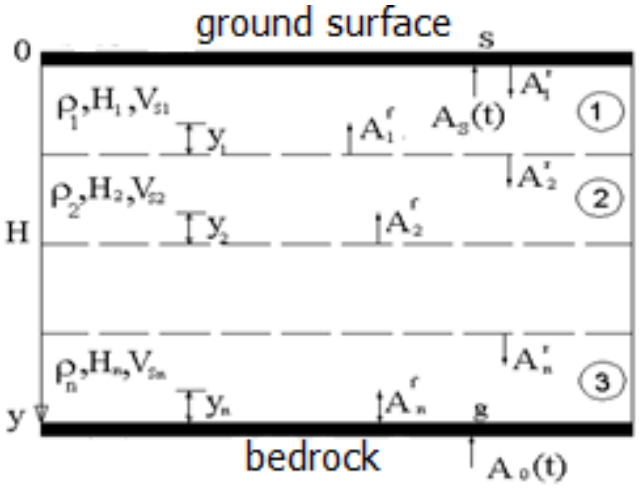

Fig. 2. Design model of non-homogeneous ground.

In the Fig. 2 are accepted following designations: $A_i^J(t)$ is value of the wave function at the t time on the bottom level of the *i*-th layer; $A_i^r(t)$ is value of the wave function at the t time on the top level of the *i*-th layer; $A_0(t)$ is the given relationship of the movement on the level of bedrock.

For any *i*-th layer of ground the wave equation of shear oscillations can be written as (Napetvaridze, 1973):

$$\frac{\partial^2 A_i(t)}{\partial t^2} - V_{si}^2 \frac{\partial^2 A_i(t)}{\partial y^2} = 0\,, \tag{15}$$

where $A_i(t)$ is the displacement of ground *i*-th layer particles; t is the time; y represents the coordinate of particle oscillation in the vertical direction; V_s is the velocity of the shear wave propagation in the ground area.

Solution of the Eq. (15) on the top of the *i*-th layer at the t time is given by

$$A_i^r(t) = \alpha_{i-1,i} A_{i-1}^r(t-\tau_{i-1}) + \beta_{i,i-1} A_i^f(t-\tau_i)\,, \tag{16}$$

where $\alpha_{i-1,i}$ is the factor of refraction under passing of wave from *i*-1-th to *i*-th layer; $\beta_{i,i-1}$ is the factor of wave reflection on the borderline between i and *i*-1 layers; τ_i represents the time of wave passage in the *i*-th layer $\tau_i = H_i/V_{si}$, where H_i and V_{si} are accordingly the thickness of ground layer and the velocity of the shear wave propagation in the i-th layer).

α and β factors are defined by

$$\alpha_{i-1,i} = 2\rho_{i-1}V_{s,i-1}/\left(\rho_{i-1}V_{s,i-1} + \rho_i V_{si}\right), \tag{17}$$

$$\beta_{i,i-1} = \left(V_{si}\rho_i - \rho_{i-1}V_{s,i-1}\right)/\left(V_{si}\rho_i + V_{s,i-1}\rho_{i-1}\right), \tag{18}$$

where ρ_i is a density of *i*-th ground layer.

Hence, finally solution of the direct problem of engineering seismology can be represented by the recurrent relations as (Napetvaridze, 1973):

$$\begin{aligned}
&A_1^r(t) = A_1^f(t-\tau_1)\,,\\
&A_1^f(t) = \alpha_{2,1}A_2^f(t-\tau_2) + \beta_{1,2}A_1^r(t-\tau_1)\,,\\
&A_2^r(t) = \alpha_{2,1}A_1^r(t-\tau_1) + \beta_{2,1}A_2^f(t-\tau_2)\,,\\
&A_2^f(t) = \alpha_{3,2}A_3^f(t-\tau_3) + \beta_{2,3}A_2^r(t-\tau_2)\,,\\
&A_i^r(t) = \alpha_{i-1,i}A_{i-1}^r(t-\tau_{i-1}) + \beta_{i,i-1}A_i^f(t-\tau_i)\,,\\
&A_i^f(t) = \alpha_{i+1,i}A_{i+1}^r(t-\tau_{i+1}) + \beta_{i,i+1}A_i^r(t-\tau_i)\,,\\
&A_n^r(t) = \alpha_{n-1,n}A_{n-1}^r(t-\tau_{n-1}) + \beta_{n,n-1}A_n^f(t-\tau_n)\,,\\
&A_n^f(t) = \alpha_{n+1,n}A_{n+1}^r(t-\tau_{n+1}) + \beta_{n,n+1}A_n^r(t-\tau_n)\,.
\end{aligned} \tag{19}$$

Value of the wave function from the bottom of i-th layer on the level of $y_i$can be calculated according to

$$A_i^{y_i}(t) = A_i^f\left(t - \frac{y_i}{V_{si}}\right) + A_i^r(t - (H_i - y_i)/V_{si})\,. \qquad (20)$$

Thus, the developed algorithm of solution the direct problem of engineering seismology is realized by the software package GAFART (Rekvava and Mdivani, 2011).

5. Simulation Results for Tbilisi City Sites

The computer code ACCSIM was used for generation of the horizontal and vertical components of synthetic accelerograms corresponding possible seismic source zones of Tbilisi region, given in Table 1. Discrete step of the simulated accelerograms was taken equal to $0.04T$. When assessing the probabilistic mean acceleration elastic response spectra and the normalized dynamic coefficient spectral curves for all sites, which are presented in Fig. 1, the required number of realizations was reduced for each synthetic accelerogram up to 20 realizations. The most novel aspect of this extension is elaboration of proper the three-components normalized dynamic coefficient spectral curves, which are computed for a 50 years exposure time and 2% and 1% probabilities of exceeding.

In Table 5 are represented values of the probabilistic mean normalized spectral dynamic coefficient of synthetic motion, generated from the source zones N3 and N6 for the sites situated in the center of Tbilisi city.

As an example, Fig. 3 shows pairs of the probabilistic mean elastic acceleration response spectra for 5% damping and the corresponding spectral curve of normalized dynamic coefficient of synthetic motion, generated from the source zone N3, for site [1]8 of soft soil characteristics for 2% in 50 years.

Table 5. Maximum values of normalized dynamic coefficient for 2%/50 and 1%/50 years.

Zone	M	Axes	Site											
			$N1$		$N2$		$N5$		$N7$		$N8$		$N10$	
			β_{max}		β_{max}		β_{max}		β_{max}		β_{max}		β_{max}	
			2%	1%	2%	1%	2%	1%	2%	1%	2%	1%	2%	1%
3	7	x	2.5	2.7	2.4	2.5	2.5	2.8	2.4	3.0	2.5	3.0	2.4	2.6
		y	1.8	2.2	2.0	2.4	2.6	3.0	2.2	2.6	2.5	2.5	2.5	2.7
		z	2.2	3.0	2.7	3.0	1.8	3.0	2.1	2.2	2.6	2.8	1.8	2.3
6	6	x	2.6	3.0	2.0	2.9	3.0	3.7	2.4	2.5	2.6	3.2	2.3	2.5
		y	2.5	2.7	2.0	2.5	2.5	3.0	2.2	2.5	2.5	3.0	2.3	2.5
		z	3.0	3.4	2.5	2.7	2.7	3.0	3.3	3.5	2.5	2.8	2.0	2.5

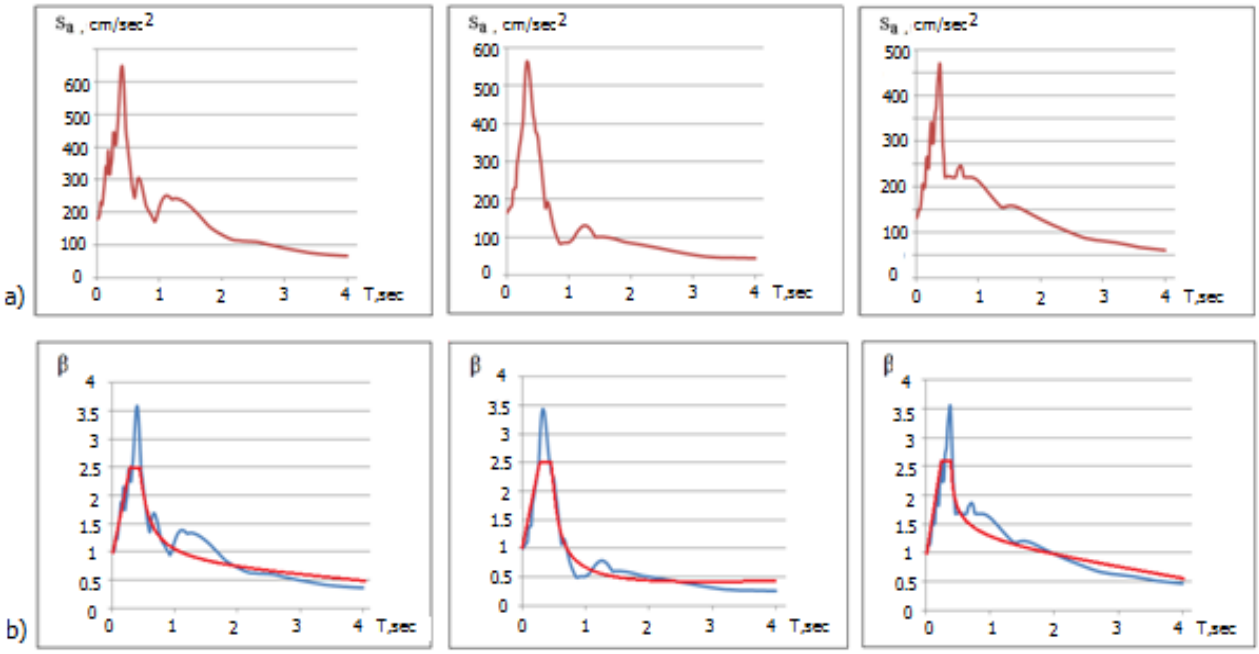

Fig. 3. Generated from zone #3 for site #8: (a) x,y,z components of acceleration response spectra; (b) spectral curves of normalized dynamic coefficient for 2% in 50 years.

Using the software GAFART was studied an influence of a typical earthquake and local geological conditions upon forming the elastic acceleration response spectra for the abovementioned sites. With that and in view from the data set (Rekvava and Mdivani, 2011) was selected five recorded on the bedrock accelerograms (EL Centro-1940, M=6.7, Santa Barbara-1980, Montenegro-1979, M=7.0, Friuli 1976, M=6.0, and Tbilisi-2002, M=4.5), which are different from each other by parameters of PGA, dominant period and duration, but by the magnitude and epicentral distance are close to predicted earthquakes characteristics for Tbilisi region.

Considering the soil profile properties (thickness, density, shear wave velocity) of these sites, received from geological test, on the basis of the abovementioned recorded ground motions were calculated the three components of time-histories on the ground surface of the sites. Then at the final phase of analysis the three components of spectral curves of normalized dynamic coefficient have been plotted. Table 6 displays the effect of local soil condition on the dynamic coefficient.

Table 6. Maximum values of normalized dynamic coefficient from different earthquakes.

Zone	Earthquake	Component	Site					
			$N1$	$N2$	$N5$	$N7$	$N8$	$N10$
			β_{max}	β_{max}	β_{max}	β_{max}	β_{max}	β_{max}
1	EL Centro	x	2.2	3.0	3.0	2.5	3.0	2.5
		y	2.2	3.0	3.0	2.5	3.0	2.5
		z	2.2	3.0	3.0	2.5	3.0	2.5
2	Santa Barbara	x	2.7	3.5	4.0	3.0	2.5	2.7
		y	2.7	3.5	4.0	3.0	2.5	2.5
		z	2.7	3.5	4.0	3.0	2.5	2.4
3	Montenegro	x	2.5	3.5	2.5	3.0	4.0	2.5
		y	2.0	3.0	3.0	3.7	3.0	2.5
		z	3.0	2.5	2.7	3.0	2.0	3.0
4	Friuli	x	2.4	3.0	3.5	3.0	3.0	2.8
		y	2.7	3.3	3.0	2.8	2.5	2.7
		z	1.8	3.0	2.3	2.3	2.5	2.5
5	Tbilisi	x	2.5	2.0	2.1	2.5	2.3	2.3
		y	2.5	2.2	3.1	2.0	2.5	2.5
		z	2.3	2.3	2.4	3.0	2.1	2.2

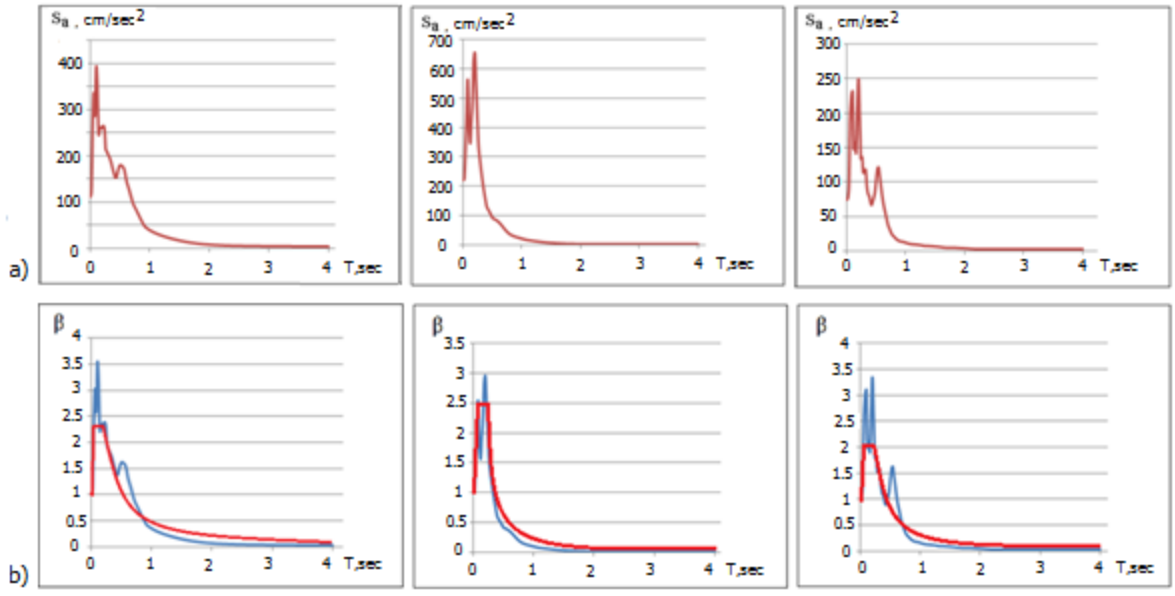

Fig. 4. Three components acceleration response spectra: (a) and spectral curves of normalized dynamic coefficient; (b) for site #8 resulting from the accelerogram calculated at the free surface from recording "Tbilisi- 2002" of the depth z=-43.1m.

Fig. 4 displays the effect of local soil condition on the normalized dynamic coefficient for the concrete site $^{1}8$ under action of Tbilisi-2002 records.

According to the obtained results was computed value of the relative seismic factor or soil amplification factor as the ratio of the maximum accelerations of the ground surface layer to the bedrock. The analysis shows that in the given soil properties of the sites under investigation the seismic factor is changed from 1.5 to 2.6.

6. Conclusions

The complex approach of simulation ground motion and construction the horizontal and vertical acceleration elastic response spectra and corresponding normalized dynamic coefficient spectral curves are proposed, which account for the location of the earthquake source zones and seismological and geological characteristics of the Tbilisi region territory and concrete construction sites of the Tbilisi city.

Based on the empirical relations and characteristics of the earthquake source zones the values of mean accelerations of ground motion for 2% and 1% probabilities of being exceeded in 50 years expected in the sites of Tbilisi city has been determined and appropriate probabilistic horizontal and vertical acceleration elastic response spectra and normalized spectral dynamic coefficients are calculated which can be used in seismic design and analysis of structures.

On the territory under examination for the concrete construction sites in result of experimental research the dynamic parameters of soil geological layers are determined and based on the theory of reflected waves the ground motion for the sites of Tbilisi city horizontal and vertical acceleration elastic response spectra and normalized spectral dynamic coefficients are calculated and their corrected shapes considering the local sites conditions for medium (II) and soft (III) categories of soil are constructed.

The value of the relative seismic factor as the ratio of the maximum accelerations of the ground surface layer to the bedrock, in the given soil properties of the sites under investigation, is changed from 1.5 to 2.6.

Maximum values (2.6-3.0) of spectral dynamic coefficient determined and based on the stochastic ground motion model under medium and soft ground conditions are up to 1.04-1.2 times larger than given in the Building code (2.5).

Maximum values (2.7-4.0) of spectral dynamic coefficient obtained from the solution of direct problem of engineering seismology under medium and soft ground conditions are 1.08-1.6 times greater than determined in the Building code (2.5).

References

Building Code (2009). Earthquake Engineering PN 01.01-09. Georgian Ministry of Economic Development, Tbilisi, Georgia.

Eurocode 8 (2004) Design of structures for earthquake resistance, part 2: General rules, seismic actions and rules for buildings (European Standard EN 1998-1:2004).

Javakhishvili Z, Varazanashvili O, Butikashvili N (1998). Interpretation macroseismic Valley of Georgia. *Journal of Georgian Geophysical Society,* 3, 85-88.

Mikhailova N, Aptikaev F (1996). Some correlation relations between parameters of seismic motion. *Journal Of Earthquake Prediction Research,* 5(2), 257-263.

Napetvaridze S (1973). Some Problems of Engineering Seismology. Mecniereba, Tbilisi, Georgia.

Rekvava P (2009). Modern Earthquake Engineering. Intellect, Tbilisi, Georgia.

Rekvava P, Mdivani K (2010). Modeling of earthquake ground motion for tbilisi region. *Global Journal of Researches in Engineering, Revolutions in Engineering*, 10(3), 2-7.

Rekvava P, Mdivani K (2011). Elaboration of the Seismic Influence Spatial Models for Performance-Based Design Considering Seismological and Engineering-Geological Conditions of Tbilisi Region. Georgian National Science Foundation, Grant N GNSF/ST08/7-484.

Smit P, Arzumznian V, Javakhishvili Z, Arefiev S, Mayer-Rosa D, Balassanian S, Chelidze T (2000). The digital accelerograph network in the Caucasus. *Earthquake Hazard and Seismic Risk Reduction,* 109-118.

Challenge Journal of Structural Mechanics

Evaluation of framed building types based on the combination of fuzzy AHP and fuzzy MOORA methods

Burak Erkayman [a,*], Fatih Mehmet Özkal [b]

[a] *Department of Industrial Engineering, Atatürk University, 25240 Erzurum, Turkey*
[b] *Department of Civil Engineering, Erzincan University, 24060 Erzincan, Turkey*

ABSTRACT

Mankind has been using different kind of materials to build shelters and after then more specific structures throughout the history. If the stone is accepted as a primitive construction material; wood, concrete and steel has spread to the construction history. However, from both of the supply and demand view, it is possible to say that defining the best solution to the construction necessities and constraints is vastly ambiguous. In other words, making decision with respect to infinite parameters is an important task. The level of uncertainty in the optimality based definition of framed building types is relatively high and need to be carefully analyzed. Therefore, in order to select a proper construction technique, combination of fuzzy AHP (analytic hierarchy process) and evaluation based on fuzzy MOORA (multi objective optimization by ratio analysis) has proposed a new useful method, in which FAHP is used for calculating priority weight of criteria and the MOORA is implemented for obtaining the final ranking of construction techniques. In addition, for expressing the applicability of the offered model, it is supported by a case study. In the rating of framed building types; cost, performance, time, fire, corrosion, esthetics and recycling is considered as important factors. As a result, this model is easy to understand and simple to implement in various areas. Also, this method is applicable for the choosing of proper alternatives in different selection problems.

ARTICLE INFO

Article history:
Received 18 April 2016
Accepted 8 June 2016

Keywords:
Fuzzy AHP
Fuzzy MOORA
Group decision making
Framed buildings
Construction techniques

1. Introduction

Lots of parameters should be considered in the comparison of framed building types such as reinforced concrete, steel or wooden constructions. Common failure titles in this comparison may be summed as calculation of cost and determination of seismic performance with regards to discrete structural elements. However, evaluation of any kind of structure should be positioned on a holistic way.

Reinforced concrete is a combination of concrete and steel bars that work together against dead/live loads and seismic forces. It has been the most common construction technique with respect to its many assumed advantages. Low construction cost based on its material puts reinforced concrete forward beyond the others. Another technique is steel construction that is preferred mostly for tall buildings and industrial structures. Steel has the highest strength through reinforced concrete and wood. Similarly to the steel construction technique, wooden construction has a significant tensile and flexural behavior in addition to its weight advantage and fire resistance disadvantage. Wood is the oldest construction material and has still a wide application field which evolved on modern approaches.

As it is seen in the above brief, all these construction techniques have some advantages and disadvantages. It is the main problem to determine which one of them is the most preferable technique. Strictly speaking, there is no absolute answer to this question. Because necessities and constraints can only point the most appropriate construction technique. Furthermore, commercial purposes

* *Corresponding author*. Tel.: +90-442-2316017 ; Fax: +90-442-2314910 ; E-mail address: erkayman@atauni.edu.tr (B. Erkayman)
ISSN: 2149-8024 / DOI: http://dx.doi.org/10.20528/cjsmec.2016.06.013

could mislead the demanders. However, a rough survey on the main construction parameters could lead a general preference feasibility for both of the supply and demand sides.

Decision making has become one of the most important activities in the modern world today despite being attacked by diverse sophisticated technology decision tools. Technology alone sometimes cannot to deliver a decision without assuming human understood ability. Human capabilities with a good insight are considered to extend effective decision making to access a decision. One of the important decision making tools that was introduced in early seventies is multi criteria decision making theory.

The theory of decision making has formed a basis for more reasonable decision making especially in the situation where multiple criteria need to be calculated. The combination of multi criteria decision making (MCDM) with fuzzy logic can be efficiently implemented for solving decision problems with diverse criteria (Sánchez-Lozano et al., 2015).

Framed building types are compared with each other and our view was based on seven criteria. These are the three common construction types which we can select for this study:

- Reinforced concrete construction
- Steel construction
- Wooden construction

In this study, framed building type selection is defined as fuzzy integrated model. In order to, relevant criteria are determined as follows:

- Construction cost
- Structural performance
- Construction time
- Fire resistance
- Corrosion resistance
- Architectural esthetics
- Recycling

The purpose of this study is determination of the best framed building type for any supply and demand sides. For this reason, practical information was obtained from a sufficient number of civil engineer scholars. Many preference parameters were presented and also their new suggestions were asked. After the review of collected responses, these seven titles were determined and the study has been performed on them. First of all, the weights of criteria are calculated by using fuzzy AHP. After that, the ERP systems are ranked according to three different parts of fuzzy MOORA method.

2. Fuzzy Set Theory

Zadeh (1975) proposed fuzzy theory as a mathematical theory for first time. It is possible to create relationship between uncertainty and vagueness in real life world problems by using fuzzy theory. If X be the universe of discourse $X = \{x_1, x_2, \dots, x_n\}$, a fuzzy set ã of X is characterized by a membership function $\mu_{\tilde{a}}(X)$, which maps each element x in X to real number within the interval [0,1]. The function values $\mu_{\tilde{a}}(x)$, the stronger degree of membership for x in ã (Kaufman and Gupta, 1991).

3. Methods

3.1. Fuzzy AHP

AHP is one of the most important MCDM methods for modeling erratic problems in diverse areas. Fuzzy AHP was introduced to eliminate the defects of traditional AHP and to facilitate adoption to real life problems (Buckley et al., 2001). Chang (1992) proposed a fuzzy AHP based on the extent analysis method which is widely used in supplier selection problems (Kilincci and Onal, 2011; Ertuğrul and Karakaşoğlu, 2007) by using of triangular fuzzy numbers for pairwise comparison scale of fuzzy AHP. The steps of FAHP are as follows (Buckley et al., 2001) :

i. Build fuzzy triangular judgment matrix

The fuzzy triangular matrix $A = (a_{ij})_{nk*nk}$ is a closed interval, where pairwise comparison judgments express by $a_{ij} = (l_{ij}, m_{ij}, u_{ij})$ fuzzy numbers.

$u_{ij} = upper\ bound, m_{ij} = median,\ l_{ij} = lower\ bound,$
$i, j = 1,2, \dots, n_k$
$n_k =$ the number of klevel indicator system

ii. Calculate comprehensive judgment matrix

The $a_{ij}^t = (u_{ij}^t, m_{ij}^t, l_{ij}^t)$ elements, express the fuzzy number which determined by decision makers $t = 1,2, \dots, T$ with comparing the indicators i and j.

$$M_{ij} = \frac{1}{T} \otimes \left(a_{ij}^1 + a_{ij}^2 + \cdots + a_{ij}^T\right). \quad (1)$$

$\otimes = multiplication\ principle\ of\ triangular\ fuzzy\ number.$

iii. Calculate comprehensive fuzzy degree

The comprehensive fuzzy degree S_i calculates as follows:

$$S_i = \sum_{j=1}^{n_k} M_{ij} \otimes \left(\sum_{i=1}^{n_k} \sum_{j=1}^{n_k} M_{ij}\right)^{-1}. \quad (2)$$

iv. Calculation of indicator weight

The best scalar measure of indicator C_i is as follows:

$$d'(C_i) = min\, V(S_i \geq S_j), \quad (3)$$

where $0 \leq V(S_i \geq S_j) \leq 1, i, j = 1,2,.., n_k$. $V(S_i \geq S_j)$ shows the possibility degree of $S_i \geq S_j$.

$$V(S_i \geq S_j) = \mu(d) = \begin{cases} \frac{l_j - u_i}{(m_i - u_i) - (m_j - l_j)} & , \quad l_j \leq u_j \\ 0 & , \quad others \end{cases}. \quad (4)$$

The single level indicator weight:

$$W' = (d'(C_1), d'(C_2), \dots, d'(C_n)). \quad (5)$$

The normalized indicator weight:

$$W = \left(d(C_1), d(C_2), \dots, d(C_n)\right), \quad (6)$$

3.2. Fuzzy MOORA

The using of multi objective optimization by ratio analysis (MOORA) was commenced by (Brauers and Zavadskas, 2006) based on recent research. This multi criteria decision making method start with matrix X which it's elements x_{ij} express *i*th alternative of *j*th criterion ($i = 1,2,\dots,m$ and $j = 1,2,\dots,n$); in addition, the fuzzy MOORA method consists of three parts such as fuzzy ratio method, fuzzy reference point and fuzzy multiplicative form.

i. Fuzzy ratio method

Step1: Decision matrix is acquired according to the Tables 4 and 5:

$$\tilde{X} = \begin{bmatrix} [x_{11}^l, x_{11}^m, x_{11}^u] & \cdots & [x_{1n}^l, x_{1n}^m, x_{1n}^u] \\ \vdots & \ddots & \vdots \\ [x_{m1}^l, x_{m1}^m, x_{ml}^u] & \cdots & [x_{mn}^l, x_{mn}^m, x_{mn}^u] \end{bmatrix}. \quad (7)$$

Step2: In this part, we normalize decision matrix since it enables us to compare alternatives with each other more accurately (Liu and Liu, 2010).

$$\tilde{X}_{ij}^* = \left(x_{ij}^{l*}, x_{ij}^{m*}, x_{ij}^{u*}\right); i = 1,2,\dots,m; j = 1,2,\dots,n, \quad (8)$$

$$X_{ij}^{l*} = \frac{x_{ij}^l}{\sqrt{\sum_{i=1}^m [\left(x_{ij}^l\right)^2 + \left(x_{ij}^m\right)^2 + \left(x_{ij}^u\right)^2]}}, \quad (9)$$

$$X_{ij}^{m*} = \frac{x_{ij}^m}{\sqrt{\sum_{i=1}^m [\left(x_{ij}^l\right)^2 + \left(x_{ij}^m\right)^2 + \left(x_{ij}^u\right)^2]}}, \quad (10)$$

$$X_{ij}^{u*} = \frac{x_{ij}^u}{\sqrt{\sum_{i=1}^m [\left(x_{ij}^l\right)^2 + \left(x_{ij}^m\right)^2 + \left(x_{ij}^u\right)^2]}}. \quad (11)$$

Step3: In this step, calculated weights of criteria from AHP are used to form weighted and normalized fuzzy matrix (Vatansever, 2013).

$$\tilde{v}_{ij} = (v_{ij}^l, v_{ij}^m, v_{ij}^u)$$
$$v_{ij}^l = w_j x_{ij}^{l*}$$
$$v_{ij}^m = w_j x_{ij}^{m*}$$
$$v_{ij}^u = w_j x_{ij}^{u*}. \quad (12)$$

Step4. Summarizing ratio $\tilde{y}_i$ calculate for each *i*th alternative as follows (Baležentis et al., 2012):

$$\tilde{y}_i = \sum_{j=1}^g \tilde{v}_{ij} - \sum_{j=g+1}^n \tilde{v}_{ij}, \quad (13)$$

where $g = 1,2,\dots,n$ denotes number of criteria to be maximized. On the other hand, $g+1,\dots,n$ denotes number of criteria to be minimized.

Step5. In this step, fuzzy numbers change to non-fuzzy numbers by BNP equation and the amounts of BNP are calculated for each alternative. As a result, the alternatives with highest values are favorable for choosing.

$$BNP_i(y_i) = \frac{\left(y_i^u - y_i^l\right) + \left(y_i^m - y_i^l\right)}{3} + y_i^l \quad (14)$$

ii. Fuzzy reference point

Fuzzy ratio system plays major role in the fuzzy reference point approach. The maximal objective reference point $\tilde{r}$ is obtained as well as second step of fuzzy ratio method. The fuzzy maximum or minimum of the *j*th criteria are calculated as follows:

$$\begin{cases} \tilde{x}_j^+ = \left(\max_i x_{ij}^{l*}, \max_i x_{ij}^{m*}, \max_i x_{ij}^{u*}\right), & j \le g \\ \tilde{x}_j^+ = \left(\min_i x_{ij}^{l*}, \min_i x_{ij}^{m*}, \min_i x_{ij}^{u*}\right), & j > g \end{cases}. \quad (15)$$

The every element of normalized matrix is calculated and final sort achieved based on deviation from the refere1nce point and the Min-Max metric of (Liu et al., 2014; Balezentiene and Streimikiene, 2013):

$$\min_i(\max_j(\tilde{r}_j, \tilde{x}_{ij}^*)), \quad (16)$$

iii. The fuzzy multiplicative form

Overall utility of *i*th alternative is obtained as follows:

$$\tilde{U}_i' = \frac{\tilde{A}_i}{\tilde{B}_i}, \quad (17)$$

where $\tilde{A}_i = (A_{i1}, A_{i2}, A_{i3}) = \prod_{j=1}^g \tilde{x}_{ij}$, i = 1,2,…,$m$ expresses the criteria of the *i*th alternative to be maximized $g = 1,2,\dots,n$ being the number objectives to be maximized and where $\tilde{B}_i = (B_{i1}, B_{i2}, B_{i3}) = \prod_{j=g+1}^n \tilde{x}_{ij}$ expresses the criteria of the *i*th alternative to be minimized with $n - g$ being the number of objectives to be minimized. We need to eliminate fuzzy numbers of overall utility $\tilde{U}_i'$ to rank the alternatives. The alternative with higher BNP is favorable for choosing (Balezentiene and Streimikiene, 2013).

4. Framed Building Characteristics – Decision Criteria

Framed building types are evaluated through the following decision criteria as: Construction cost, structural performance, construction time, fire resistance, corrosion resistance, architectural esthetics, recycling.

4.1. Construction cost

Construction cost of and type of structure actually depends of many other parameters. While the expense for structural material could be said that has the main portion, it is more complex than this evaluation. Because production, transport and installation stages totally specify the initial construction cost. Installation cost regarding qualified labor (especially for steel and wooden construction) should not be neglected. Reinforced concrete has a significant advantage on this parameter. It is also obvious that this parameter is generally assumed as one of the most important preference criteria.

4.2. Structural performance

Any type of building is expected to have a high structural performance against dead/live loads and seismic forces. Substantial properties of construction materials that affect their structural performance could be defined as compression/tensile/flexural strength, ductility and stiffness. However, especially for seismic performance, strength/weight proportion is the main factor. Repeated reversible forces are highly subjected to the structural elements' weight and reinforced concrete structures recede into background considering their excess weight.

4.3. Construction time

Steel and wooden construction types are ahead of reinforced concrete construction considering this parameter. Because steel and wooden structural elements are pre-fabricated, these techniques could be applied independent of climate conditions. However, reinforced concrete construction is executed totally on the field. Rain, snow, hot&cold weather conditions prevents the labor and also concrete casting while steel and wooden construction is based mostly on the mounting of prefabricated elements.

4.4. Fire resistance

Despite some possible precaution methods, fire is crucial for firstly wood and then steel. One can say that carbonization delay the collapse of wooden structures, it is obvious that wood gets affected and damaged faster than steel. Additionally, reinforced concrete should not be assumed in a similar way as steel construction. Owing to the concrete cover on the steel rebar, reinforced concrete has the highest fire and high temperature resistance in comparison to steel and wooden structures.

4.5. Corrosion resistance

Traditionally, corrosion has a significant negative effect on metal materials. Steel construction has the biggest disadvantage regarding to this parameter although many precaution methods against corrosion are available. However, similarly as the fire protection, they increase the construction cost and should be taken in consideration without these additional solutions. For reinforced concrete structures, concrete cover on the steel rebar decrease corrosion effect. Moreover, corrosion is an undesirable situation for wooden structures, lifetime of timber is affected more by other negative factors.

4.6. Architectural esthetics

This parameter has actually a subjective aspect and esthetical look ranking could be applied based on the common opinion. However, most important indicator of architectural esthetics should be the diversity level of architectural design. Especially regarding to the low weight and high tensile/flexural strength of steel and wood materials; much number of extraordinary designs are possible than reinforced concrete construction. Moreover, natural look of wooden construction brings an additional positive value than the other techniques.

4.7. Recycling

Nowadays, recycling has been one of the most important arguments in all mankind productions. Despite the long lifetime of buildings, recycling should be considered for material selection. Furthermore, exhaustion of natural sources is possible to be implemented in this evaluation. Hence, steel is the foremost material regarding to its recycling capability.

5. Illustrative Example

The useful data have been acquired from the survey throughout civil engineer scholars and it was seen that the level of uncertainty in the selection of framed building types is relatively high and need to be carefully analyzed. Therefore, in order to select a proper construction technique, combination of fuzzy AHP (FAHP) and evaluation based on fuzzy MOORA (multi objective optimization by ratio analysis) has proposed a new useful method, in which FAHP is used for calculating priority weight of criteria and the MOORA is implemented for obtaining the final ranking of framed building types. Fig. 1 shows the hierarchical structure of the model. Decision making group, which has a significant background in this field, selected 7 main criteria. This group also confirmed the convenience of three construction types as our alternatives. In this study, linguistic variables are used then they are converted into triangular fuzzy numbers (Table 1). Accordingly, a systematic approach based on combination of fuzzy AHP with fuzzy MOORA is proposed to determine the best construction technique. Table 2 shows the comparison of 7 decision criteria with each other. The abbreviations are; equally important: EI, moderately important: MI, important: I, very important: VI, much more important: MMI. The weights of criteria that were calculated by FAHP is presented in Table 3.

5.1. Determination of criteria weights

In this section, the fuzzy scale of Chang (1996) is used through fuzzy AHP for calculating the weights of criteria.

Table 1. The fuzzy scale of Chang (1996).

Linguistic variables	Fuzzy scale	Response scale
Equally Important	(1,1,1)	(1,1,1)
Moderately Important	(2/3,1,3/2)	(2/3,1,3/2)
Important	(3/2,2,5/2)	(2/5,1/2,2/3)
Very Important	(5/2,3,7/2)	(2/7,1/3,2/5)
Much More Important	(7/2,4,9/2)	(2/9,1/4,2/7)

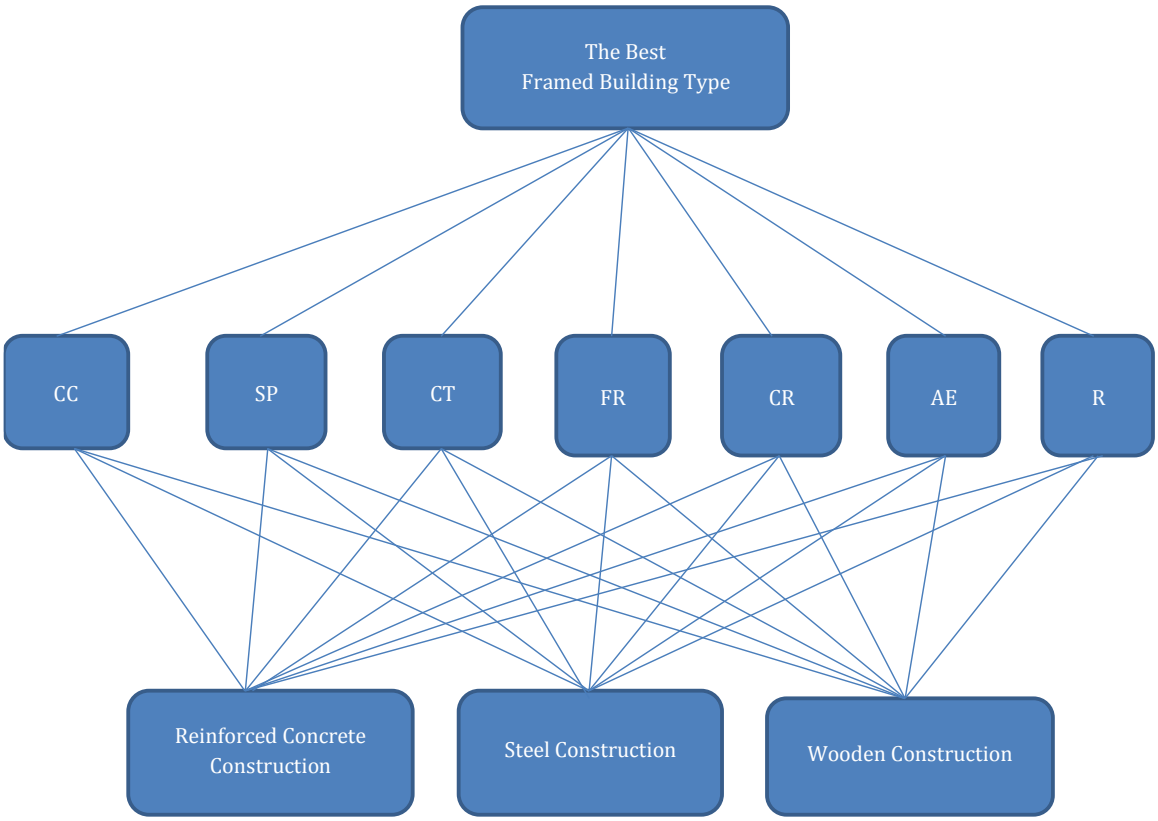

Fig. 1. Hierarchical structure of the model.

Table 2. Pairwise comparison matrix of criteria.

	SP	CT	FR	CC	AE	CR	R
SP	-	MI	I	EI	I	I	MI
CT		-	I	MI	I	I	I
FR			-	I	MI	EI	I
CC				-	I	I	I
AE					-	MI	EI
CR						-	MI
R							-

Table 3. The weights of criteria calculated by FAHP.

Criteria	W
Structural Performance	0.23
Construction Time	0.26
Fire Resistance	0.1
Construction Cost	0.26
Architecture Esthetics	0.05
Corrosion Resistance	0.05
Recycling	0.05

5.2. Selection of the framed building type

Fuzzy MOORA is used for the selection of framed building types. While Chen's fuzzy linguistic scale is used which is shown in Table 4, fuzzy evaluation matrix for framed building types are as in Table 5. After calculation the rank of systems were acquired, the ranking of framed building types are given on Table 6.

Table 4. Chen's fuzzy linguistic scale (Chen, 1992).

Linguistic variables	Fuzzy scale
Very Low (VL)	(0,0,0.1)
Low (L)	(0,0.1,0.3)
Medium Low (ML)	(0.1,0.3,0.5)
Medium (M)	(0.3,0.5,0.7)
Medium High (MH)	(0.5,0.7,0.9)
High (H)	(0.7,0.9,1)
Very High (VH)	(0.9,1,1)

Table 5. Fuzzy evaluation matrix for ERP system types.

	SP	CT	FR	CC	AE	CR	R
Reinforced Concrete Construction	ML	ML	VH	MH	ML	MH	ML
Steel Construction	VH	MH	MH	ML	M	M	VH
Wooden Construction	M	MH	ML	ML	VH	VH	MH

Table 6. Comparison between system types based on criteria.

	SP	CT	FR	CC	AE	CR	R
Reinforced Concrete Construction	(0.1,0.3,0.5)	(0.1,0.3,0.5)	(0.9,1,1)	(0.5,0.7,0.9)	(0,0.1,0.3)	(0.5,0.7,0.9)	(0.1,0.3,0.5)
Steel Construction	(0.9,1,1)	(0.5,0.7,0.9)	(0.5,0.7,0.9)	(0.1,0.3,0.5)	(0.3,0.5,0.7)	(0.3,0.5,0.7)	(0.9,1,1)
Wooden Construction	(0.3,0.5,0.7)	(0.5,0.7,0.9)	(0.1,0.3,0.5)	(0.1,0.3,0.5)	(0.9,1,1)	(0.9,1,1)	(0.5,0.7,0.9)

Table 7. Normalized aggregated ratings for each alternative.

	SP	CT	FR	CC	AE	CR	R
Reinforced Concrete Construction	(0.05,0.149,0.248)	(0.054,0.161,0.269)	(0.415,0.461,0.461)	(0.333,0.467,0.6)	(0.05,0.15,0.25)	(0.224,0.313,0.402)	(0.046,0.138,0.23)
Steel Construction	(0.447,0.496,0.496)	(0.269,0.377,0.484)	(0.23,0.32,0.415)	(0.067,0.2,0.333)	(0.15,0.25,0.35)	(0.134,0.224,0.313)	(0.415,0.461,0.461)
Wooden Construction	(0.198,0.248,0.347)	(0.269,0.377,0.484)	(0.046,0.138,0.23)	(0.067,0.2,0.333)	(0.45,0.5,0.5)	(0.402,0.402,0.447)	(0.23,0.32,0.415)

According to the calculations based on FAHP method, steel construction is selected as the best solution (1st) throughout the considered framed building techniques. Wooden and then reinforced concrete constructions are the 2nd and 3rd in the final ranking.

6. Conclusions

The main objective of this study was to propose comprehensive criteria to evaluate framed building types by using fuzzy AHP and valuable ranking of framed building types by using fuzzy MOORA. This paper contributes to civil engineering literature as well as the validity of developed criteria for framed building types based on the guidance of scholars. It is possible to consider different parameters and different weight ratios to seek the optimal solution. Another parametric evaluation of construction techniques will yield new results. However, this paper has an importance to enlighten the related studies and make scholars discuss on the selection of framed building types. Choosing of a suitable construction technique is a difficult MCDM problem that includes both quantitative and qualitative objectives. It is difficult to

measure the performance of the existing construction types, which we managed to do that by getting help from civil engineer scholars. This study, proposed a fuzzy integrated model that can assess and choose the best framed building type by using of FAHP and FMOORA methods. Implementing of a practical decision making method for assessment and evaluating construction techniques is the major contribution of this study. For the next studies, this integrated method can be adjusted to diverse MCDM problems.

The proposed model may be used to evaluate alternatives successfully through various selection problems. Future researches may try to extend this study as an integration of more fuzzy integrated MCDM techniques to solve many other decision making problems on many other disciplines.

Table 8. Weighted normalize fuzzy decision matrix.

	SP	CT	FR	CC	AE	CR	R
Reinforced Concrete Construction	(0.011,0.034,0.057)	(0.014,0.042,0.07)	(0.04,0.046,0.046)	(0.087,0.12,0.156)	(0.002,0.007,0.012)	(0.011,0.016,0.02)	(0.002,0.007,0.011)
Steel Construction	(0.103,0.114,0.114)	(0.07,0.1,0.126)	(0.023,0.03,0.04)	(0.017,0.052,0.087)	(0.007,0.012,0.017)	(0.007,0.011,0.016)	(0.021,0.023,0.023)
Wooden Construction	(0.046,0.057,0.08)	(0.07,0.098,0.126)	(0.005,0.014,0.023)	(0.017,0.052,0.087)	(0.022,0.025,0.025)	(0.02,0.02,0.022)	(0.011,0.016,0.021)

Table 9. The fuzzy ratio method.

	$\tilde{y}_i$	BNP	Rank
Reinforced Concrete Construction	(-0.032,-0.053,-0.079)	-0.05447	3
Steel Construction	(0.073,0.043,-0.001)	0.038578	1
Wooden Construction	(0.017,-0.018,-0.041)	-0.01409	2

Table 10. The fuzzy reference point approach.

	SP	CT	FR	CC	AE	CR	R	$\max_j d(\tilde{r}_j, \tilde{x}^*_{ij})$	Rank
Reinforced Concrete Construction	0.583011	0	0	0.46188	0.588103	0.204939	0.541289	0.588103	3
Steel Construction	0	0.373002	0.23495	0	0.418854	0.349285	0	0.418854	1
Wooden Construction	0.381209	0.373002	0.541289	0	0	0	0.23495	0.541289	2

Table 11. The fuzzy multiplicative form.

	$\widetilde{U}_i'$	BNP	Rank
Reinforced Concrete Construction	(0.001,0.09,2.25)	0.780333	3
Steel Construction	(0.081,0.833,8.82)	3.244778	1
Wooden Construction	(0.027,0.5,6.3)	2.275667	2

REFERENCES

Balezentiene L, Streimikiene DBT (2013). Fuzzy decision support methodology for sustainable energy crop selection. *Renewable and Sustainable Energy Reviews*, 17, 83-93.

Baležentis A, Baležentis T, Brauers WKM (2012). Personnel selection based on computing with words and fuzzy MULTIMOORA. *Expert Systems with Applications*, 39(9), 7961-7967.

Brauers WKM, Zavadskas EK (2006). The MOORA method and its application to privatization in a transition economy. *Control and Cybernetics*, 35, 445-469.

Buckley JJ, Feuring T, Hayashi Y (2001). Fuzzy hierarchical analysis revisited. *European Journal of Operational Research*, 129, 48-64.

Chang DY (1992). Extent Analysis and Synthetic Decision. *In: Optimization Techniques and Applications*. World Scientific, 1, 352-355, Singapore.

Chang DY (1996). Application of the extent analysis method on fuzzy AHP. *European Journal of Operational Research*, 95, 649-655.

Chen SJ (1992). Fuzzy Multiple Attribute Decision Making Methods and Applications. Springer-Verlag, New York.

Ertuğrul İ, Karakaşoğlu N (2007). Comparison of fuzzy AHP and fuzzy TOPSIS methods for facility location selection. *The International Journal of Advanced Manufacturing Technology*, 39(7-8), 783-795.

Kaufman A, Gupta MM (1991). Introduction to Fuzzy Arithmetic. Van Nostrand Reinhold Company, New York.

Kilincci O, Onal SA (2011). Fuzzy AHP approach for supplier selection in a washing machine company. *Expert systems with Applications*, 38(8), 9656-9664.

Liu HC, Fan XJ, Li P, Chen YZ (2014). Evaluating the risk of failure modes with extended MULTIMOORA method under fuzzy environment. *Engineering Applications of Artificial Intelligence*, 34, 168-177.

Liu W, Liu PD (2010). Hybrid multiple attribute decision making method based on relative approach degree of grey relation projection. *African Journal of Business Management*, 4(17), 3716-3724.

Sánchez-Lozano JM, Serna J, Dolón-Payán A (2015). Evaluating military training aircrafts through the combination of multi-criteria decision making processes with fuzzy logic. A case study in the Spanish Air Force Academy. *Aerospace Science and Technology*, 42, 58-65.

Vatansever K, Ulukoy M (2013). Kurumsal kaynak planlaması sistemlerinin bulanık AHP ve bulanık MOORA yöntemleriyle seçimi: Üretim sektöründe bir uygulama. *CBU Sosyal Bilimler Dergisi*, 39(9), 274-293 (in Turkish).

Zadeh LA (1975). The concept of a linguistic variable and its application to approximate reasoning. *Information Sciences*, 8, 199-249.

Challenge Journal of Structural Mechanics

A Poisson method application to the assessment of the earthquake hazard in the North Anatolian Fault Zone, Turkey

Tuğba Türker [a,*], Yusuf Bayrak [b]

[a] *Department of Geophysical Engineering, Karadeniz Technical University, 61080 Trabzon, Turkey*
[b] *Faculty of Patnos Sultan Alparslan Natural Sciences and Engineering, Ağrı İbrahim Çeçen University, 04100 Ağrı, Turkey*

ABSTRACT

North Anatolian Fault (NAF) is one from the most important strike-slip fault zones in the world and located among regions in the highest seismic activity. The NAFZ observed very large earthquakes from the past to present. The aim of this study; the important parameters of Gutenberg-Richter relationship (*a* and *b* values) estimated and this parameters taking into account, earthquakes were examined in the between years 1900-2015 for 10 different seismic source regions in the NAFZ. After that estimated occurrence probabilities and return periods of occurring earthquakes in fault zone in the next years, and is being assessed with Poisson method the earthquake hazard of the NAFZ. The 10 different seismic source regions are determined the relationships between the cumulative number-magnitude which estimated *a* and *b* parameters with the equation of *LogN=a-bM* in the Gutenberg-Richter. A homogenous earthquake catalog for M_S magnitude which is equal or larger than 4.0 is used for the time period between 1900 and 2015. The database of catalog used in the study has been created from International Seismological Center (ISC) and Boğazici University Kandilli observation and earthquake research institute (KOERI). The earthquake data were obtained until from 1900 to 1974 from KOERI and ISC until from 1974 to 2015 from KOERI. The probabilities of the earthquake occurring are estimated for the next 10, 20, 30, 40, 50, 60, 70, 80, 90 and 100 years in the 10 different seismic source regions. The highest earthquake occur probabilities in 10 different seismic source regions in the next years estimated that the region Tokat-Erzincan (Region 9) 99% with an earthquake occur probability for magnitude 6.5 which the return period 24.7 year, 92% with an earthquake occur probability for magnitude 7 which the return period 39.1 year, 80% with an earthquake occur probability for magnitude 7.5 which the return period 62.1 year, 64% with an earthquake occur probability for magnitude 8 which the return period 98.5 year. For the Marmara Region (Region 2) in the next 100 year estimated that 89% with an earthquake occur probability for magnitude 6 which the return period 44.9 year, 45% with an earthquake occur probability for magnitude 6.5 which the return period 87 year, 45% with an earthquake occur probability for magnitude 7 which the return period 168.6 year.

ARTICLE INFO

Article history:
Received 23 April 2016
Accepted 16 June 2016

Keywords:
North Anatolian Fault Zone
Earthquake hazard
Poisson method
Seismic source regions

1. Introduction

The earthquake hazard of regions represented a possible potential or level of expected hazard and caused by geological structure features, tectonic movements, geophysical fields etc. At the same time, the satisfactory evaluation of earthquake hazard was one of the major problems of engineer seismology. The appraisal of earthquake hazard of the territory is realized using essentiality and probabilistic methods. The indifferent information

* *Corresponding author*. Tel.: +90-462-3773417 ; Fax: +90-462-3257405 ; E-mail address: tturker@ktu.edu.tr (T. Türker)
ISSN: 2149-8024 / DOI: http://dx.doi.org/10.20528/cjsmec.2016.06.014

of some parameters and random character of seismic events were caused the probabilistic analysis of earthquake hazard evaluation included some models of seismic sources, the earthquake return periods, the seismic signal attenuation, and distance addiction, and much uncertainty. Although in the obligation analysis of earthquake hazard evaluation the uncertainty was not believed, just the extreme seismic effect is estimated in the real territory, using near earthquake source with constant magnitudes. (Zaalishvili, 2012).

The probabilistic evaluation described first by Cornell which used in most earthquake hazard analysis, and usually receivable for four important information (Reiter 1991).

- Description of earthquake source regions
- Description of recurrence characteristic for each region
- Evaluation of earthquake effect
- Description of hazard at the territory.

The amount, sizes, and location of future earthquakes were determined a true approach by probabilistic estimates. (Bazzuro and Cornell, 1999).

In the past years, stochastic models of earthquake occurrence have been recommended (Kagan, 1996). The firstly reasons for the stochastic model formulation, the small number of parameters evaluated, the different of regions could be applied and the about ease with which hazard although a few sources might be combined. The hazard evaluation most important for earthquake forecasts knowledgeable determinations in of earthquakes hazard and exigency responsibility (Kagan, 2010). The occurring randomly in time, space and magnitude have long been determined by earthquake events. According to an assumption, earthquakes estimated a stochastic process free sequence of events space and extrication all of the energy at a point, space and in time. The happening of a next event was not attached to at the time, size or location of the last or no of the proceeding events. The detached supposition pleased the Poisson process. In accordance with the Poisson process, if a large earthquake consisted on at a point in time, the likelihood of another large event occurred in the near future is not changed (Anagnos and Kiremidjian, 1988). The Poisson model was well definitional earthquake occurrence which used for determined of the earthquake hazard analysis extensively in the time (Cornell, 1968).

The different researchers have applied the Poisson models in the world. The Poisson distribution used for determined the statistical distributions of earthquake numbers by Kagan (2010). The negative binomial distribution (NBD) has got a higher variance than the Poisson law, which could be shown (Kagan, 1973a; 1973b). The generalized Poisson distributions could be used to about earthquake numbers (Cornell, 1968). The some arbitrary compounding distributions from the empirical observations on the earthquake sequences which determined earlier for earthquake occurrences for the compound Poisson process models (Moharir, 1992) and compound Poisson models determined as alternatives to the Poisson process model (Singh 1983). The earthquake sequences which used estimating seismic risk relate to Poisson model (Molchan et al., 1970). Lenord et al. (2001) and more extensively and appropriated method based on the Poisson distribution which assumed different unknown variances for the frequencies, equal to the means.

The NAFZ has been the highest earthquake activity among regions in the world. Most large earthquakes have occurred on this fault system in Turkey. A lot of studies have been made to evaluate of earthquake hazards in the NAFZ. Semi-Markov method is applied for earthquakes larger than 5.5 magnitude occurred between 1900 to 1986 years (Altınok, 1988). Öncel et al. (1996) and Mäntyniemi and Kijko (1991) studied earthquake risk using maximum likelihood method. The earthquake hazard parameters are estimated with Kijko and Sellevoll method (Bayrak et al., 2011). Türker and Bayrak (2015b) determined the earthquake hazard using the Bayesian method in the NAFZ. Also, Bayrak and Türker investigated the earthquake hazard using different statistics methods in different areas of Turkey (Bayrak and Türker, 2015a; 2016a; 2016b).

The aim of this study; the important parameters of Gutenberg-Richter relationship (a and b values) estimated and these parameters taking into account, earthquakes were examined in the instrumental period for 10 different seismic source regions in the NAFZ. After that, estimated occurrence probabilities and return periods of occurring earthquakes in fault zone in the future years (10, 20, 30, 40, 50, 60, 70, 80, 90 and 100), and is appraised with Poisson method the earthquake hazard of the NAFZ.

2. Data and Seismic Source Regions

In this study; is used the instrumental earthquake catalog by Bayrak et al. (2009). A homogenous earthquake catalog for M_S magnitude which is equal or larger than 4.0 is used for the time period between 1900 and 2015. The catalogs contain the origin time, different magnitudes scales (M_B-body wave magnitude, M_S-surface wave magnitude, M_L-local magnitude, M_D-duration magnitude, and M_W-moment magnitude), epicenter and depth information of earthquakes. The database of catalog used in the study has been created from International Seismological Center (ISC) and Boğaziçi University Kandilli observation and earthquake research institute (KOERI). The earthquake data were obtained until from 1900 to 1974 from KOERI and ISC until from 1974 to 2015 from KOERI.

We prepared a homogenous data catalog for that period fulfill the basic requirement of homogeneity of M_S magnitude using relationship which is equal or larger than 4.0, and used only instrumental part of the earthquake catalogue. We applied decluster on the earthquake catalog. Earthquake catalogs were frequently declustered which using a pioneer to modeling the residual events as a substantiation of a spatially inhomogeneous in temporally homogeneous Poisson process (Luen and Stark, 2012).

We updated different nine seismic sources defined by Bayrak et al. (2011). We divided Region 3 given by Bayrak et al. (2011) into two different source regions considering Düzce Faults is a different source. Finally, 10 different seismic source regions shown in Fig. 1 are defined to study earthquake hazard parameters of NAFZ.

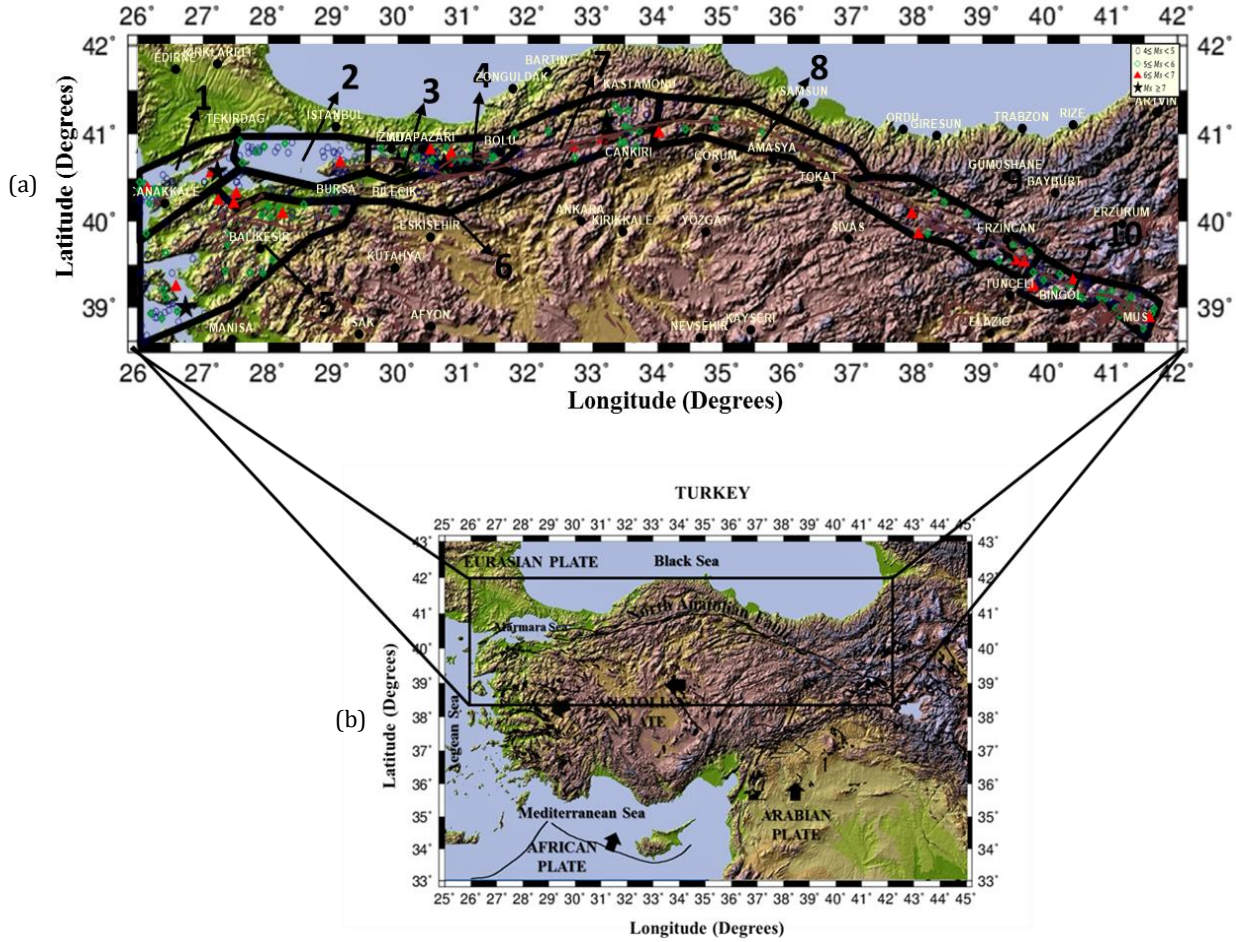

Fig. 1. a) The 10 different seismic source regions are shown on the North Anatolian Fault Zone (NAFZ); b) The epicenter of $M_S \geq 4.0$ are shown with different symbols. The NAFZ is demonstrated on Turkey map.

We divided into 10 different seismic source regions based on epicenter distribution, tectonics, seismicity and focal mechanism solutions as shown in Table 1.

3. Tectonic in the North Anatolian Fault Zone

The tectonic and seismicity of Turkey which were formed with plate movements in between African, Arabian, Eurasian and Anatolian (McKenzie, 1972; Alptekin, 1978; Dewey 1986; Şengör, 1979; Şengör et al., 1985). Many the large earthquakes occurred on the North Anatolian fault zone along which Turkey is moving westward. The North Anatolian Fault Zone (NAFZ) from tectonism the East Anatolian convergent zone and the Hellenic Arc occurred that the motion of Asia Minor is compensated by the completion of oceanic crust (McKenzie, 1972). The NAFZ has been a dextral strike-slip fault zone (Ketin, 1948) extending about 1200 km (Bozkurt, 2001) across northern Turkey and marking the boundary between the Anatolian and Eurasian plates (Ketin, 1969; Şengör et al., 1985; Barka, 1996; Şaroğlu, 1988). Developing hard localization in a usually westerly widening right-lateral kerogen in northern Turkey commonly along an interface arranging subduction-expansion material to its south and older and rigid continental basements to its north was occurred in the NAFZ.

Table 1. Seismic source regions.

Region	Region Name
1	Saroz Gulf
2	Marmara Sea
3	İzmit-Sakarya
4	Sakarya-Düzce
5	The Southern Branch of NAF
6	The Southern of Marmara
7	Düzce-Tosya
8	Tosya-Erbaa
9	Tokat-Erzincan
10	The East of Erzincan

Morphologically different and seismically active extends from the Gulf of Saros in the northern Aegean Sea from Karlıova, paralleling approximately the southern Black Sea support and keeping a rather ordinary distance of some 100 km to the coast, connecting the Aegean taphrogen (Şengör et al., 2005) with the East Anatolian high plateau (Koçyiğit et al., 2001; Şengör et al.,

2003). The fault occurred roundly 13 to 11 Ma ago in the east and propagated westward. It achieved the Sea of Marmara no earlier than 200 ka ago, though shear concerned deformation in a wide zone there had anyway introduced in the late Miocene (Şengör et al., 2005). The NAFZ starts around Karlıova triple junction in the east, and it runs NW to Vezirköprü that it makes a left bend and constant westward. Around Kargı, it makes another left bend and then runs in an SW direction (Bozkurt, 2001). The NAFZ is 85±5 km (Bozkurt, 2001; Şengör et al., 2003). Along of the NAFZ, the right-lateral slip has a rate of 24±1 mm/yr (McClusky et al., 2000; Flerit et al., 2004; Reilinger et al., 2006).

The western part of the NAFZ is an in the Marmara Sea region and the NAFZ divided into a complex fault structure, however, the eastern part of the NAFZ is a narrow strike-slip zone. The transition of the strike-slip regime in the east into a stress regime with N-S extension formed from this branching. The next, if the predominant E-W purposed graben structures in Western Anatolia could accountable, the Aegean region could have been typical. The northern branch of NAFZ is the most active fault zone in the Sea of Marmara according to the southern branch of NAFZ. The North branch exists as a zone comprised of boundary faults, normal faults and reverse faults in the Sea of Marmara. The NAFZ is young (~5 Ma) and has about 85 km of cumulative displacement (Hubert-Ferrari et al., 2009).

The NAFZ has been devastating earthquakes along with both historical and instrumental periods so the most active fault zone in Turkey. Historical investigations of major earthquakes along the NAFZ have revealed that in the twentieth century, ruptures migrated westward after the 1939 Erzincan earthquake in eastern Turkey (Barka and Kadinsky-Cade, 1988; Barka, 1996). This fault observed a lot of earthquakes of $M_S \geqslant 7.0$. In the instrumental period, the earthquakes in the NAFZ migrated from east to west and this process have begun with 1939 Erzincan earthquake (M_S=7.8).

4. Method

The Poisson method used one of the most common models to estimate the earthquake occurrences. According to the Poisson model was not affected since passing the time by the formation of a previous earthquake, distribution of waiting time by the formation of the next earthquake (Özdemir et al., 2000). The Poisson model is especially important for large earthquakes.

The sequence of events forms a Poisson process where the occurrence of a subsequent event did not depend on time, size or location of the last any of the preceding events. $N(t)$ as the number of events in the interval (0,t) the counting sequence ($N(t)$, t>=0) is Poisson provided.

$$P\{N(t+s)-N(t)=k\}=\frac{e^{-\lambda s}(\lambda s)^k}{k!} \quad k=0,1,2,\ldots;\ \lambda>0. \quad (1)$$

This relationship has been used as a model of the earthquake process in the Poisson process (Lomnitz, 1966).

The interval times for the Poisson process $\{T_1, T_2, T_3, \ldots\ldots, T_n\}$ should be exponentially distributed with probability density function $f_T(t)$ or $f_M(m)$and cumulative distribution $F_T(t)$ or $F_M(m)$ given.

$$f_T(t)=\lambda e^{-\lambda t} \qquad t\geq 0, \lambda>0, \quad (2)$$

$$F_T(t)=1-e^{-\lambda t} \qquad t\geq 0, \lambda>0, \quad (3)$$

where λ is the rate of occurrence of events. The Gutenberg-Richter relationship describing the number of earthquake events, $N(m)$, of a given magnitude, m or greater in time t was given.

$$Log\ N(m)=\ a-bm, \quad (4)$$

where a and b are earthquake hazard parameters. Thus for a given magnitude of exceedance the frequency of occurrence.

$$\lambda(t)=e^{\alpha-\beta m} \qquad m_o\leq m\leq m_{max}, \quad (5)$$

where m_o and m_{max} are the lower and upper bound magnitudes respectively. The lower magnitude arises from practical considerations. The upper magnitude is determined by the maximum earthquake capacity of a fault.

The earthquake hazard parameters for investigated area with the Poisson method were calculated using different equations.

$$a'=\ a-\ log\ (b*ln10), \quad (6)$$

$$a_1\ =\ a-\ log\ T, \quad (7)$$

$$a_1'=\ a'-\ log\ T. \quad (8)$$

T in this equation shows period for the next years and calculated for 100 years. The normal frequency value was used for annual average the number occurring of earthquakes which were shown by the following equation.

$$N(M)=10^{a_1'-b*M}. \quad (9)$$

$N(M)$ value indicated determining of the earthquake risk and has been calculated according to the seismic parameters.

$$R(M)=1-e^{-N(M)*T}. \quad (10)$$

T value in this model was different from other models and used to calculate of the earthquake occurring risk.

The return periods according to the Poisson model was calculated for the next years using the following equation.

$$Q(M)=\frac{1}{N(M)}. \quad (11)$$

The risk rate of the Poisson process is equal to the constant implying that the probability of occurrence of an earthquake in a future small increment of time, Δt, remains constant regardless of the size of the last event or the elapsed time since its occurrence.

5. Chi-Square Test for Poisson method

The chi-square test has used the fact that, conditional on the total number of events and the add distribution of the numbers of events in the probabilities.

The test statistic is;

$$\chi^2 = \sum_{k=1}^{K} \frac{(N_k - \hat{\lambda})^2}{\hat{\lambda}} \qquad k = \{1, \dots\dots, K\}. \tag{12}$$

If the hypothesis for applied Poisson method was true, the distribution of X^2 was determined from the Chi-square with K-1 degrees of freedom. The chi-square test involved choosing the number of intervals K. The chi-square test investigated only at the change of the observed number of events across intervals.

6. Results and Discussions

The NAFZ is one of the most seismically active regions of the Turkey and has been affected large earthquakes in the past years. The Poisson method is applied in order to check the potentiality of the different seismic source regions in the NAFZ for the future earthquake hazard. For this purpose, a homogeneous and complete seismicity database of the instrumental period during is used in 10 different seismic source regions in the examined region. For this aim; a and b parameters of Gutenberg-Richter relationship, the annual occurring number of earthquakes, return periods and earthquake risk in the next years.

The 10 different seismic source regions are estimated a and b parameters with equation (Eqs. (4) and (5)) of $LogN$=a-bM in the Gutenberg-Richter which are determined the relationships between the cumulative number-magnitude in shown Fig. 2. The earthquake hazard parameters are estimated for the 10 different seismic source regions of the NAFZ and shown in Table 2.

The b value is lower than the local mean value of 1.0, which indicates that the data consists of the larger earthquake and high differential crustal stress in the region (Wiemer and Katsumata, 1999; Wiemer and Wyss, 2002).

Table 2. The earthquake hazard parameters are estimated for 10 different seismic source regions on the NAFZ.

Region	Region name	a	$b \pm \sigma_b$	a/b	a'	a_1	a_1'	N	M_{max}^{obs}
1	Saroz Gulf	4.75	0.630±0.08	7.53	3.66	1.75	1.66	65	7.3
2	Marmara Sea	5.00	0.688±0.09	7.26	3.79	1.92	1.78	53	7.3
3	İzmit-Sakarya	4.92	0.685±0.09	7.18	3.79	1.92	1.79	59	7.8
4	Sakarya-Düzce	4.68	0.611±0.07	7.65	3.60	1.68	1.60	87	7.2
5	The Southern Branch of NAF	5.64	0.859±0.1	6.56	4.39	2.64	2.39	44	7.0
6	The Southern of Marmara	5.56	0.731±0.06	7.60	4.39	2.56	2.39	117	7.2
7	Düzce-Tosya	4.53	0.548±0.05	8.26	3.51	1.53	1.51	54	7.3
8	Tosya-Erbaa	4.42	0.617±0.1	7.16	3.34	1.42	1.34	20	7.1
9	Tokat-Erzincan	4.18	0.501±0.05	8.34	3.21	1.18	1.21	44	7.9
10	The east of Erzincan	5.12	0.651±0.04	7.86	4.01	2.12	2.01	94	6.8

The b values which is one of the most important earthquake hazard parameters are estimated using Eq. (4) with Poisson method for 10 different seismogenic source regions of the NAFZ. The map of estimated b values is plotted (Fig. 6). The estimated b values for the 10 different regions of the NAFZ vary between 0.501 and 0.859. The highest b value is observed in region 5 covering the Southern Branch of NAFZ, while the lowest b value is observed in region 9 covering the Tokat-Erzincan. The a/b values are estimated with Poisson method for 10 different seismogenic source regions. The map of estimated a/b values is plotted (Fig. 7). The highest a/b value is observed in region 9 covering the Tokat-Erzincan. The lowest a/b value is observed in region 5 covering the Southern Branch of NAFZ.

We plotted the maps of the occurrences probability of the earthquakes and return periods in the 6.5, 7.0, 7.5 and 8.0 magnitudes in next 100 years, respectively that shown in Figs. 8 and 9. The calculated changes between regions observed from a region to another region, clearly.

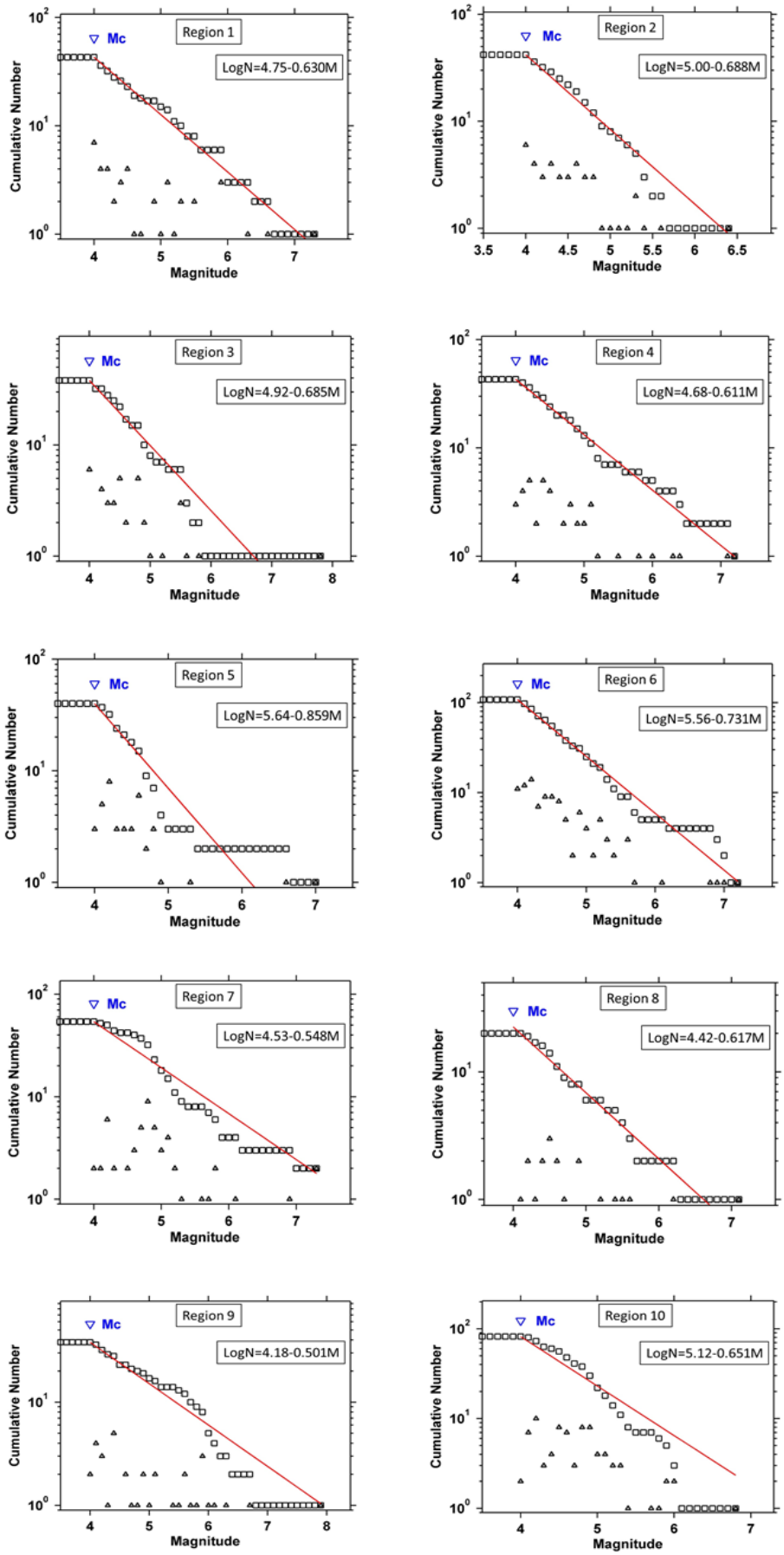

Fig. 2. The Magnitude-Frequency (Gutenberg-Richter) relationships are shown for occurring earthquakes on the NAFZ. The overall catalog plotted is observed both the cumulative (squares) and noncumulative form (triangles) in frequency magnitude distribution.

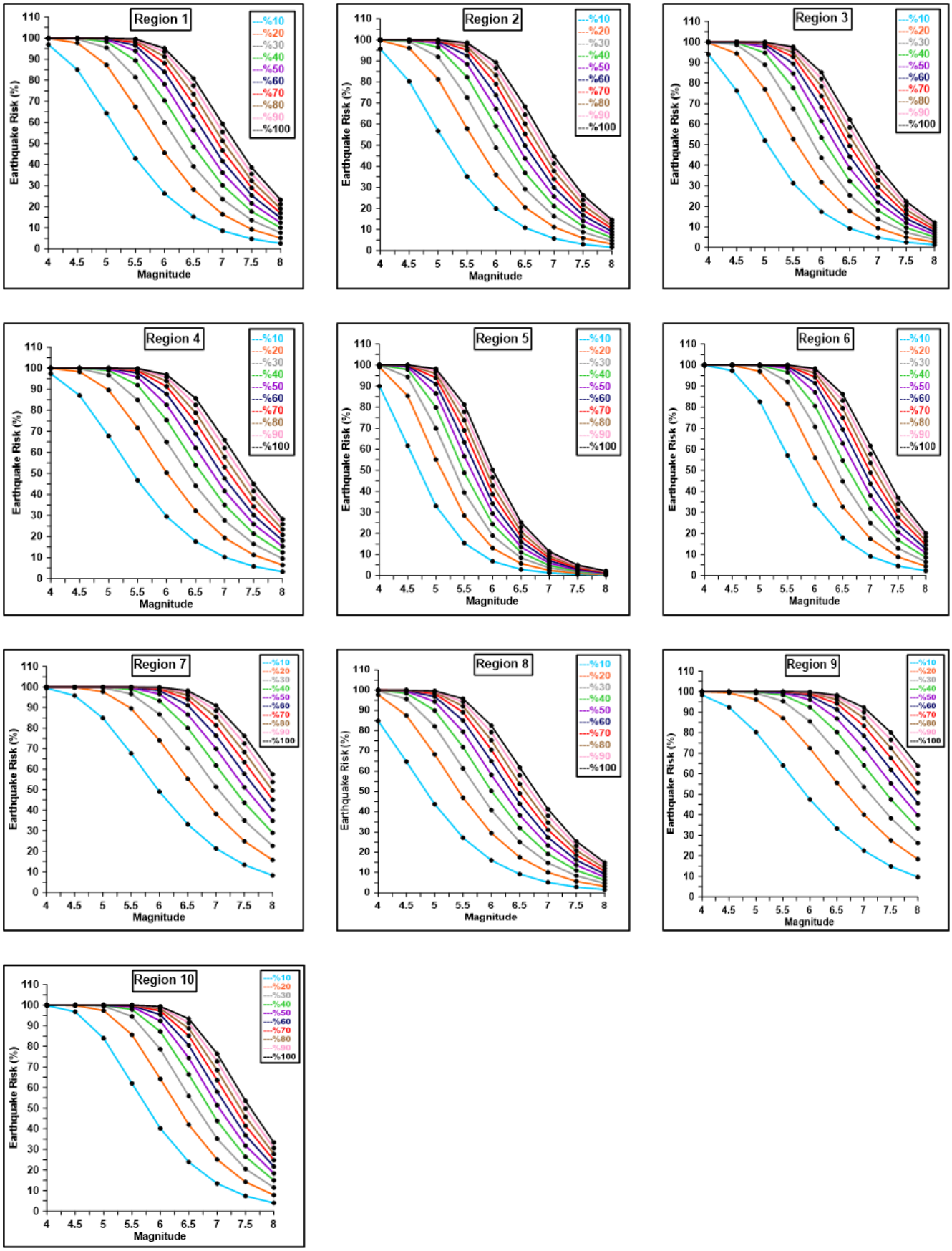

Fig. 3. The earthquake risk (%) values are estimated for the 10 different seismic source regions.

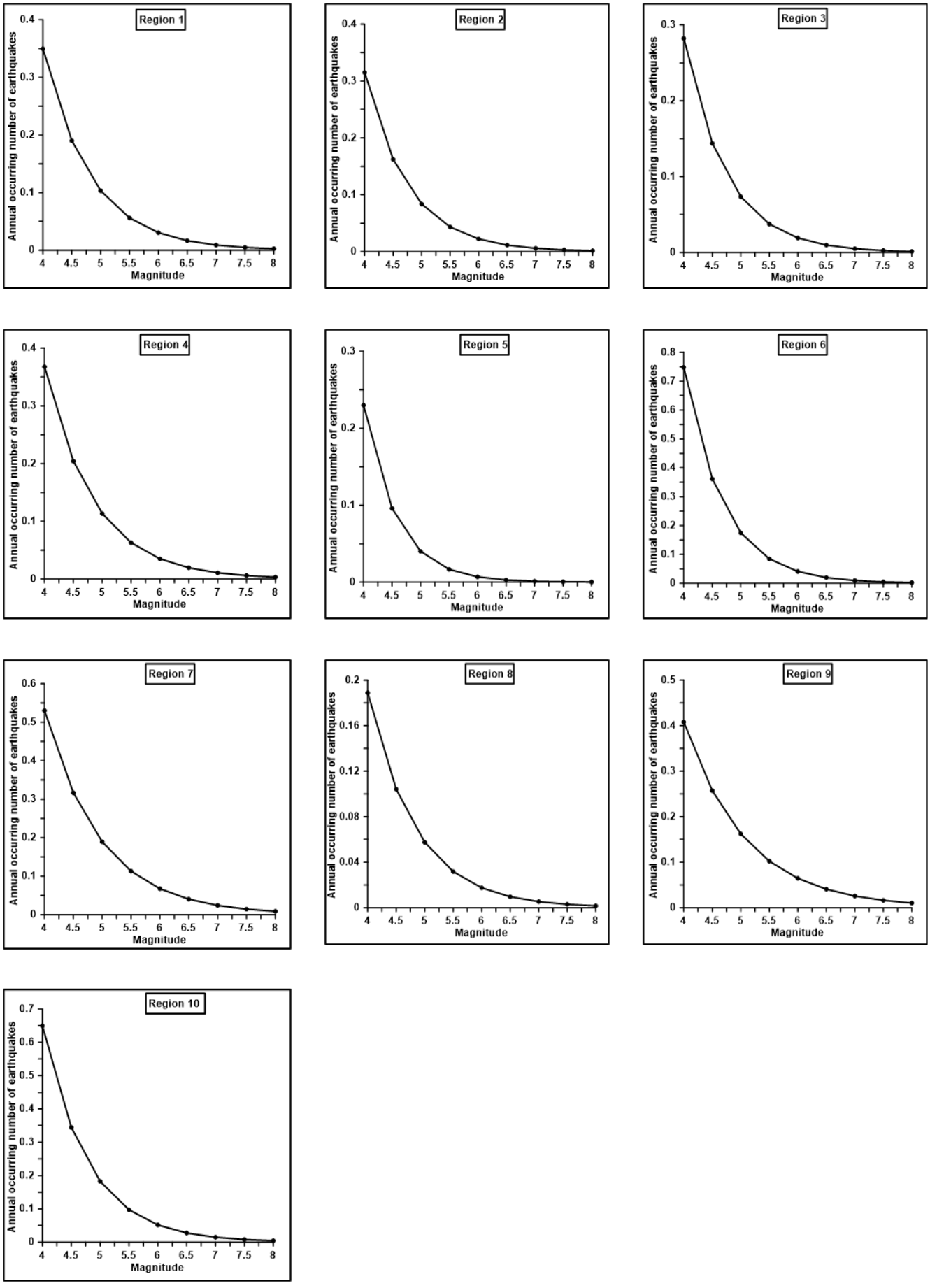

Fig. 4. The annual occurring number of earthquakes are estimated for the 10 different seismic source regions.

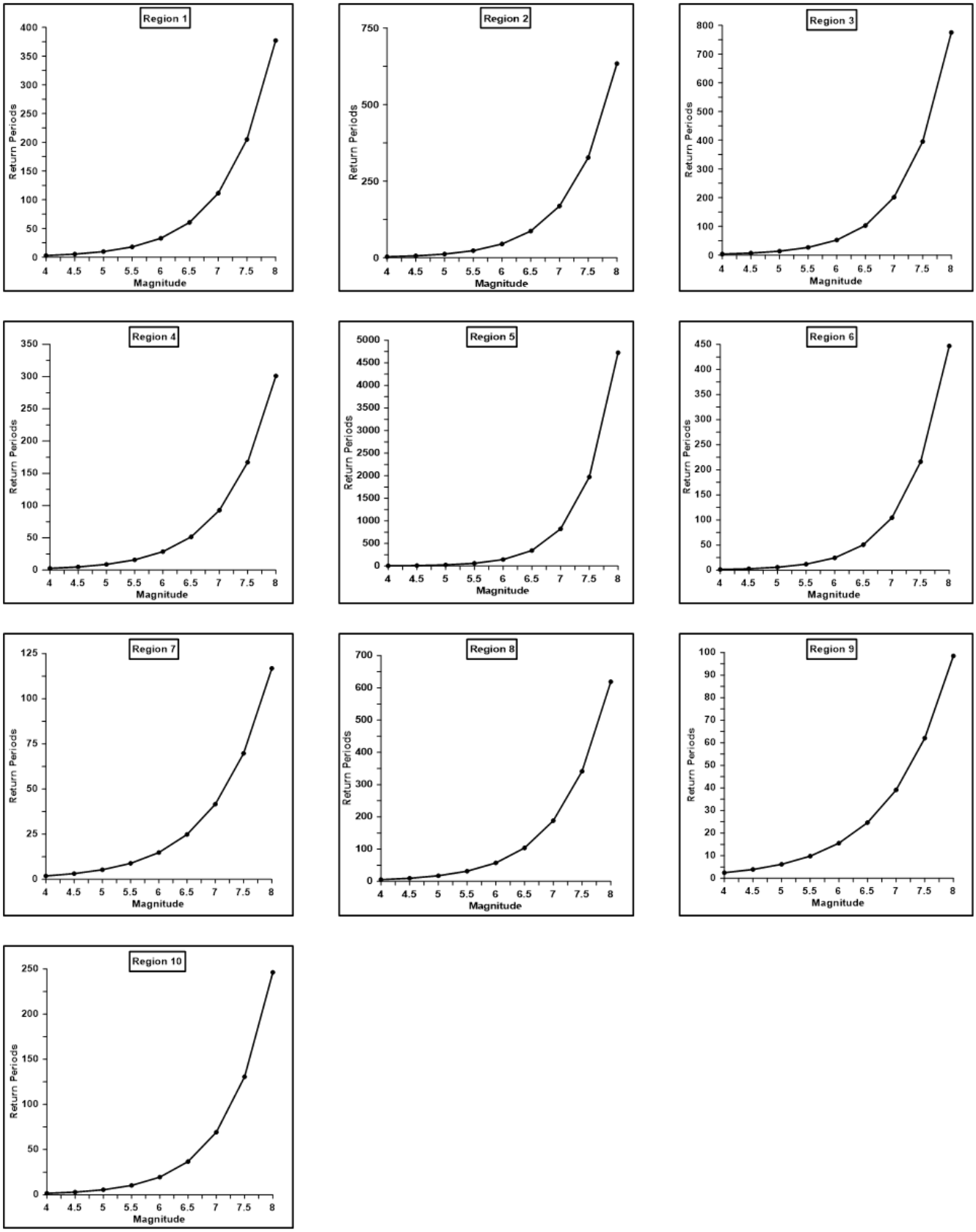

Fig. 5. The return periods are estimated for the 10 different seismic source regions.

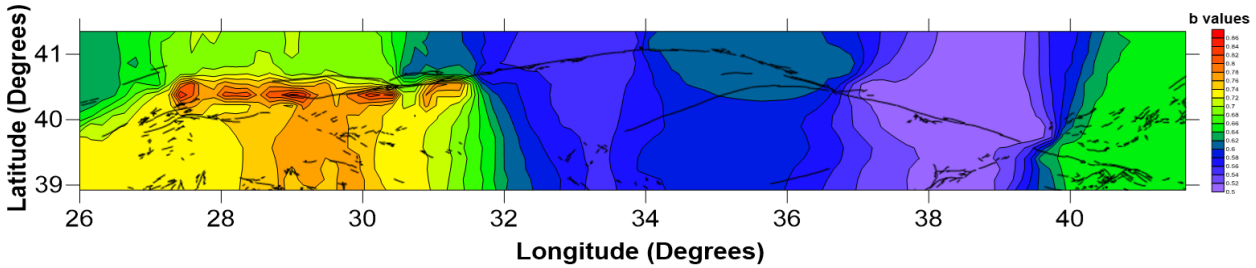

Fig. 6. The map of estimated b values are plotted for 10 different seismic source regions of the NAFZ.

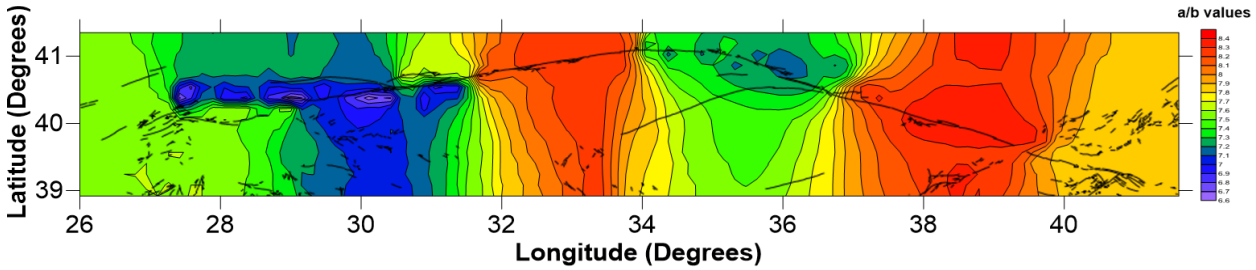

Fig. 7. The map of estimated a/b values are plotted for 10 different seismic source regions of the NAFZ.

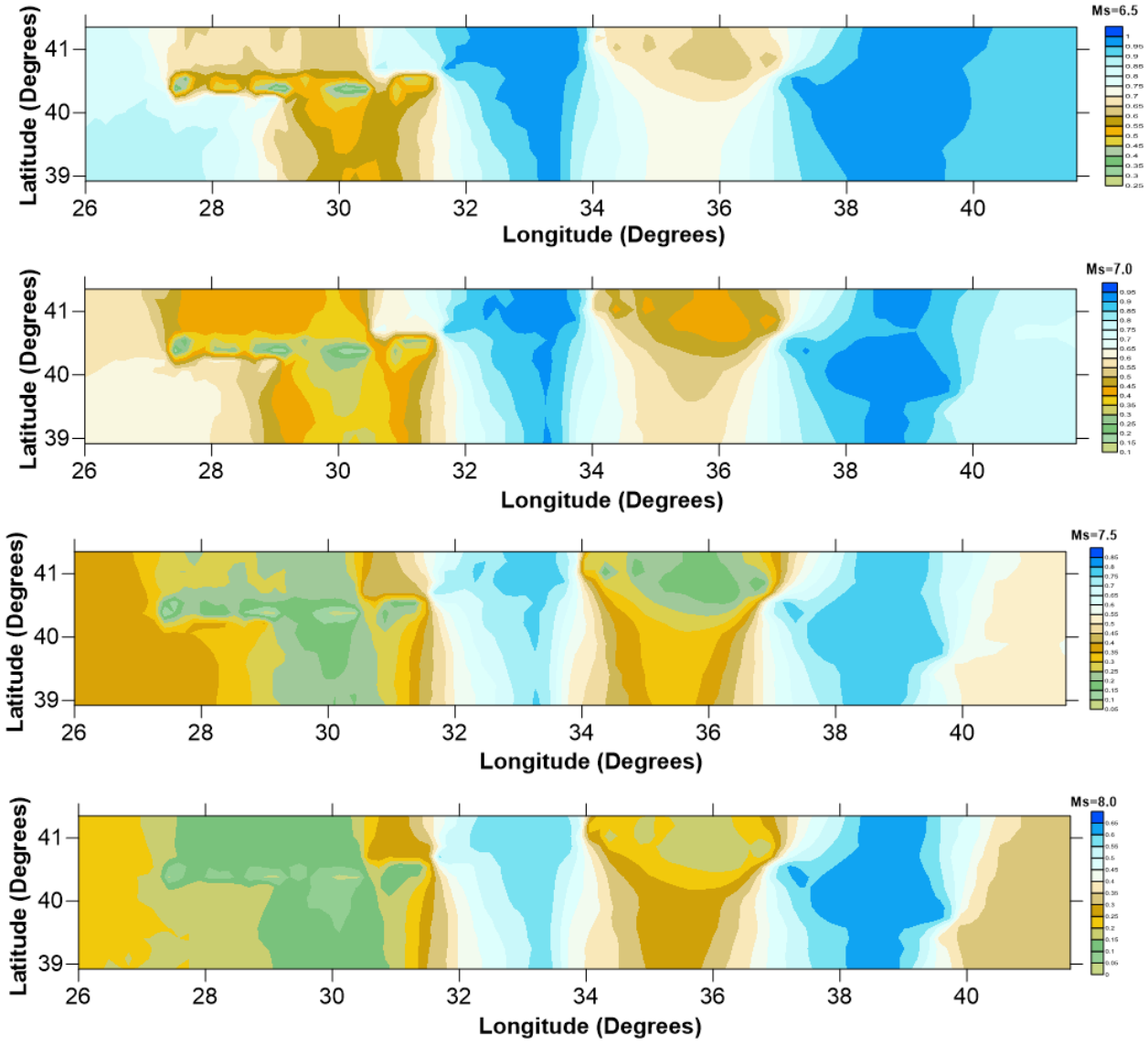

Fig. 8. The maps of the occurrences probability of the earthquakes in the 6.5, 7.0, 7.5 and 8.0 magnitudes are plotted in next 100 years, respectively.

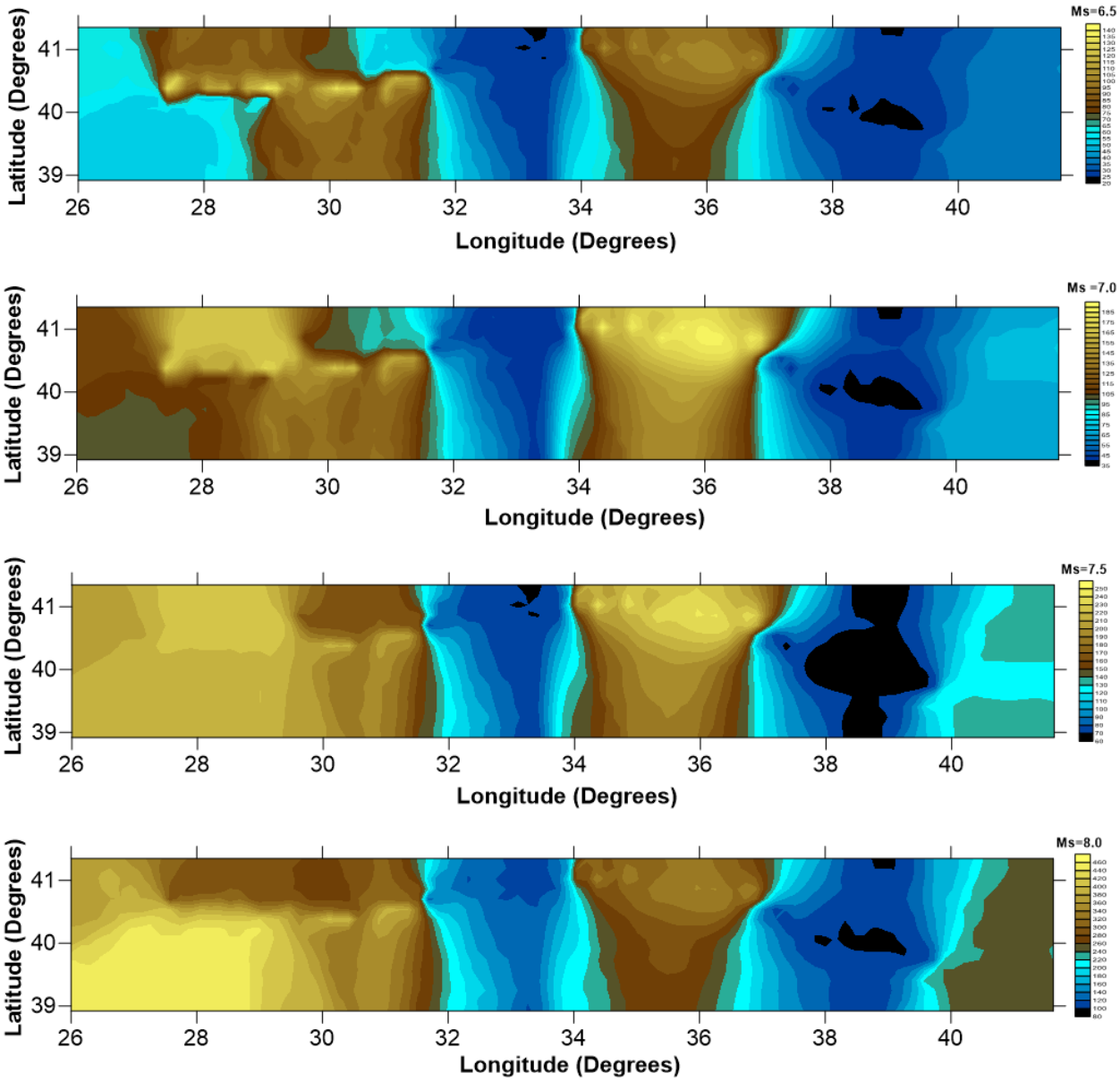

Fig. 9. The maps of the return periods in the 6.5, 7.0, 7.5 and 8.0 magnitudes are plotted for in next 100 years, respectively.

The probabilities of the earthquake occurring are estimated for the future 10, 20, 30, 40, 50, 60, 70, 80, 90 and 100 years in the 10 different seismic source regions and are shown in Fig. 3. The highest earthquake occurring probabilities in 10 different seismic source regions in the next years estimated that the region 9. We are estimated annual occurring number of earthquakes ($N(M)$) using Eq. (10) for 10 different seismic regions which are shown in Fig. 4. The region 9 is observed 0.0644 annual occurring number of magnitude of 6 magnitude, 0.0406 annual occurring number of magnitude of 6.5 magnitude, 0.0256 annual occurring number of magnitude of 7 magnitude, 0.0161 annual occurring number of magnitude of 7.5 magnitude, 0.0102 annual occurring number of magnitude of 8 magnitude. If region 2 observed 0.0223 annual occurring number of magnitude of 6 magnitude, 0.0115 annual occurring number of magnitude of 6.5 magnitude, 0.0059 annual occurring number of magnitude of 7 magnitude.

Earthquake recurrence times (return periods, $Q(M)$) estimated using the parameters of Gutenberg-Richter relationship and are shown in Fig. 5. The region Tokat-Erzincan (Region 9) is estimated for the future 100 years using Eqs. (9) and (11), respectively. The region 9 is estimated 99% with an earthquake occur probability for magnitude 6.5 which the return period 24.7 year, 92% with an earthquake occur probability for magnitude 7 which the return period 39.1 year, 80% with an earthquake occur probability for magnitude 7.5 which the return period 62.1 year, 64% with an earthquake occur probability for magnitude 8 which the return period 98.5 year. For the Marmara Region (Region 2) in the next 100 year is estimated that 89% with an earthquake occur probability for magnitude 6 which the return period 44.9 year, 45% with an earthquake occur probability for magnitude 6.5 which the return period 87 year, 45% with an earthquake occur probability for magnitude 7 which the return period 168.6 year.

In the past, Bayrak and Türker (2015b) estimated an earthquake occurrence probability (in the next 100 years) in region Tokat-Erzincan using the Bayesian method for the NAFZ. In this study, we are estimated the same of results. Both the Bayesian method and the Poisson method are estimated an earthquake occurrence probability with most probably in the region Tokat-Erzincan for the next 100 years in the NAFZ.

7. Conclusions

In this study, The NAFZ was estimated earthquake hazard parameters (a and b values and their different values of Gutenberg-Richter relationship) in the future years for instrumental catalog during complete seismic catalogue with M_S≥4.0. For this aim, the annual occurring number of earthquakes, return periods and earthquake risk were estimated in the next 100 years. a and b values for this time period were estimated to be equal to 0.501 and 0.859, respectively. b values were observed the data form of larger earthquakes and high diversity crustal stress. We were applied the chi-square test for estimated values with Poisson method. Therefore, we were tested to the accuracy of the Poisson method. According to the chi-square test was applied for Poisson method and significance level estimated as α=0.05 in this study. Also, whole estimates were determined with Matlab program. Maps were plotted using GMT program. The annual occurring number of earthquakes were estimated for magnitudes 6.5, 7, 7.5 and 8 at region 9 while 6, 6.5 and 7 at region 2 in the NAFZ. This values were estimated respectively in region 9, 0.0644 for magnitude 6, 0.0406 for magnitude 6.5, 0.0256 for magnitude 7, 0.0161 for magnitude 7.5, 0.0102 for magnitude 8. In region 2, 0.0223 for magnitude 6, 0.0115 for magnitude 6.5, 0.0059 for magnitude 7, 0.0031 for magnitude 7.5. Also, the return periods were estimated for magnitude 6.5, 7, 7.5, and 8 at region 9, while 6, 6.5 and 7 at region 2. This values were estimated in region 9, respectively which 24.7 years for magnitude 6.5, 39.1 years for magnitude 7, 62.1 years for magnitude 7.5, 98.5 years for magnitude 8. Their earthquake risk values were estimated respectively, 99%, 92%, 80% and 64%. If region 2, 44.9 years for magnitude 6, 87 years for magnitude 6.5, 168.6 years for magnitude 7. Their earthquake risk values estimated respectively, 89%, 45% and 45%.

References

Alptekin Ö (1978). Magnitude-Frequency Relationships and Deformation Release for the Earthquakes in and around Turkey. *Thesis for Promoting to Associate Professor Level.* Karadeniz Technical University, Trabzon (in Turkish).

Altınok Y (1988). Seismic risk estimation of the North Anatolian Fault Zone using Semi-Markov Model. *Jeofizik*, 2, 44-58.

Anagnos T, Kiremidjian AS (1988). A review of earthquake occurrence models for seismic hazard analysis. *Probabilistic Engineering Mechanics*, 3, 3-11.

Barka A (1996). Slip distribution along the North Anatolian Fault associated with the large earthquakes of the period 1939 to 1967. *Bulletin of the Seismological Society of America*, 86, 1238–1254.

Barka A, Kadinsky-Cade K (1988). Strike-slip fault geometry in Turkey and its influence on earthquake activity. *Tectonics*, 7, 663-684.

Bayrak Y, Çınar H, Bayrak E (2011). The North Anatolian Fault Zone: An evaluation of earthqauke hazard parameters. *New Frontiers in Tectonic Research-At The Midst of Plate Convergence*, *Edited by Scatter U*, 269-288.

Bayrak Y, Oztürk S, Cınar H, Kalafat D, Tsapanos T, Koravos CG, Leventakis GA (2009). Estimating earthquake hazard parameters from instrumental data for different regions in and around Turkey. *Engineering Geology*, 105, 200–210.

Bayrak Y, Türker T (2016a). The determination of earthquake hazard parameters deduced from Bayesian approach for different seismic source regions of Western Anatolia. *Pure and Applied Geophysics*, 173, 205-220.

Bayrak Y, Türker T (2016b). The evaluation of the earthquake hazard using the exponential distribution method for different seismic source regions in and around Ağrı. *International Conference on Advances in Natural and Applied Sciences*, *Icanas 2016*, *Antalya*, *Turkey*, 1726, 1, 0200001,1-0200001,4.

Bazzurro P, Cornell CA (1999). Disaggregation of Seismic Hazard. *Bulletin of the Seismological Society of America*, 89, 501-520.

Bozkurt E (2001). Neotectonics of Turkey-a synthesis. *Geodinamica Acta.* 14, 3-30.

Cornell CA (1968). Engineering risk in seismic analysis. *Bull. Seism. Soc. Am.* 54, 583-1606.

Dewey JF, Hempton MR, Kidd WSF, Şaroğlu F, Şengör AMC (1986). Shortening of continental litosphere: The tectonics of Eastern Anatolia-young collision zone, in collision tectonics. *Edited by Coward MP and Ries AC. Geological Society*, *London*, *Special Publication* 19:3-36.

Flerit F, Armijo R, King G, Meyer B (2004). The Mechanical interaction between the propagating North Anatolian Fault and the back-arc extension in the Aegean. *Earth and Planetary Science Letters*, 224, 347–362.

Hubert-Ferrari A, Armijo R, King G, Meyer B, Barka A (2002). Morphology, displacement and slip rates along the North Anatolian Fault, Turkey. *Journal of Geophysical Research*, 107(10), 1029-1059.

Kagan YY (1973a). A probabilistic description of the seismic regime, Izv. Acad. Sci. USSR, (English translation). Scanned versions of the Russian and English text are available at http://eq.ess.ucla.edu/~kagan/pse 1973 index.html. *Physics of the Solid Earth*, 213-219.

Kagan YY (1973b). Statistical methods in the study of the seismic process (with discussion: Comments by M. S. Bartlett, A. G. Hawkes, and J. W. Tukey). Scanned version of text is available at http://moho.ess.ucla.edu/~kagan/Kagan 1973b.pdf. *Bulletin of the International Statistical Institute*, 45(3), 437-453.

Kagan YY (1996). Comment on "The Gutenberg-Richter or characteristic earthquake distribution, which is it?" by Steven G. Wesnousky. *Bulletin of the Seismological Society of America*, 86, 274-285.

Kagan YY (2010). Statistical distributions of earthquake numbers: consequence of branching process. *Geophysical Journal International*, 180(3), 1313–1328.

Ketin I (1948). Über die tektonisch-mechanischen Folgerungen aus den grossen anatolischen Erdbeben des letzten Dezenniums. *Geologische Rundschau*, 36, 77-83 (in German).

Ketin I (1969). Über die nordanatolische Horizontalverschiebung. *Bulletin of the Mineral Research and Exploration Institute of Turkey*, 72, 1-28 (in German).

Koçyiğit A, Yılmaz A, Adamia A, Kuloshyili S (2001). Neotectonics of East Anatolian Plateau (Turkey) and Lesser Caucasus: implication for transition from thrusting to strike-slip faulting. *Geodinamica Acta.* 14, 177-195.

Lomnitz C (1966). Statistical prediction of earthquakes. *Reviews of Geophysics*, 4, 377-393.

Luen B, Stark PB (2012). Poisson tests of declustered catalogues. *Geophysical Journal International*, 189(1), 691–700.

Mäntyniemi P, Kijko A (1991). Seismic hazard in East Africa: An example of the application of incomplete and uncertain data. *Natural Hazards*, 4, 421-430.

McClusky S, Balassanian S, Barka A, Demir C, Ergintav S, Georgiev I, Gürkan O, Hamburger M, Kahle KHH, Kastens K, Kekelidze G, King

R, Kotzev V, Lenk O, Mahmoud S, Mishin A, Nadariya M, Ouzounis A, Paradissis D, Peter Y, Prilepin M, Reilinger R, Şanlı I, Seeger H, Tealeb A, Toksöz MN, Veis G (2000). Global positioning system constraints on plate kinematics and dynamics in the Eastern Mediterranean and Caucasu. *Journal of Geophysical Research*, 105(B3), 5695–5719.

McKenzie DP (1972). Active tectonics of the Mediterranean region. Geophysical *Journal of Royal Astronomical Society*, 30, 109-185.

Moharir PS (1992). Estimation of the compounding distribution in the compound Poisson process model for earthquakes. *Proceedings of the Indian Academy of Science (Earth and Planetary Science Letters)*, 101, 347-359.

Molchan GM, Keılıs-Borok VI, Vılkovıch GV (1970). Seismicity and principal seismic effects. *Geophysical Journal*, 21, 235-411.

Öncel AO, Main L, Alptekin Ö, Cowie P (1996). Spatial variations of the fractal properties of seismicity in the Anatolian Fault Zones. *Tectonophysics*, 257, 189-202.

Özdemir F, Necioğlu A, Bağcı GF (2000). Geophysic. *JFMO Press*, 14, 1-2.

Reilinger R, McClusky S, Vernant P, Lawrence S, Ergintav S, Cakmak R, Özener H, Kadirov F, Guliev I, Stepanyan R, Nadariya M, Hahubia G, Mahmoud S, Sakr K, ArRajehi A, Paradissis D, Al-Aydrus A, Prilepin M, Guseva T, Evren E, Dmitrotsa A, Filikov SV, Gomez F, Al-Ghazzi R, Karam G (2006). GPS constraints on continental deformation in the Africa-Arabia- Eurasia continental collision zone and implications for the dynamics of plate interactions. *Journal of Geophysical Researches*, 111, B0541.

Reiter L (1991). Earthquake Hazard Analysis. Columbia Univ. Press, New York, 1-245.

Şaroğlu F (1988). Age and off-set of The North Anatolian Fault. *Journal Pure Applied Science*, 21, 65-79.

Şengör AMC (1979). The North Anatolian transform fault: its age, offset and tectonic significance. *Journal of the Geological Society*, 136, 269-282.

Şengör AMC, Görür N, Şaroğlu F (1985). Strike-slip faulting and related basin formation in zones of tectonic escape: Turkey as a case study. *The Society of Economic Paleontologists and Mineralogists*, *Special Publication*, 37, 227-264.

Şengör AMC, Özeren S, Zor E, Genç T (2003). East Anatolian high plateau as a mantle-supported, N-S shortened domal structure. *Geophysical Research Letters*, 30(24), 1-4.

Singh H (1983). Compound Poisson process models for earthquake occurrences. *M. Tech. Dissertation.* University of Roorkee, Roorkee.

Türker T, Bayrak Y (2015a). Assessment of the earthquake hazard analyses with Bayesian method in the Eastern Anatolian and around. *Activite Tectonic Research Group Congress*, Sakarya, Turkey.

Türker T, Bayrak Y (2015b). The earthquake hazard analysis using bayesian method of the North Anatolia fault. *5th International Earthquake Symposium*, Kocaeli, Türkiye, 366-367.

Wiemer S, Katsumata K (1999). Spatial variability of seismicity parameters in aftershock zones. *Journal of Geophysical Research*, 13, 135-151.

Wiemer S, Wyss M (2002). Mapping spatial variability of the frequencymagnitude distribution of earthquakes. *Advances in Geophysics*, 45, 259–302.

Zaalishvili VB (2012). Assessment of Seismic Hazard of Territory. *In: Earthquake Engineering*, *edited by Halil Sezen*, InTech, Rijeka, 26-64.

Challenge Journal of Structural Mechanics

Test on dynamic performance of silt-concrete structure system under cyclic loading with different frequency

Liyun Li *, Xiuli Du, Xiaoqiong Wang, Shengxia Zhang, Aijun Yao

Key Laboratory of Urban Security and Disaster Engineering of Ministry of Education, Beijing University of Technology, Beijing 100124, China

ABSTRACT

In order to study the dynamic response of the soil-structure system and the contact performance between soil and structure under cyclic loading, a Suspensory Ring Test Apparatus was designed by the authors, and a series of tests had been carried out. The physical properties of the test silt were that ρ=1.59g/cm^3, ω_P=14.26%, ω_L=21.77%. In the paper, The Suspensory Ring Test Apparatus was introduced firstly. Then, the test data were analyzed in two aspects, that was (1) the damage mechanism of the soil-structure system, (2) the factors which affected on contact performance between silt and concrete structure under cyclic loading, such as moisture content, loading frequency, roughness, and so on. Finally, some conclusions were also proposed.

ARTICLE INFO

Article history:
Received 3 May 2016
Accepted 19 June 2016

Keywords:
soil-structure system
dynamic response
contact performance
damage mechanism

1. Introduction

Soil and Structure Interaction (SSI) is very important to study the dynamic response and damage of underground structure, where the description of contact performance between soil and structure is a key problem. Now, there have been many research fruits on the aspect. For example, Potyondyj (1961), as a pioneer, studied the Skin friction performance between various soils and construction materials using direct shear apparatus. Yoshini and Kishida (1981) designed a ring torsion apparatus for evaluating friction between soils and metal surfaces. Desai et al. (1985) discussed the mechanical properties of Soil-structure interface under cyclic loading. Zhang and Zhang (2003) designed an apparatus called TH-20t Cyclic Shear Apparatus for Soil-structure Interface, and many experimental studies have been carried out using this apparatus. Westgate and DeJong (2006) researched the evolution of sand-structure interface response during monotonic shear using particle image velocimetry. Zhang et al. (2008) developed a 3D soil-structure interface test apparatus. Li and Li (2010) developed a test apparatus which was patient of unrestricted deformation of soil in interface area along shear direction. Cai et al. (2010) and Li et al. (2012) improved their test apparatus to research the contact performance between soil and structure respectively. We know that the mechanical performance of material is affected by loading velocity, so, we think loading frequency maybe affect the mechanical performance of material, due to the earthquake includes many different frequency waves. But the literatures about the influence of loading frequency on contact performance between soil and structure are very few. At the same time, these above research did not considering the soil's deformation during test. In order to study the dynamic performance of soil and structure system comprehensively, based on DYS-200-1-05 shaking table system, we designed a Suspensory Ring Test Apparatus (Li et al., 2013). Using the apparatus, the dynamic performance of silt and concrete structure system was researched, and some conclusions were proposed in this paper.

2. Suspensory Ring Test Apparatus

The suspensory ring test apparatus was designed by reforming the DYS-200-1-05 shaking table system. Fig. 1 is its Skeleton drawing. The DYS-200-1-05 shaking table system include the output power system which provide

* *Corresponding author*. Tel.: +86-10-6739-1931 ; Fax: +86-10-6739-2430 ; E-mail address: lly@bjut.edu.cn (L. Li)
ISSN: 2149-8024 / DOI: http://dx.doi.org/10.20528/cjsmec.2016.06.015

the horizontal force and the table system to fix the test structure, where the low frequency can reach 0.5Hz, the vibration displacement can arrive 40mm, and the maximum vertical loading is 100kg. The table system is connected to the output power system with connector and dynamic force sensor. During testing, the structure board was fixed on the table, the suspensory ring container was hanged above the structure slab, and the contact area between soil and structure would be not changed due to the size of structure slab was larger than the diameter of the container. The suspensory ring container was made of latex film around with several aluminum ring, thus the soil can horizontal deform in test. The diameter of two containers was 150mm and 100mm respectively, and the aluminum ring's size was 3mm×5mm (thickness×height) with 5mm space. The displacement sensor 1 (DIS1) was located on the structure board, the displacement sensor 2 (DIS2) lied on the lowest aluminum ring contact the structure, and the displacement sensor 3 (DIS3) lied on the aluminum ring near the lowest one, parallel to the interface between soil and structure. Then, the two shear deformation SD1=DIS1-DIS2 and SD2=DIS2-DIS3 stand for the shear deformation on contact interface between soil and structure and that on soil body respectively. The vertical external force can be input on the top of the soil with additional weight. The dynamic force sensor was a MCL-Z force sensor, used to record the force history along the interface.

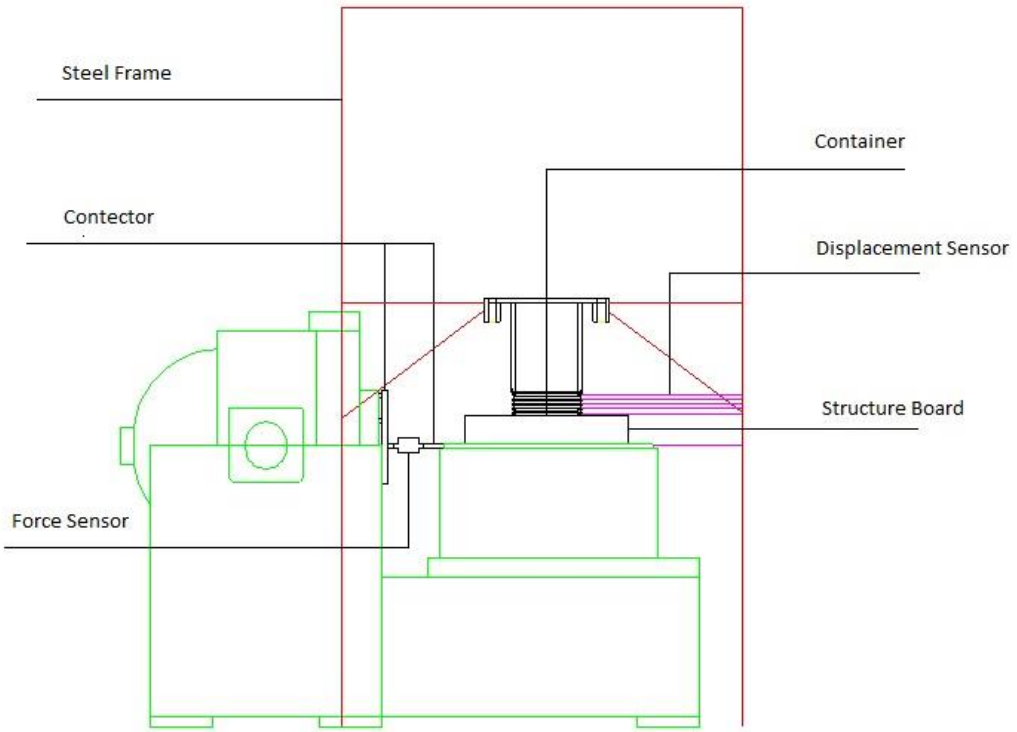

Fig. 1. Skeleton drawing.

The apparatus' features and applications include the following aspects. Firstly, the vertical force on the interface was constant, and the horizontal force paralleled to the interface can be carried out by different frequency. Secondly, the shear distortion of the test soil was considered, thereby, the relationship between destroy of soil-structure system and that of soil can be studied in test. Thirdly, the influence of some factors including the load frequency and velocity on the contact performance between soil and structure can be researched.

Fig. 2 is the relation between loading frequency and ratio of force to displacement in different assembling stage, where there is nothing on the shaking table at stage I, the structure board has been fixed on the shaking table at stage II, and the container has been hanged above the structure board at stage III. As shown in Fig. 2, the ratio of force to displacement at stage II is consistent with that at stage III, thus, the friction is very low between the container and the structure board, and the incremental force could only be caused by the soil in container during test. So, the shear force along the interface is $SF=F_{III}-F_{II}$.

3. Overview of the Experiments

In order to study the response of the soil-structure system and the contact performance between soil and structure under cyclic loading systematically, a series of tests had been carried out by using the suspensory ring test apparatus designed by the authors. The test soil was silt, whose physical properties were that ρ_d=1.59g/cm^3, w_P=14.26%, w_L=21.77%, c=6.26kPa, and φ=34.96°. One of the test structures was a plain concrete board (STR1), the other was concrete board covered with reinforcing net of 20mm with the diameter of 2.0mm (STR2). Table 1 shows the test cases.

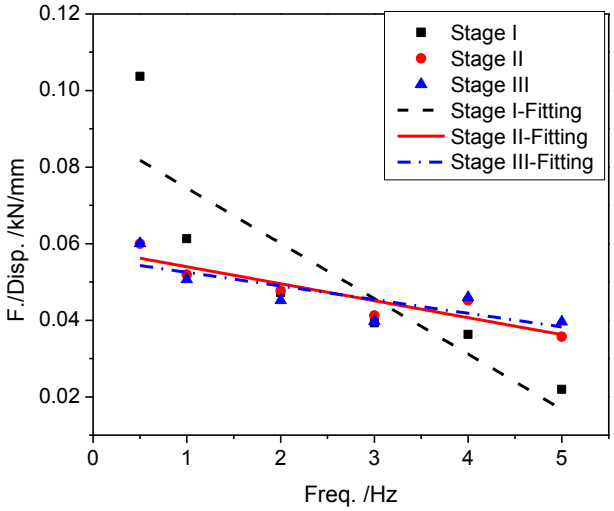

Fig. 2. Relation between loading frequency and ratio of force to displacement.

Table 1. Test cases.

Loading Freq. (Hz)	Moisture content (%)					
	14.3	8.1	7.1	6.3	5.4	4.1
0.5	√	√				
1.0	√	√		√		
1.5	√	√		√		
2.0	√	√	√	√	√	√
2.5	√	√	√	√	√	
3.0	√	√	√	√	√	√
3.5			√		√	√
4.0	√		√	√	√	√
5.0	√		√	√	√	√
6.0			√		√	√

4. Analysis of Test Results

4.1. Mechanism of silt-structure system

Fig. 3 is a typical record curves under 0.5Hz loading, where the moisture content of silt is 14.3%. Fig. 4 is the shear deformation curve deduced from Fig. 3. From Fig. 3, we find that the increasing of the displacements is slower than that of shear force along the interface between soil and structure. Fig. 4 indicates that the shear deformation on the interface between soil and structure is different to that on soil, the shear deformation on the interface increases fast with the increasing in shear force until the destruction, but, the shear deformation on the soil is basically unchanged. Finally, the damage of the silt-structure system is taken place on the interface between soil and structure. But, the other test data represent that the shear deformation on the soil can be larger than that on the interface when the loading frequency reached a certain value, we will talk about it in the following.

As shown in Fig. 5, the SD2/SD1 is related to the moisture content of soil and the loading frequency, which indicate that the SD2/SD1 increase and then decrease with the increasing in loading frequency, and the peak value of SD2/SD1 increase with the increasing in moisture content of soil. Because SD1 and SD1 stand for the shear deformation on contact interface between soil and structure and that on soil body respectively, the system damaged will be found in soil when SD2/SD1>1.0.

Fig. 6 is a typical hysteresis loop, where the moisture content of silt is 14.3%. Fig. 6 presents that the development of the deformation can be divided into three phases. First, the size of hysteresis loop is very small, and its long axis is almost horizontal, where the shear force and shear deformation are all low. Second, the shear force increases quickly, and the long axis of hysteresis loop turns into vertical direction. Third, the shear deformation is larger and larger with the increasing in shear force, and the size of hysteresis loop also become large to a value, and its long axis is going to horizon again. So, the damage of the soil-structure system will be occurred between the

second phase and the third phase, and that the energy dissipation may be used to study the contact performance because of the hysteresis loop represents the energy dissipation during deformation under cyclic loading. Fig. 7 is a typical relationship between energy dissipation and number of loading cycle which also indicate that the development of deformation of the soil-structure system includes three phases. Fig. 8 shows that the monocycle energy will decrease and the number of cycle will increase with the increasing in loading frequency to cause the soil-structure system damaged. So, the total energy dissipation will be employed in order to eliminate the influence of the number of cycle in the following study.

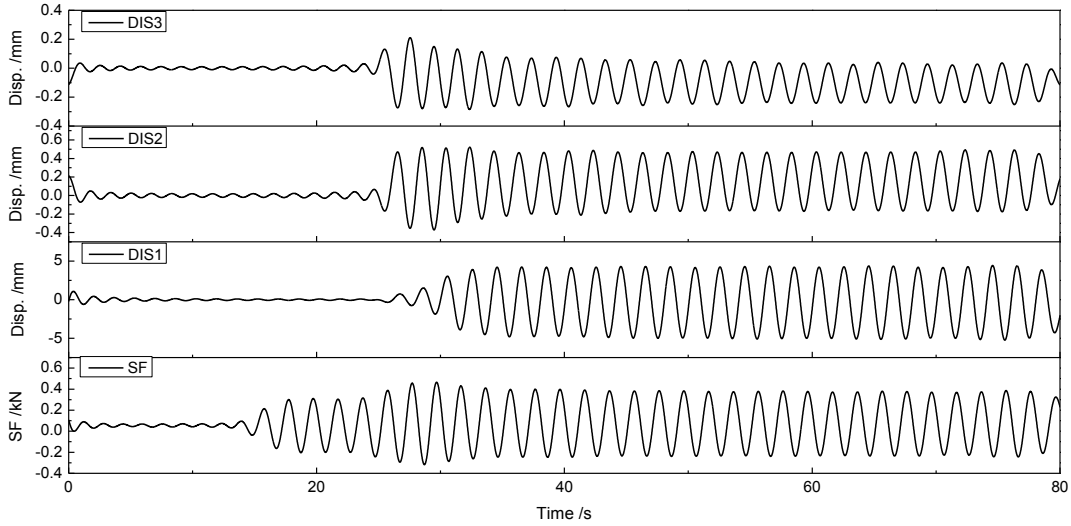

Fig. 3. Typical record curves.

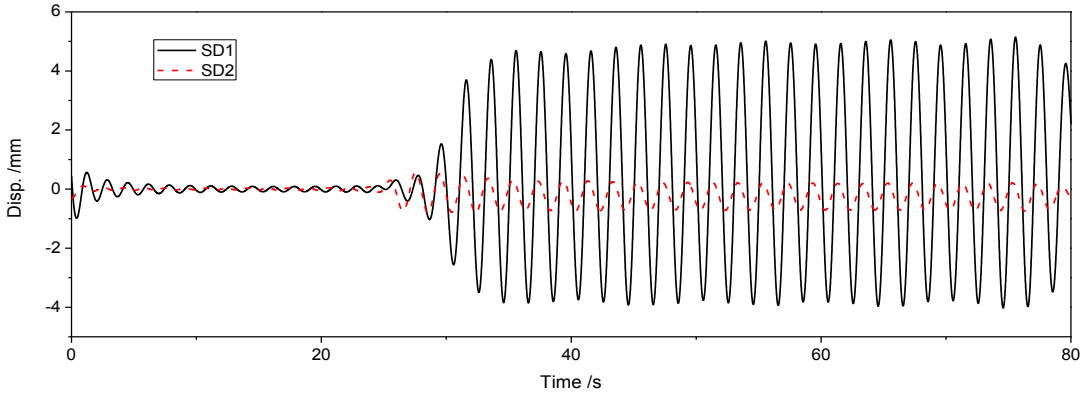

Fig. 4. History curve of shear deformation.

4.2. Influence of moisture content and loading frequency

Fig. 9 presents the relation between the total energy dissipation and the moisture content, and Fig. 10 is the relation between the total energy dissipation and the loading frequency. The two figures indicate that the total energy dissipation causing the system to damage will decrease with the increasing in moisture content and the loading frequency, which can be fitted with formula of $y=ax^b$ respectively. From Fig. 9 and 10, we also find that the relations among the total energy dissipation, moisture content, and loading frequency were coupling.

4.3. Influence of contact size and roughness on interface

Table 2 shows the total energy dissipation on different case under different loading frequency, including contact diameter with 150mm, 100mm, and different roughness of STR1, STR2. From Table 2, we find that the total energy dissipation on different cases all decrease with the increasing in loading frequency, the total energy dissipation on large contact size case are larger than that on small contact size case, and the influence of roughness are also obvious which present that the total energy dissipation on STR2 are less than that on STR1.

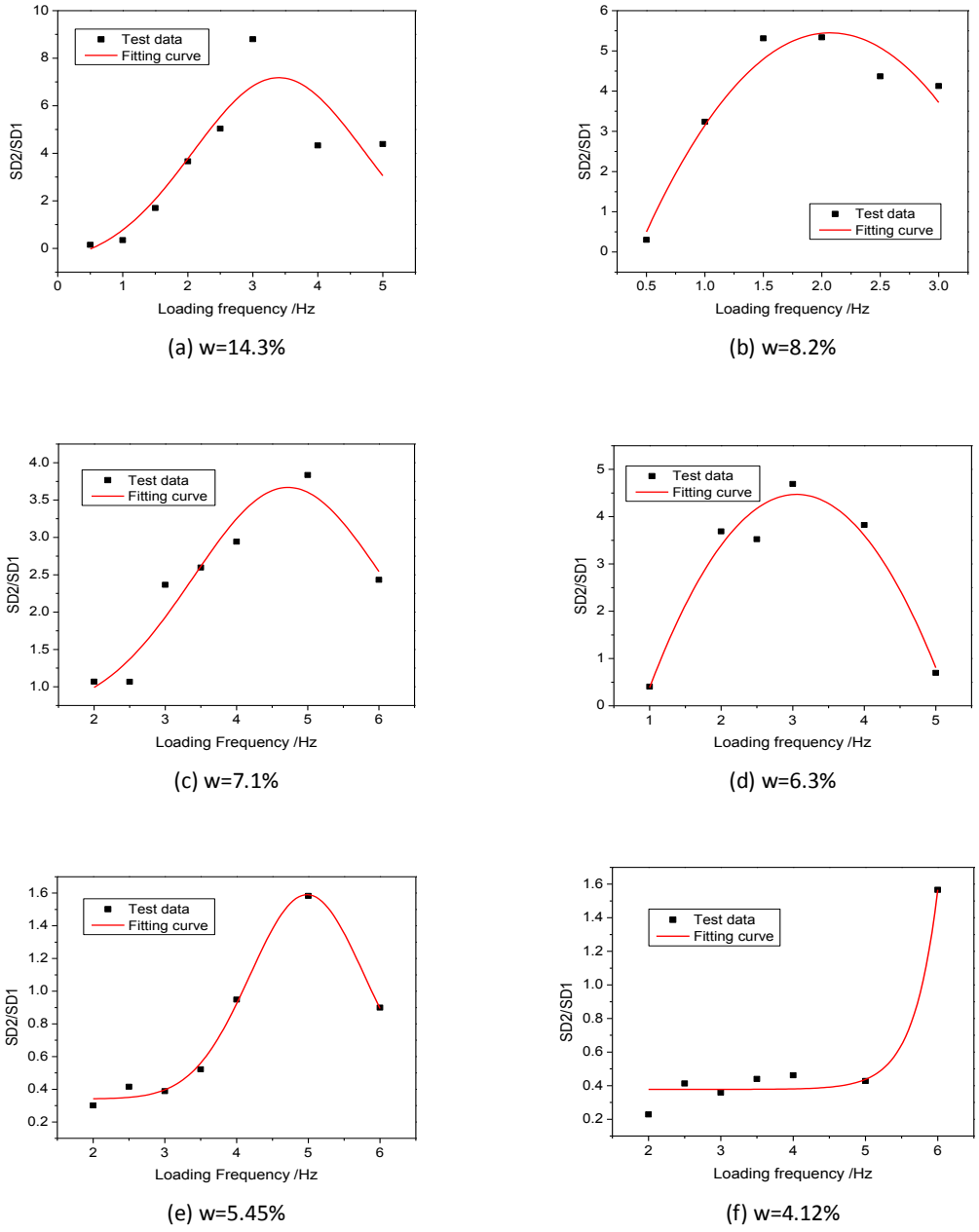

Fig. 5. Relationship curve between SD2/SD1 and loading frequency.

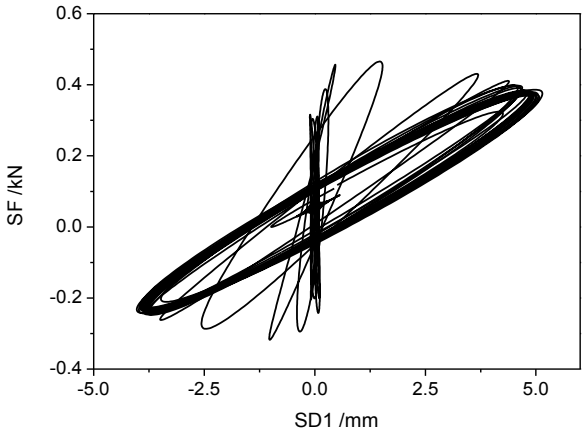

Fig. 6. Typical hysteresis loops.

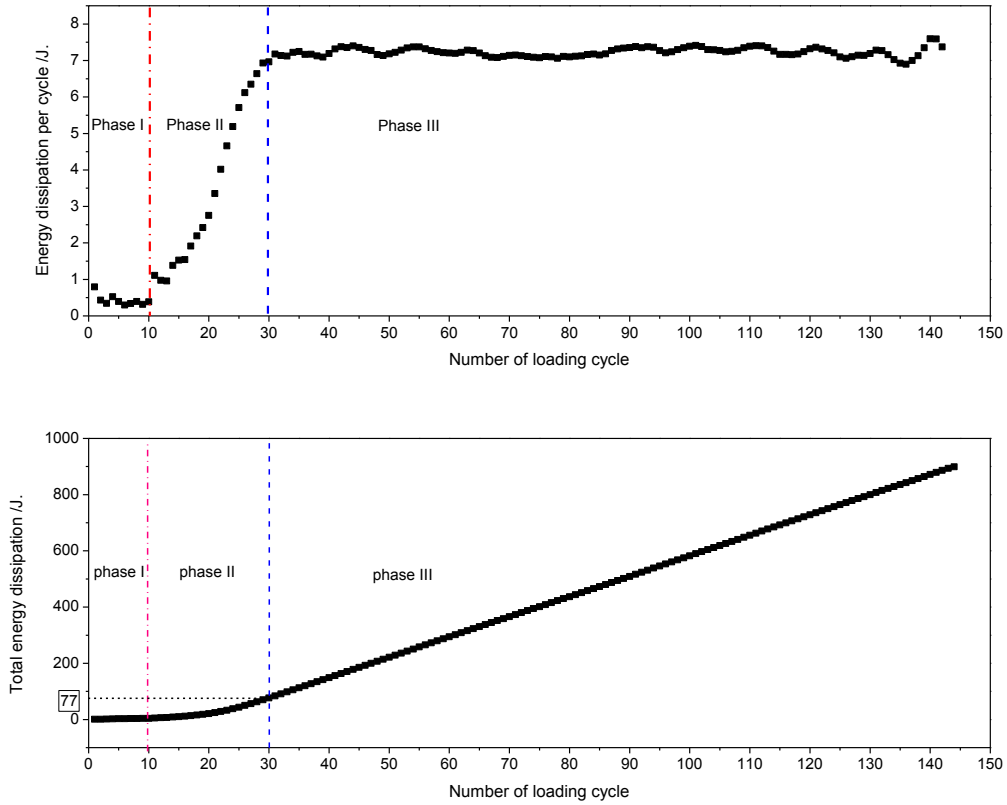

Fig. 7. Relationship between energy dissipation and loading cycle.

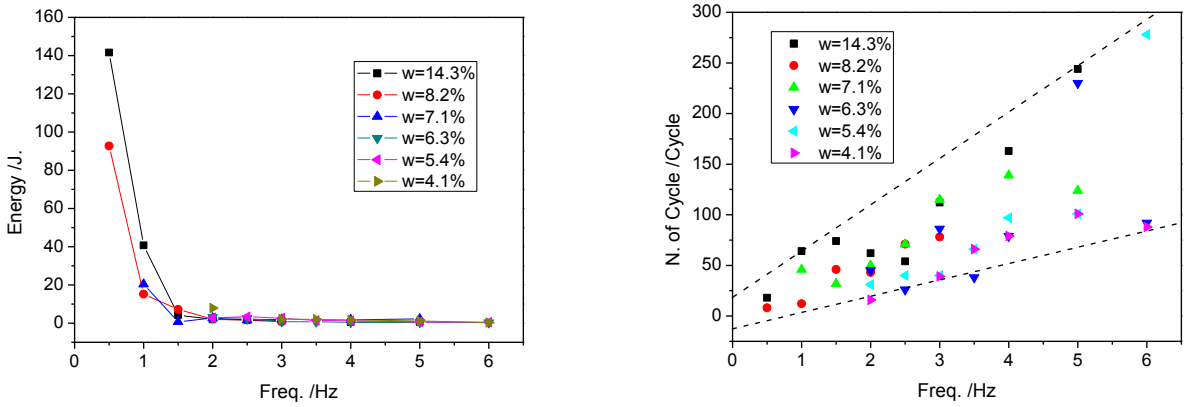

Fig. 8. Monocycle Energy and Number of Cycle while the system damaged.

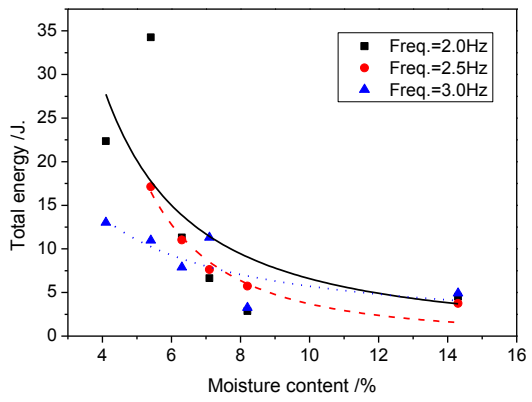

Fig. 9. Total energy versus Moisture content.

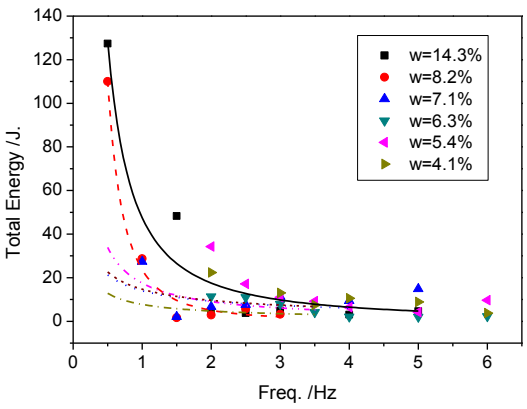

Fig. 10. Total energy versus loading frequency.

Table 2. Total energy dissipation on different cases.

Case Freq. /Hz	D=150mm and STR1	D=100mm and STR1	D=150mm and STR2
2.0	11.31	3.71	3.24
2.5	11.03	2.29	6.59
3.0	7.90	1.49	14.56
3.5	4.15	0.79	2.61
4.0	2.11	1.84	4.44
5.0	1.97	1.49	1.85
6.0	2.24	0.97	2.18

5. Conclusions

In this paper, the dynamic response of the soil-structure system and the contact performance between silt and structure under cyclic loading was studied, using a Suspensory Ring Test Apparatus designed by the authors, where the physical properties of the test silt were that ρ=1.59g/cm^3, ω_P=14.26%, ω_L=21.77%. Firstly, the Suspensory Ring Test Apparatus was introduced. Then, the test data are analyzed and some conclusions were gained. (1) The increasing of the displacements is slower than that of shear force along the interface between soil and structure. (2) The damage position of the soil-structure system was different when the loading frequency and moisture content were different. (3) The factors affected on contact performance between silt and concrete structure under cyclic loading were studied, such as moisture content, loading frequency, contact size, and roughness.

Acknowledgements

This paper has been funded by grants from the National Science Foundation of P.R. China (No: 51278017, No: 51421005).

References

Cai ZY, Mao JF, Fu H (2010). Development of NHRI-4000 high performance with large contact surface direct shear apparatus. *Chinese Journal of Geotechnical Engineering*, 32(9), 1319-1322 (in Chinese).

Desai CS, Drumm EC, Zaman MM (1985). Cyclic testing and modeling of interfaces. *Journal of Geotechnical Engineering*, 111(6), 793–815.

Li D, Li N (2010). Development and application of test apparatus for soil-structure interface. *Engineering Journal of Wuhan University*, 43(3), 390-393 (in Chinese).

Li L, Zhang S, Wang X (2013). Development in a Suspensory Ring Test Apparatus for Studying Dynamic Contact Performance between Soil and Structure. *Earthquake Engineering and Engineering Vibration*, 33(4), 248-255 (in Chinese).

Li S, Meng F, Chen J (2012). Development of shear test device with interface visualization for soil-structure interaction and its application. *Chinese Journal of Rock Mechanics and Engineering*, 31(1), 180-188 (in Chinese).

Potyondyj G (1961). Skin friction between various soils and construction materials. *Geotechnique*, 11(4), 339-353.

Westgate ZJ, DeJong JT (2006). Evolution of sand-structure interface response during monotonic shear using particle image velocimetry. *GeoCongress ASCE Conference Proceedings*, 1-6.

Yoshini Y, Kishida TA (1981). Ring torsion apparatus for evaluating friction between soils and metal surfaces. *Geotechnical Testing Journal*, 4(4), 145–152.

Zhang G, Zhang JM (2003). Development and application of cyclic shear apparatus for soil-structure interface. *Chinese Journal of Geotechnical Engineering*, 25(2), 149-153 (in Chinese).

Zhang JM, Hou WJ, Zhang G (2008). Development of a 3D soil-structure interface test apparatus and its application. *Chinese Journal of Geotechnical Engineering*, 30(6), 889-894 (in Chinese).

Challenge Journal of Structural Mechanics

An experimental study on impact of anchor bars at the steel frames with infilled walls

Atila Kumbasaroğlu [a,*], Ahmet Budak [b]

[a] *Department of Civil Engineering, Erzincan University, 24060 Erzincan, Turkey*
[b] *Department of Civil Engineering, Atatürk University, 25240 Erzurum, Turkey*

ABSTRACT

In this study, a series of experimental study was conducted to investigate the effect of anchor bars on steel frame systems where the connections were provided by anchor bars between frame and infilled walls. Seven one over four scaled specimens having one story and one bay of frames were tested. Experimental study was carried out by damage-controlled and incrementally applied load up to loading cracks. The test results relieved that with the help of using anchor bars the capacity of energy absorption with initial stiffness were increased. It has been found that the frames without using anchor bars failure at the loading edge, the crushing behavior of infilled walls and separations at free edges were occurred. These observed failure behaviors replies with tensile cracking for the frames having anchor bars. There for it should be underlined that anchor bars have a significant effect on improving the behavior of the frames.

ARTICLE INFO

Article history:
Received 24 April 2016
Accepted 21 June 2016

Keywords:
Infilled walls
Anchor bars
Energy absorption capacity
Initial stiffness

1. Introduction

Infilled walls mainly defined as a wall which separates the place from each other. Infilled walls directly affect the structural behavior. Although infilled walls affect the structural behavior of buildings, it has not been consider for the structural design analysis (Budak, 1997). This may be explained by the difficulties and the non-practical calculation methods which were provided by the available literature.

In the available literature considerable research has been conducted particularly the behavior of infilled walls under the impact of lateral loading. For this purposes the capacity of infilled walls load-carrying capacities, ductile, stiffness and energy absorption properties were examined. Performed studies generally used hysteretic and cycling loadings were applied (Öztürkoğlu et al., 2015; Aksoy et al., 2015; Özdemir et al., 2014; Yakut et al., 2013; Peynirci, 2007; Kara, 2006; Celep et al., 2003; Ataman, 2003; Orbay, 2001). Depending on the increases by loads some regions between frame and infilled walls are separated, and cracks occurred at inside of the infilled walls. Since separations and cracks depending on the changing loads occurred between infilled walls and the frames where infilled walls are in contact with those cracking regions; friction forces appear. Beside of occurred friction forces, damping provided by infilled walls increase overall strength and stiffness with energy absorption (Budak, 1997). Up to a certain value of slippage, slipping of anchor bars provides ductility and the capacity of energy absorption (Yalciner et al., 2015).

In Turkey, lessons learned from previous earthquake show that most of the constructed buildings with infilled walls cause ductile problems, non-adequate lateral stiffness for the damaged buildings (Kızıloğlu, 2006). In order to repair and strengthening of such buildings against to further expected earthquakes, it has been began to use anchor bars for infilled walls (Tekeli et al., 2014; Özen et al., 2014; Erdem et al., 2004).

In contrast to previous studies in this study the behavior of steel frames constructed with infilled walls by using anchor bars were examined. It is believed that infilled walls with anchor bars provide better stability of the structural systems under the applied lateral loads.

* *Corresponding author*. Tel.: +90-446-2240088 ; Fax: +90-446-2240077 ; E-mail address: akumbasaroglu@erzincan.edu.tr (A. Kumbasaroğlu)
ISSN: 2149-8024 / DOI: http://dx.doi.org/10.20528/cjsmec.2016.06.016

2. Assumptions of the Current Study

The assumptions done for the current study were listed below:

- Monolithic loading has been applied until the cracking loading. Thus applied lateral loading of infilled walls distributed as diagonal that because of the bending behavior of the system an effective experimental program was performed.
- The placing of anchor bars at column-beam joints were done according to the conventional densification.
- The infilled model was preferred as slenderness walls. This may be explain by the bending behavior for the infilled walls which are having slenderness ratio less than 20.
- For the trial test four millimeter diameter of aggregate was used according to the described guideline by ACI. In order to observe the cracking patterns seven millimeter diameter of aggregate were selected for the real tests.
- For ϕ4 millimeter diameter of anchor bars were selected to provide the ratio of total area of anchor bars to area of infilled walls which was 0.8 (Phan et al., 1995).

3. Experimental Program and Setup

3.1. Experimental program

In this study, seven one over four scaled specimens having one story and one bay of frames were tested. While the material of the infilled walls was done by in-place concrete, the frame was constructed with steel profile. Fig. 1 shows the connections between frame and infilled walls provided by anchor bars. All specimens were cured for seven days. The characteristic properties for the samples were given in Table 1. The tests were ended until the defined damaged degree was provided where the loading program was done by using incremental loading and damage-controlled.

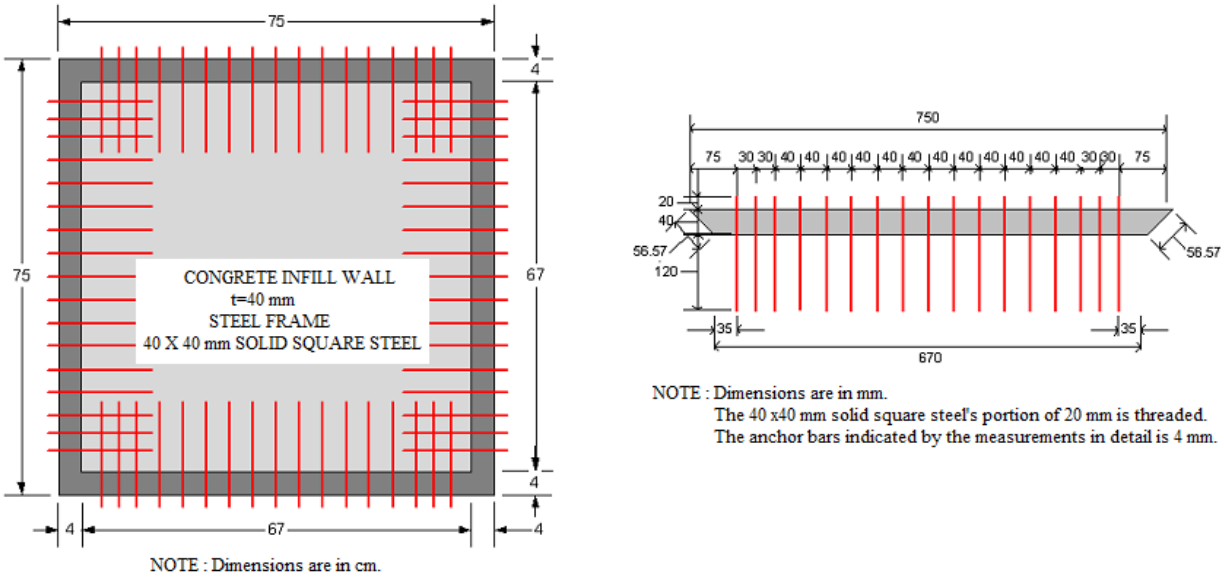

Fig. 1. Demonstration of test specimen.

3.2. The setup of the experimental study

Fig. 2 shows the setup for the performed experimental study. Steel frames with infilled walls were hold with the help of its own weight at the setup platform and the loads were applied to the edge of the frame.

The damage degree to the cracking loading constitutes the linear curvature region of load-displacement and separation of walls at free support. In this study the considered cracking loading was not limited by initial cracking or interface surface cracking. The loading was continued until tension and cross cracking occurs at the surface of the infilled walls, crushing occurs at fixed support and edge failure-crushing, separation of infilled walls at free supports.

After obtaining the damage to the cracking load while the load constant since the displacements were continued and the behavior of the system exceed the plastic region in order to be able to discuss the contribution of the anchor bars the experimental tests were ended.

The expectation until the occurring of the cracking loading was initial cracking or interface cracking, tensile or cross cracking, crushing of walls supports and edge failure-crushing and separation of walls at free supports.

Table 1. Characteristics of test specimens.

Frame without Infilled Wall		Steel Frame	$E_{\text{steel frame}}$=198000 MPa $\gamma_{\text{steel frame}}$=7,25e-6 kg/mm^3 $\upsilon_{\text{steel frame}}$=0,30
Frame with Infilled Walls	First Test Specimen	Steel Frame	$E_{\text{steel frame}}$=198000 MPa $\gamma_{\text{steel frame}}$=7.25e-6 kg/mm^3 $\upsilon_{\text{steel frame}}$=0.30
		Infilled Walls	$E_{\text{infilled walls}}$=17300 MPa $\gamma_{\text{infilled walls}}$=2.20e-6 kg/mm^3 $\upsilon_{\text{infilled walls}}$=0.20 $\sigma_{\text{infilled walls}}$=11.14 MPa
	Second Test Specimen	Steel Frame	$E_{\text{steel frame}}$=198000 MPa $\gamma_{\text{steel frame}}$=7.25e-6 kg/mm^3 $\upsilon_{\text{steel frame}}$=0.30
		Infilled Walls	$E_{\text{infilled walls}}$=13400 MPa $\gamma_{\text{infilled walls}}$=2.20e-6 kg/mm^3 $\upsilon_{\text{infilled walls}}$=0.20 $\sigma_{\text{infilled walls}}$=3.57 MPa
	Third Test Specimen	Steel Frame	$E_{\text{steel frame}}$=198000 MPa $\gamma_{\text{steel frame}}$=7.25e-6 kg/mm^3 $\upsilon_{\text{steel frame}}$=0.30
		Infilled Walls	$E_{\text{infilled walls}}$=19300 MPa $\gamma_{\text{infilled walls}}$=2.20e-6 kg/mm^3 $\upsilon_{\text{infilled walls}}$=0.20 $\sigma_{\text{infilled walls}}$=15.10 MPa
	Forth Test Specimen	Steel Frame	$E_{\text{steel frame}}$=198000 MPa $\gamma_{\text{steel frame}}$=7.25e-6 kg/mm^3 $\upsilon_{\text{steel frame}}$=0.30
		Infilled Walls	$E_{\text{infilled walls}}$=18900 MPa $\gamma_{\text{infilled walls}}$=2.20e-6 kg/mm^3 $\upsilon_{\text{infilled walls}}$=0.20 $\sigma_{\text{infilled walls}}$=13.95 MPa
Frame with Infilled Walls + Anchor Bars	First Test Specimen	Steel Frame	$E_{\text{steel frame}}$=198000 MPa $\gamma_{\text{steel frame}}$=7.25e-6 kg/mm^3 $\upsilon_{\text{steel frame}}$=0.30
		Infilled Walls	$E_{\text{infilled walls}}$=18900 MPa $\gamma_{\text{infilled walls}}$=2.20e-6 kg/mm^3 $\upsilon_{\text{infilled walls}}$=0.20 $\sigma_{\text{infilled walls}}$=13.95 MPa
		Anchor Bars	$E_{\text{anchor bar}}$=123000 MPa $\gamma_{\text{anchor bar}}$=7.80e-6 kg/mm3 $\upsilon_{\text{anchor bar}}$=0.30
	Second Test Specimen	Steel Frame	$E_{\text{steel frame}}$=198000 MPa $\gamma_{\text{steel frame}}$=7.25e-6 kg/mm^3 $\upsilon_{\text{steel frame}}$=0.30
		Infilled Walls	$E_{\text{infilled walls}}$=16500 MPa $\gamma_{\text{infilled walls}}$=2.20e-6 kg/mm^3 $\upsilon_{\text{infilled walls}}$=0.20 $\sigma_{\text{infilled walls}}$=10.49 MPa
		Anchor Bars	$E_{\text{anchor bar}}$=123000 MPa $\gamma_{\text{anchor bar}}$=7.80e-6 kg/mm3 $\upsilon_{\text{anchor bar}}$=0.30
Note: E: Modulus of Elasticity, γ: Density, υ: Poisson's Ratio and σ: The average compressive strength of infilled wall			

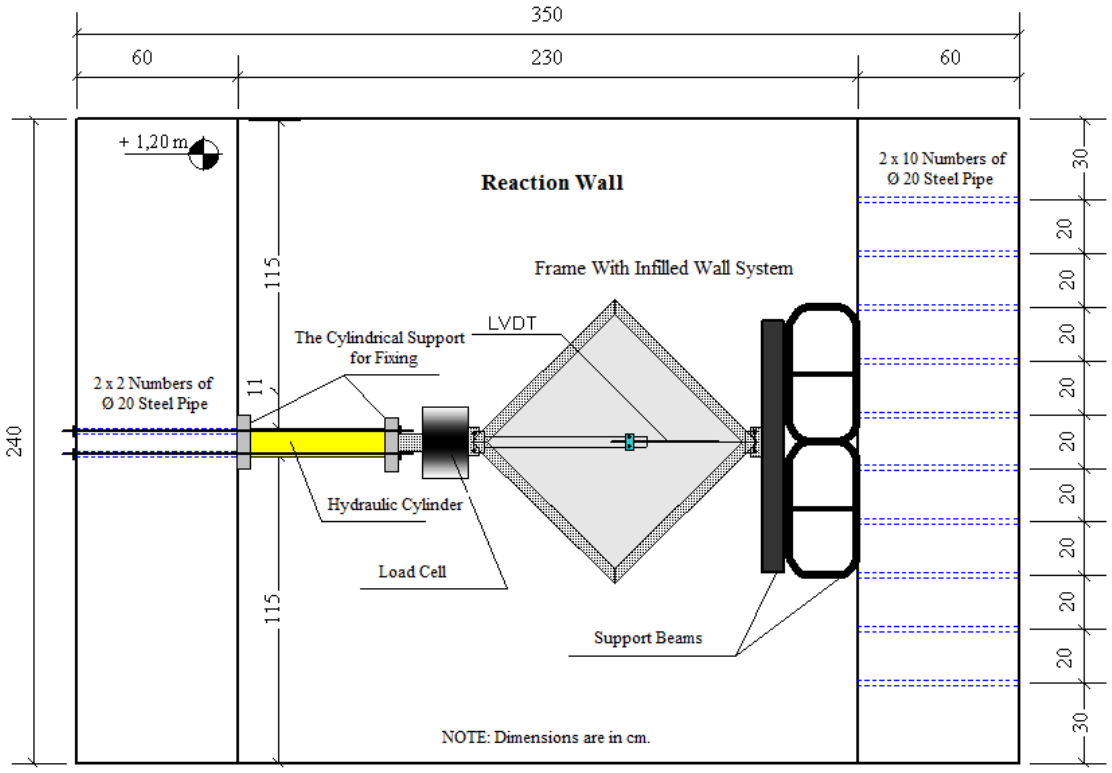

Fig. 2. Experimental setup.

4. Experimental Results

For each samples load-displacement curves were obtained and by using those results the capacity of energy absorption with initial stiffness were calculated. At the obtained load-displacement curve since initial stiffness was calculated at the 1.50 mm displacement, the capacity of the energy absorption was also calculated based on these quantities.

Table 2 gives the obtained load-displacement curve with cracking patterns occurred at cracking load. Based on obtained test, results initial stiffness with capacity of energy absorption summarized in Table 3.

By using the material constant of the concrete infilled walls damage level occurred until to the cracking loading, with the assumption of the plane strain, stress-based evaluation was done by calculating the shear stresses occurred at infilled walls. Obtained tests results for the average shear stresses were summarized in Table 4.

In this study also plane stresses were recorded by installing the strain gauges to the anchor bars. The interaction between the frames lends to bending and the slippage of the infilled walls was investigated. The installed strain gauges are shown in Fig. 3. Table 5 also shows the transferred loads to the infilled walls and plane stresses passes to anchor bars.

Table 3. Displacement-based evaluation of the test specimens.

Frame With Infilled Wall Systems		Load (N)	Energy Absorption Capacity (Joule) (10^{-3})	Initial Stiffness (N/m) (10^{6})
Frame without Infilled Wall		4264	3.23	2.80
Frame with Infilled Walls	First Test Specimen	71906	59.05	57.35
	Second Test Specimen	17896	15.51	15.96
	Third Test Specimen	34695	27.98	29.69
	Forth Test Specimen	84323	69.35	131.06
Frame with Infilled Walls + Anchor Bars	First Test Specimen	82752	71.26	72.12
	Second Test Specimen	70892	59.75	56.72

Table 2. Load-displacement curves of the experimental specimen and the damage pattern in cracking load.

Frame without Infilled Wall		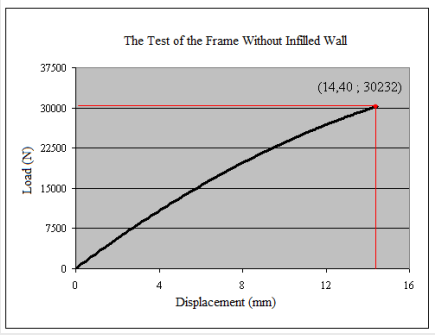	
Frame with Infilled Walls	First Test Specimen	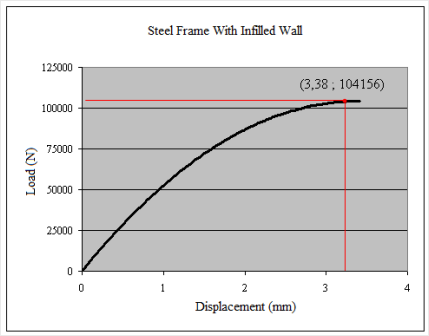	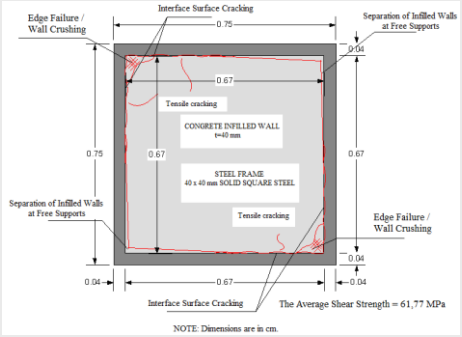
	Second Test Specimen	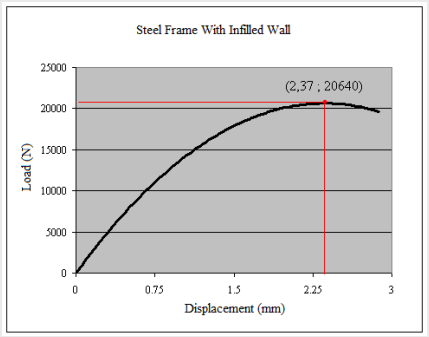	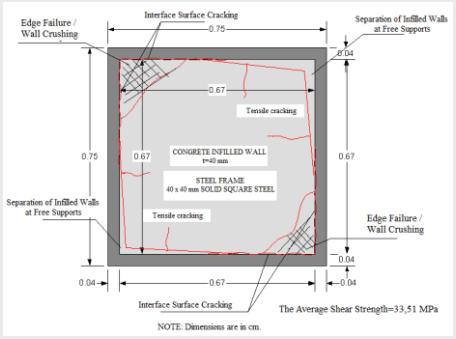
	Third Test Specimen	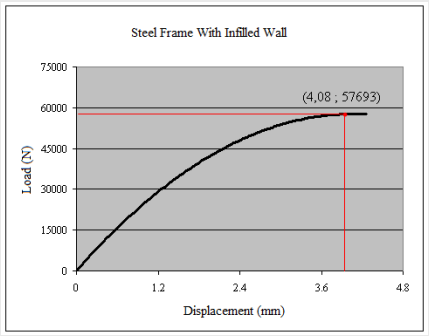	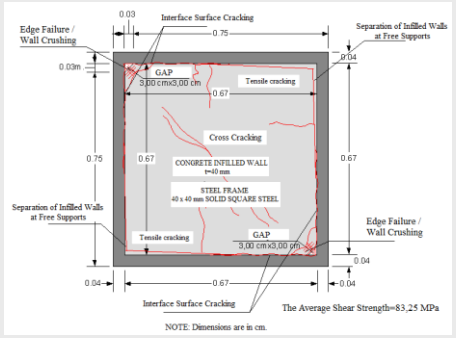
	Forth Test Specimen	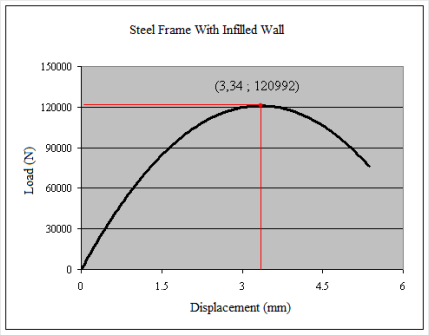	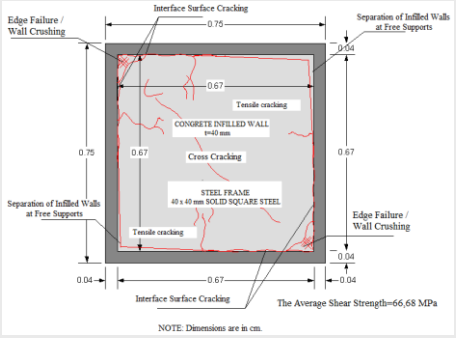

* Table 2			
Frame with Infilled Walls + Anchor Bars	First Test Specimen	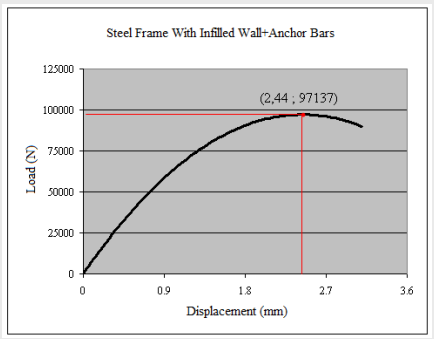	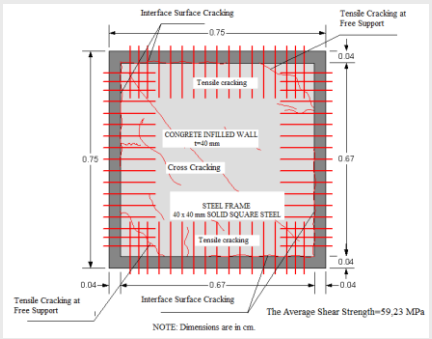
	Second Test Specimen	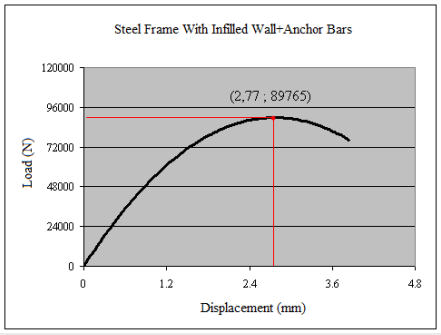	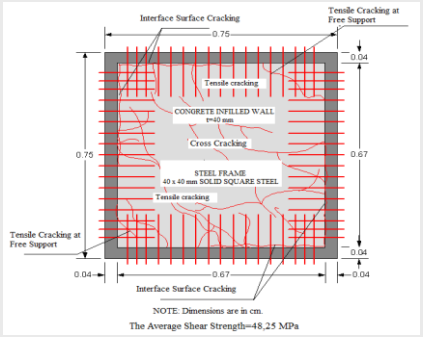

Table 4. Stress-based evaluation of the test specimens.

Frame With Infilled Wall Systems		Cracking Load (N)	The Average Shear Strength (MPa)	The Average Compression Strength of Infilled Wall (MPa)
Frame without Infilled Wall		-	-	-
Frame with Infilled Walls	First Test Specimen	104156	61.77	11.14
	Second Test Specimen	20640	33.51	3.57
	Third Test Specimen	57693	83.25	15.10
	Forth Test Specimen	120992	66.68	13.95
Frame with Infilled Walls + Anchor Bars	First Test Specimen	97137	59.23	20.44
	Second Test Specimen	89765	48.25	10.49

5. Discussions of the Test Results

When the obtained results of load-displacement curve and the capacity of energy absorption were examined, the tests results 1.52 times less for infilled walls without anchor bars, 20.28 for times of frame without infilled walls. The test results of the capacity of energy absorption are summarized in Fig. 4.

When the tests results consider for the initial stiffness the obtained results for the initial stiffness was 1.18 times was more for the anchor system compare to frames without anchor bars and 23.13 times compare to frames without infilled walls at the displacement of 1.50 mm and the load corresponding to cracking load. The test results of the initial stiffness are summarized in Fig. 5.

As shown in Fig. 6, it has been found that there have been no significant differences for the obtained results of shear stresses between the frame with infilled walls having anchor bars and the infilled walls frames not having anchor bars. According these results steel frames transfers the loads uniformly and provide adequate confinement.

Obtained results of the plane stresses and transferred normal loads passes through anchor bars having fixed support and free support are shown in Table 6.

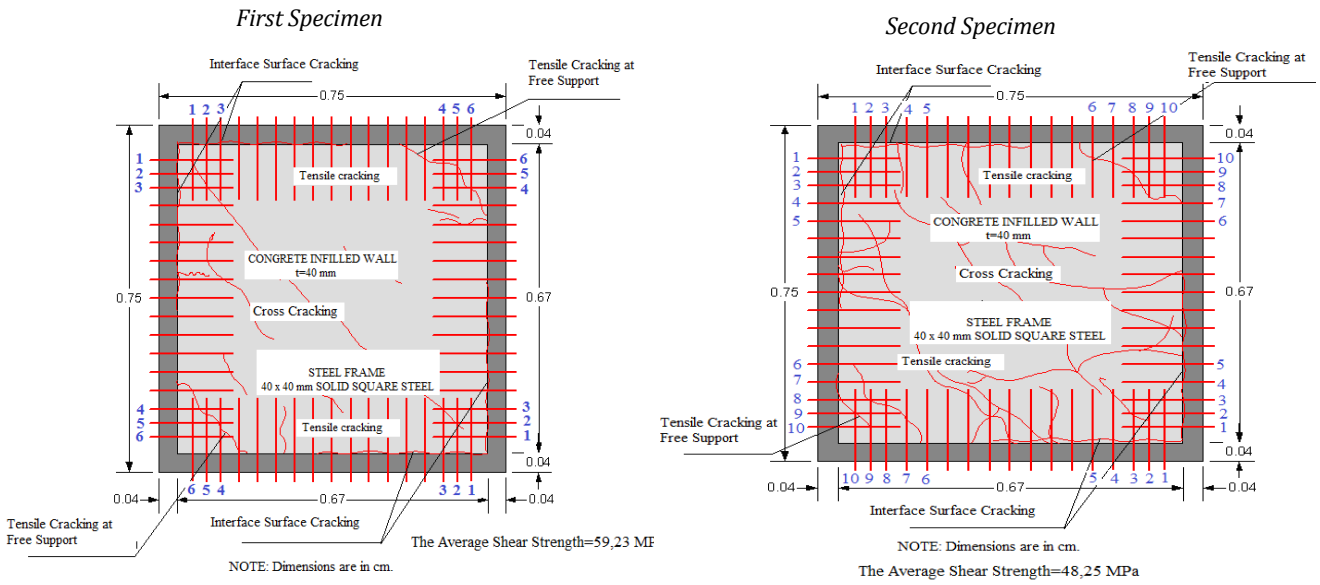

Fig. 3. Installation of strain gauges.

Table 5. Transferred loads to the infilled walls and plane stresses passes to anchor bars.

Frame with Infilled Wall Systems		Plane Stresses Passes to Anchor Bars	Transferred Normal Loads to the Infilled Walls
Frame with Infilled Walls + Anchor Bars	First Specimen	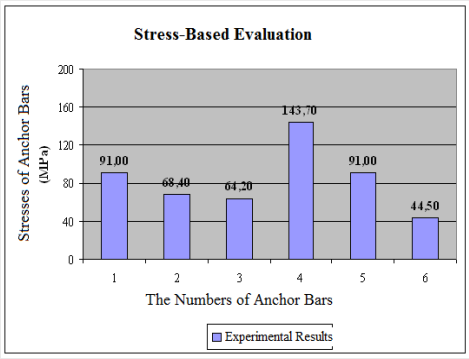	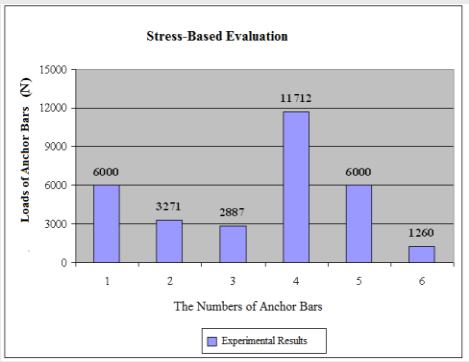
	Second Specimen	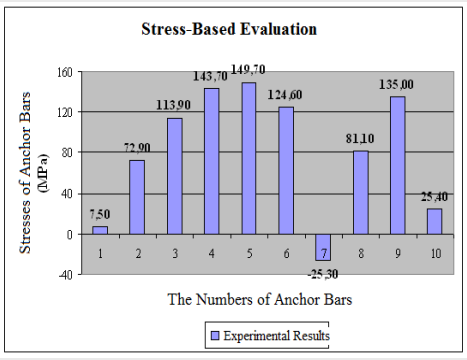	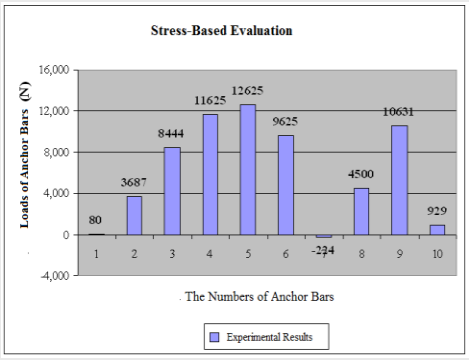

In Fig. 7 for the first sample plane stresses of the anchor bars at the fixed support were approximately 25% more compare to free support. For the second sample these results were approximately achieved to 43%.

At the first sample with the help of anchor bars transferred normal loads to the infilled walls was approximately 56% more for the fixed support compare to free support. For the second sample these values reduced to 43% at the fixed support compare to free support. According to results with the help of anchor bars plane stresses occurred at the steel frame systems successfully were distributed.

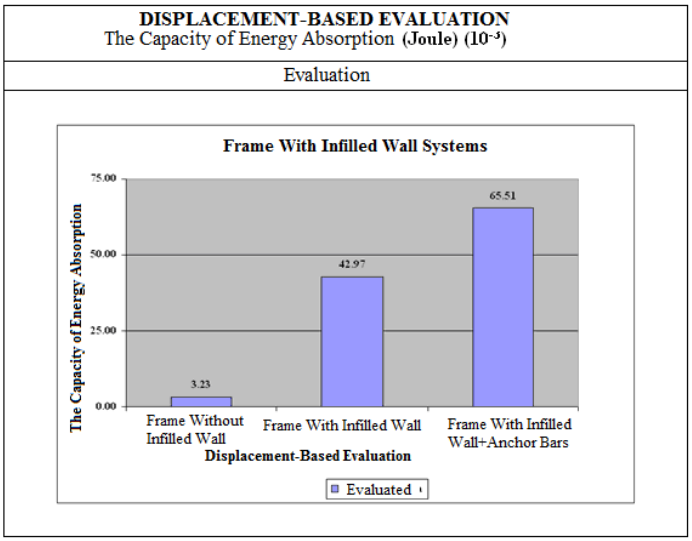

Fig. 4. Test results of the energy absorption capacity.

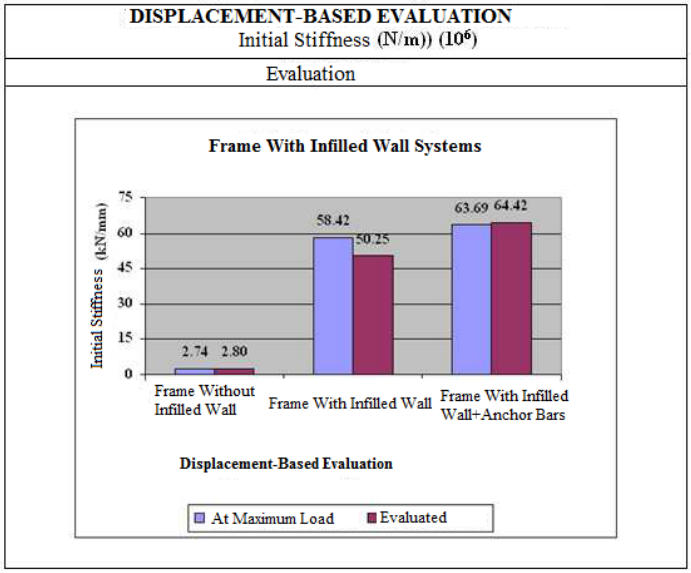

Fig. 5. Test results of the initial stiffness.

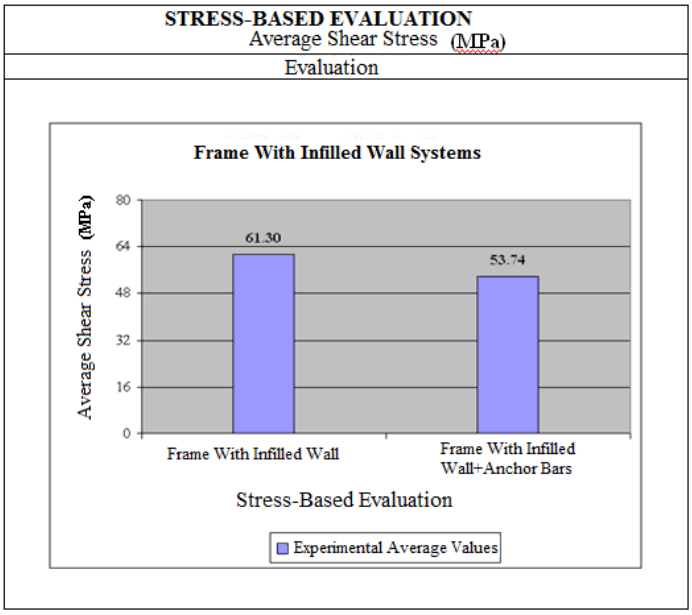

Fig. 6. Test results of the average shear stresses.

Table 6. Obtained results of the plane stresses and transfer normal loads passes through anchor bars having fixed support and free support.

Frame with Infilled Wall Systems		Plane Stresses Passes to Anchor Bars	Transferred Normal Loads to the Infilled Walls
Frame with Infilled Walls + Anchor Bars	First Specimen	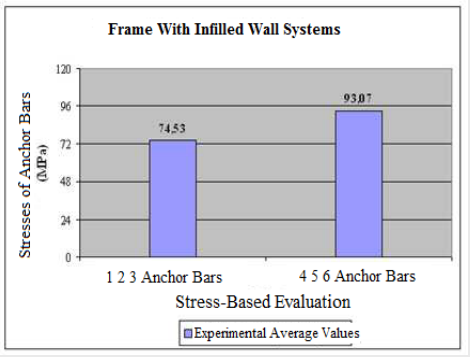	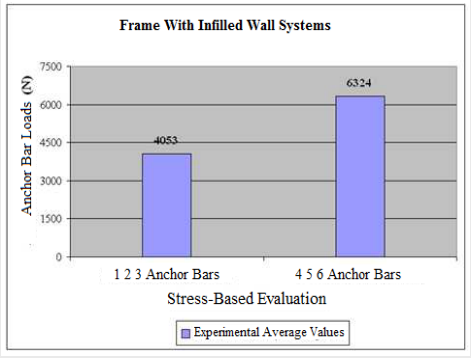
	Second Specimen	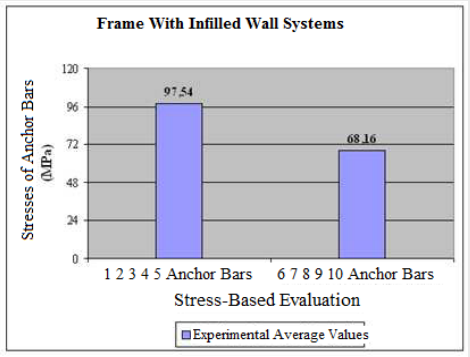	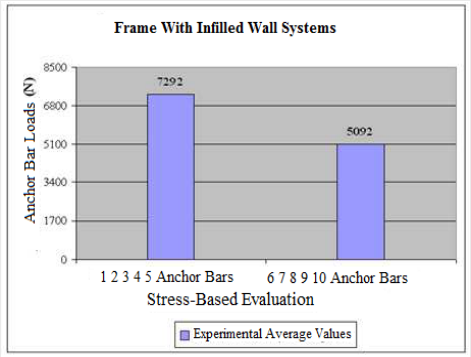

6. Conclusions

Test results indicated that placed anchor bars for the steel frames remarkable increase the capacity of the energy a sorption and initial stiffness. It has been found that average shear stresses were not change significantly. These may be explained by the rigidity of the steel frames and the applied load until to the cracking loads. While the behavior of the edge failure/wall crushing occurred at the applied load on the edge of the infilled walls frames not having anchor bars, the separation of the walls occurred at free edges. This behavior was replaced with tensile cracking for infilled walls frames having anchor bars. As a results it can be concluded that the behavior of the system obviously improved by anchor bars. It is believed that obtained results may provide the guideline for the earthquake codes.

Acknowledgements

This work was supported by the Scientific Research Projects Commission of Atatürk University under grant number BAP-2004/111.

References

Aksoy HB, Avşar Ö (2015). Dolgu duvarların betonarme çerçeve davranışına etkisinin basitleştirilmiş bir yöntemle dikkate alınması. *Pamukkale University Journal of Engineering Sciences*, 21(3), 115-122 (in Turkish).

Ataman S (2003). Betonarme Çerçevelerin Betonarme Dolgu Duvarlarla Güçlendirilmesi. *MSc thesis*, Mustafa Kemal University, Hatay (in Turkish).

Budak A (1997). Dolgu Duvarlı Çerçevelerin Sonlu Elemanlar Yöntemi ile Malzeme Bakımından Doğrusal Olmayan Hesabı. *Ph.D thesis*, Karadeniz Technical University, Trabzon (in Turkish).

Celep Z, Gençoğlu M (2003). Deprem etkisindeki betonarme çerçeve taşıyıcı sistem davranışına bölme duvarların etkisi. *5th National Conference of Earthquake Engineering*, 26-30 Mayıs, İstanbul, AT21, 1-9 (in Turkish).

Erdem I, Akyüz U, Ersoy U, Ozcebe G (2004). Experimental and analytical studies on the strengthening of RC frames. *13th World Conference on Earthquake Engineering*. Vancouver, B.C., Canada. P.no. 673.

Kara ME (2006). Sünek Olmayan Betonarme Çerçevelerin Betonarme Parasal Dolgu Duvarlarıyla Güçlendirilmesi. *Ph.D thesis*, Gazi University, Ankara (in Turkish).

Kızıloğlu MY (2006). Deprem Etkisi Altında Dolgu Duvarların Betonarme Çerçeve Yapılar Üzerindeki Etkisi. *MSc thesis*, Yıldız Technical University, İstanbul (in Turkish).

Orbay A (2001). Dolgulu çerçevelerin dayanım ve davranışı bir yaklaşık hesaplama yöntemi eldeleri. *XII. National Mechanics Congress*, Konya (in Turkish).

Özdemir H, Eren İ (2014). Çerçeveye yapılan ankraj aralığının bölme duvarlı çerçeve güçlendirmesine etkisi. *Journal of the Graduate*

School of Natural and Applied Sciences of Erciyes University, 30(4), 248-256 (in Turkish).

Özen MA, Yılmaz S (2014). Tensile performance of retrofitting anchors. *2nd European Conference on Earthquake Engineering and Seismology*, İstanbul.

Öztürkoğlu O, Uçar T, Yeşilce Y (2015). Kısmi boşluklu dolgu duvarların betonarme binaların deprem davranışına etkisinin incelenmesi. *International Burdur Earthquake & Environment Symposium (IBEES2015)*, 7-9 May 2015, Mehmet Akif Ersoy University, Burdur (in Turkish).

Peynirci R (2007). Betonarme Çerçeve Sistemlerde Dolgu Duvarların Deprem Davranışına Katkısı. *MSc thesis*, Afyon Kocatepe University, Afyon (in Turkish).

Phan LT, Cheok GS, Todd DR (1995). Strengthening methodology for lightly reinforced concrete frames: Recommended design guidelines for strengthening with infill walls. Building M-D Fire Research Laboratory, National Institute of Standards and Technology Gaithersburg, Md 20899.

Tekeli H, Akyürek O, Deniz M, Hersat E, Kara N, Tosun U, Kaya F (2014). Betonarme çerçevede dolgu duvarların hasır çelik donatılı sıva ile güçlendirilmesi. *BEÜ Journal of Natural Sciences*, 3(2), 179-191 (in Turkish).

Yakut A, Binici B, Demirel İO, Özcebe G (2013). Dolgu duvarların deprem davranışına etkisi. *2nd Turkey Conference of Earthquake Engineering and Sismology*, 25-27 September 2013, Hatay (in Turkish).

Yalciner H, Sensoy S, Eren O (2015). Seismic performance assessment of a corroded 50-year-old reinforced concrete building. *Journal of Structural Engineering*, 10.1061 / (ASCE) ST. 1943-541X.0001263, 05015001.